Aus dem

Department für Augenheilkunde Tübingen

Sektion Experimentelle Vitroretinale Chirurgie

Investigation of the role of melanosomes and radicals in photoreceptor disc clearance by the retinal pigment epithelium

Inaugural-Dissertation
zur Erlangung des Doktorgrades
der Medizin

der Medizinischen Fakultät
der Eberhard Karls Universität
zu Tübingen

vorgelegt von

Lyu, Yanan

2022

Dekan: Professor Dr. B. Pichler

1. Berichterstatter Professor Dr. U. Schraermeyer
2. Berichterstatter: Professor Dr. S. Clark

Tag der Disputation: 14.11.2022

Table of contents

List of Figures

List of tables

List of Abbreviations

A2E	N-retinylidene-N-retinyl-ethanolamine
AAV	adeno-associated virus
Ad-Tyr	adenoviral tyrosinase vector
ACU-4429	emixustat
ALK-001	C20-D3-retinyl acetate
AMD	age-related macular degeneration
AF	autofluorescence
cSLO	confocal scanning laser ophthalmoscopy
DHA	docosahexaenoic acid
EM	electron microscope
ERG	electroretinography
FA	fluorescein angiography
HPLC	high-performance liquid chromatography
hESCs	human embryonic stem cells
H_2O_2	hydrogen peroxide
IOD	integrated optical density
ISDN	Isosorbide dinitrate
MLF	melanolipofuscin
NIR-AF	Near-infrared AF
NIR-R	near-infrared reflectance
NO•	nitric oxide
N-Ret-PE	N-retinylidene-phosphatidylethanolamine
O2•-	superoxide
OCTA	optical coherence tomography angiography
ONH	optic nerve head
ONOO-	peroxynitrite
OS	outer segments
OsO4	Osmium tetraoxide solution
PBS	phosphate buffered saline
PE	phosphatidylethanolamine
RPE65	RPE-specific 65 kDa retinoid isomerase

RPE	retinal pigment epithelium
SIN-1	3-morpholinosydnonimine
Stargazer	STG-001
SD-OCT	spectral-domain optical coherence tomography
SW-AF	Short-wavelength autofluorescence
TLMs	thin lamellar membranes
UAC	uranyl acetate
VA	visual acuity

1. Introduction

1.1 Lipofuscin accumulation-related retinal disorder

Stargardt disease, first demonstrated by Karl Stargardt in 1909, is one of the most frequent causes of hereditary macular dystrophies in humans (Stargardt, 1909, Tsang and Sharma, 2018). Its prevalence is approximately 1:8000–10,000 (Michaelides et al., 2003, Tsang and Sharma, 2018, Cremers et al., 2020). The hallmark is the accumulation of lipofuscin in the retinal pigment epithelium (RPE). Onset usually occurs in childhood or early adolescence, at about 10–15 years of age (Tsang and Sharma, 2018). However, in some cases, the disorder onset occurs later in life (Lambertus et al., 2016). The age of onset relates to the severity of the underlying disease course, childhood-onset Stargardt disease is correlated with more deleterious variants, while a later age of onset is often associated with a milder prognosis (Tanna et al., 2017, Tanaka et al., 2018, Lambertus et al., 2015, Rotenstreich et al., 2003). Normally, determining the actual age of disease beginning is difficult since many patients may be unaware of the visual impairment or still have maintained central vision due to the fovea function sparing (van Huet et al., 2014, Bax et al., 2019). In the beginning, ophthalmoscopy might also exhibit a normal fundus or mild retinal abnormalities (Tanna et al., 2017).

The clinical features of this autosomal recessive disorder vary widely due to the severity of the underlying ABCA4 variants (Tanna et al., 2017, Zernant et al., 2014, van Driel et al., 1998). Stargardt disease usually presents as progressive bilateral central visual impairment with progressive bilateral atrophy of the foveal retinal pigment epithelium, and the presence of yellowish flecks in fundus microscopy, defined as lipofuscin deposits (van Huet et al., 2014, Haji Abdollahi and Hirose, 2013). Patients typically present with reduced central visual function, with highly variable visual acuity (VA), depending on the degree of foveal involvement (Fujinami et al., 2013c).

Owing to an accumulation of lipofuscin fluorophores in the RPE, the before-mentioned yellowish flecks are hyperautofluorescent on fundus autofluorescence (AF). Fundus AF enables the investigation of lipofuscin distribution in the RPE cell as well as oxidized melanin (Schmitz-Valckenberg et

al., 2008, Taubitz et al., 2019). Fujinami et al demonstrated the relationship between AF subtype and genotype (Fujinami et al., 2013b). Full-field and multifocal electroretinography (ERG) are also helpful in diagnosis, Lois et al categorized the Stargardt macular dystrophy–fundus flavimaculatus into three phenotypic subtypes based on the electrophysiological attributes (Lois et al., 2001). Group 1 is classified as having severe pattern ERG abnormality with normal full-field ERGs; Group 2 has additional loss of photopic ERG, indicating cone dysfunction; and Group 3 has abnormalities of both the photopic and scotopic ERG (Lois et al., 2001). Instead of indicating various phases in the course of the disease, these groupings have also been proved to have prognostic implications. Based on the cross-sectional data, Group 1 may have a more positive prognosis (Fujinami et al., 2013a). Fundus fluorescein angiography (FA) normally illustrates a dark choroidal phase resulting from the blockage effect of lipofuscin deposition (Westerfeld and Mukai, 2008). Spectral-domain optical coherence tomography (SD-OCT) is a vital tool allowing for thorough three-dimensional visualization of morphological alterations in Stargardt disease including RPE abnormalities; loss of outer retinal; disruption of the photoreceptor segments, retinal atrophy, and different types of retinal flecks (Adhi et al., 2015, Ergun et al., 2005, Ritter et al., 2013). Furthermore, it could recognize childhood-onset Stargardt disease by demonstrating hyperreflectivity at the base of the foveal outer nuclear layer before symptoms are noticed (Khan et al., 2018). Optical coherence tomography angiography (OCTA) could also help analyze the retinal vascular network and retina changes noninvasively; thinning of retinal layers together with the alterations of the vascular network could be observed in OCTA (Arrigo et al., 2019).

Another retinal disorder that is highly related to lipofuscin accumulation is dry age-related macular degeneration (AMD). AMD is the leading cause of impaired visual acuity and even blindness in the elderly group (Nowak, 2006, Ramkumar et al., 2010). In 2020, its global prevalence is estimated to be 200 million (Stahl, 2020, Wong et al., 2014). Clinically, AMD Patients often complain of either acute or insidious vision loss accompanied by vision deformity if macular is involved (Stahl, 2020). Dry AMD, also known as nonexudative AMD, is

characterized by lipofuscin accumulation, drusen formation, and RPE degeneration (Bandello et al., 2017, Ramkumar et al., 2010). So far, the mechanisms of drusen development and macular atrophy lesions in dry AMD have not been thoroughly studied. The accumulation of cytotoxic pigment lipofuscin is shown to be related to RPE degeneration and cell death (Pan et al., 2021, Abalem et al., 2019).

For diagnosis, dilated fundus examination should be conducted for signs such as drusen deposits, hemorrhage, exudate, and other changes (Thomas et al., 2021). OCT is important for the evaluation of macular in AMD patients, it helps to distinguish between wet and dry AMD and characterize AMD stage (Thomas et al., 2021). FA is the gold standard for conforming pathologic blood vessels (choroidal neovascularization) in AMD (Thomas et al., 2021, Stahl, 2020). OCTA also assists the investigation of the vascular network of the retina and choroid as a noninvasive tool which is replacing the traditional FA gradually (Thomas et al., 2021).

1.2 ABCA4 gene mutation and animal models

Variants in the ABCA4 gene are known to be responsible for several phenotypic patterns of hereditary retinopathy including Stargardt disease and cone-rod dystrophy (Allikmets et al., 1997, Cremers et al., 1998). To date, more than 1000 disease-causing variations in the ABCA4 gene have been discovered and the number is still getting bigger (Cremers et al., 2020). This gene encodes ATP-binding cassette transporter protein, which flips N-retinylidene-phosphatidylethanolamine (N-Ret-PE) out of the intradiscal space into the cytoplasmic surface of disc membranes (Quazi and Molday, 2014, Lenis et al., 2018, Westerfeld and Mukai, 2008). It is a part of the visual cycle. It is possible that the link between all-trans-retinal and phosphatidylethanolamine (PE) will be broken during this process. As a result, all-trans-retinal is converted to all-trans-retinol and transported to the RPE. It is eventually converted back to 11-cis retinal (Westerfeld and Mukai, 2008). By doing so, removal of all-trans-retinal and 11-cis-retinal is accomplished. Hence, impaired ABCA4 function could lead to accumulation of N-ret-PE, then generate the formation of N-retinylidene-N-retinyl-ethanolamine (A2E) and other bisretinoids, also known as lipofuscin

(Yamamoto et al., 2012, Sparrow and Boulton, 2005, Molday, 2007, Sparrow et al., 2000, Sparrow et al., 2012). The excessive A2E formation causes RPE cell dysfunction and subsequent degeneration of photoreceptors and RPE, and RPE cell death eventually resulting in vision loss (Pan et al., 2021, Taubitz et al., 2018).

Abca4$^{-/-}$ *mice* were generated for the Stargardt disease animal model and for lipofuscin genesis in general (Weng et al., 1999, Taubitz et al., 2018). Pigmented *Abca4*$^{-/-}$ mouse is the first Stargardt disease animal model that is bred on a 129 background (Fang et al., 2020, Taubitz et al., 2018). This model has been widely used as it exhibits a number of typical Stargardt pathological alterations that helps the understanding of this pathological process, including an accelerated deposition of lipofuscin granules in the RPE, delayed dark adaption and so on (Weng et al., 1999, Charbel Issa et al., 2013). However, this model has its own limitations, such as the lack of macula and the absence of retinal degeneration (Charbel Issa et al., 2013). Because of the lacking retinal degeneration, this model is known as an early-stage Stargardt model. A second animal model is the albino *Abca4*$^{-/-}$ mouse, it was generated with a BALB/c genetic background (Radu et al., 2004, Wu et al., 2010). Compared to pigmented *Abca4*$^{-/-}$ mouse, albino *Abca4*$^{-/-}$ mouse exhibits retinal degeneration and loss of photoreceptor nuclei (Radu et al., 2008, Wu et al., 2010, Taubitz et al., 2018). A third model is the pigmented *Abca4*$^{-/-}$*Rdh8*$^{-/-}$ mouse strain, which is generated by the hybrid of *Abca4*$^{-/-}$ mice and *Rdh8*$^{-/-}$ mice with a mixed 129.B6 background (Maeda et al., 2008, Taubitz et al., 2018). In this model, regional retinal degeneration, reduced thickness of the photoreceptor layer, and formation of rosette and drusen were detected (Maeda et al., 2008, Taubitz et al., 2018).

1.3 Pigment granules in RPE cell

1.3.1 Melanin

RPE is a monolayer of cuboidal cells located between the photoreceptors and choriocapillaris that is comprised of three major pigments: lipofuscin, melanosomes, and melanolipofuscin (MLF). Melanin is known to be photoprotective against phototoxic and oxidative stress in the RPE (Boulton and

Dayhaw-Barker, 2001, Hu et al., 2008). It can protect the photoreceptors and RPE from photooxidative damage by acting as a physical photo-screen directly and by absorbing light and scavenging free radicals (Feeney-Burns, 1980, Seagle et al., 2005, Kennedy et al., 1995, Feeney-Burns et al., 1984, Hu et al., 2008). During aging, the oxidized melanosomes turn into pro-oxidants that can be phototoxic to human RPE cells and cause RPE dysfunction (Rózanowski et al., 2008b, Rózanowski et al., 2008a, Rózanowska et al., 2002, Dayhaw-Barker et al., 2001). This change is related to the RPE especially. Whereas skin and choroidal melanocytes could renew the melanosomes because of the continuous tyrosinase expression, the key enzyme of melanogenesis, melanosomes in the RPE were assumed to only form during the embryonic period, it is still unclear whether melanin turn-over in the RPE also happens in adult life (Sarna, 1992, Feeney, 1978, Taubitz et al., 2019, Schraermeyer and Heimann, 1999). Premelanosomes were identified in the retina on rare occasions, implying a probably delayed turnover of melanosomes in adult RPE, though not to a substantial degree (Dorey et al., 1990, Schraermeyer, 1992). However, this idea is controversial (Hu et al., 2008). Orlow et al proposed that melanosomes are specialized lysosomes for that melanosomes share several features with lysosomes (Orlow, 1995).

Melanin acts like an energy transducer that could participate in electron transfer reactions. It can transform different forms of energy into electrical energy or heat (Hill, 1992). Melanin could not only absorb superoxide radicals, but it could also generate radicals (Hill, 1992). It was reported that the melanotic fungal species could even live in the high-radiation environment caused by the damaged reactor at Chernobyl and could use the radiation for better growth (Kothamasi et al., 2019, Casadevall et al., 2017). Melanin also has stable free radicals trapped in itself; Melanin is able to take part in redox reactions because of these radicals (Godechal and Gallez, 2011). The intrinsic free radical inside melanin could be a good indicator of melanin integrity, which also decreases during aging (Rózanowski et al., 2008b).

Near-infrared AF (NIR-AF) (excitation 787 nm, emission>800 nm) was developed for the ocular melanin investigation (Keilhauer and Delori, 2006). It

has been an effective way for researchers to study the age-related RPE changes and allows clinicians to monitor ocular diseases including Stargardt disease and AMD (Greenstein et al., 2015, Duncker et al., 2014, Battaglia Parodi et al., 2020). Taubitz et al (Taubitz et al., 2019) showed that NIR-AF of RPE and choroidal melanosomes increases with oxidative stress and age, they suggested that rather than an intrinsic property of melanin, NIR-AF should be regarded as aged or oxidized melanin marker.

Evidence stresses the protective role of melanin in reducing lipofuscin buildup in the RPE cells. The concentrations of RPE lipofuscin and RPE melanin were found to be inversely related (Weiter et al., 1986). Greenberg et al reported that fundus autofluorescence, which is primarily caused by lipofuscin, was significantly higher in whites and lower in blacks and Asians when compared to Hispanics (Greenberg et al., 2013). According to a meta-analysis performed by Jin et al, both early and late AMD were less frequent in Chinese communities globally among those aged 50 and over, compared to Caucasian populations (Jin et al., 2019). Within the 1500 microm central macular zone, white participants were substantially more likely to develop big drusen and focal pigmentation than blacks, as well as to proceed from medium-to-large-sized drusen or pigment abnormalities (Chang et al., 2008). Bressler et al had similar results, they added that black individuals may have a central zone defense mechanism against important fundus features like large drusen, and focal pigment abnormalities (Bressler et al., 2008). White people were more likely to have AMD than black people. AMD was found in 2.1 percent of white people over the age of 70 while no cases of AMD were found among the 243 black subjects in the same age range (Friedman et al., 1999). Sarna et al reported that RPE melanin content decreased 2.5-fold between the first and the ninth decade of human life (Sarna et al., 2003), one of the main explanations for this decline, according to Dontsov et al, is melanin degradation in melanolipofuscin granules caused by superoxide radicals created during photoinduced oxygen reduction by lipofuscin fluorophores (Dontsov et al., 2017).

Besides, *Abca4*$^{-/-}$ mice accumulate lipofuscin more rapidly and only develop retinal degeneration in albino strains compared to pigmented strains (Wu et al.,

2010, Radu et al., 2011, Taubitz et al., 2018), implying that connection with melanin is a positive response. Taubitz et al described the vacuole structures filled with membranous material in the albino *Abca4*$^{-/-}$ mice, this structure can be barely seen in the pigmented *Abca4*$^{-/-}$ mice (Taubitz et al., 2018). It is possible that these differences are related to melanin. The vacuole-like structure will be further discussed in this study.

1.3.2 Lipofuscin

In the human eye, aging is accompanied by the accumulation of lipofuscin granules, which is a hallmark of aged RPE and is associated with Stargardt disease and AMD (Julien-Schraermeyer et al., 2020). Lipofuscin, a highly fluorescent substance, accumulates not only in the RPE but also in several tissues, especially in metabolically active postmitotic cells (Boulton et al., 2004, Terman and Brunk, 2004). In many cells, lipofuscin originates from autophagocytosed cellular components. In terms of RPE cells, the accumulation of the age pigment-lipofuscin granules derives partially from the incomplete degradation residues of phagocytized photoreceptor outer segments (Kennedy et al., 1995, Sparrow and Boulton, 2005, Zhang et al., 2019). In RPE cells, lipofuscin contains lipid, protein and fluorescent compounds, but majority of its composition is still unclear (Kennedy et al., 1995, Ng et al., 2008). Bisretinoids is one of the components of lipofuscin, the most extensively characterized among which is A2E (Călin et al., 2021, Boyer et al., 2012, Adler et al., 2015).

Despite extensive investigations, the mechanism through which lipofuscin impairs RPE function remains unknown. Excessive deposition of this substance has been linked to retinal aging and macular degeneration (Taubitz et al., 2018, Sparrow et al., 2012). Lipofuscin fluorophores can produce reactive oxygen species when exposed to blue light; it has also been hypothesized that photooxidative processes mediated by these lipofuscin fluorophores cause chronic oxidative stress in the RPE (Dontsov et al., 2022). Even at low concentrations, A2E can cause RPE cell death (Mihai and Washington, 2014). According to Zhou et al, after photoactivation and cleavage, bisretinoids pigments of RPE serve to activate complement thus leading to chronic inflammation (Zhou et al., 2009). Lipofuscin is also able to inhibit enzyme

activity (Wassell et al., 1999). Lipofuscin clumps in lysosomes, causing lysosomal membrane permeabilization and aberrant necroptosis, as shown by Pan et al (Pan et al., 2021). Because of lipofuscin's cytotoxic effects, lifelong acquired RPE lipofuscin is hypothesized to play a role in the development and progression of AMD and Stargardt disease (Fang et al., 2022). Lipofuscin accumulation reversal could be an appealing therapeutic strategy, it might significantly improve visual quality.

For decades, one of the most widely held beliefs has been that lipofuscin cannot be degraded by enzymes (Boulton et al., 2004, Terman and Brunk, 2004, Ueda et al., 2016). However, retinal reactions are unavoidable and occur in both young and healthy people. The absence of lipofuscin production in these individuals suggests that some bisretinoid degradation may occur. Likewise, whereas lipofuscin chemistry develops earlier and more extensively in Stargardt patients than in normal aging (Charbel Issa et al., 2013), they have had normal eye function for years before the visual acuity declines. Again, this points to a mechanism for degrading lipofuscin, which decreases with age and is overwhelmed more rapidly in Stargardt disease. Studies have shown that the lipofuscin can be degraded after treatment with superoxide radical generators ($O_2^{\bullet-}$) (will be reviewed in **1.5**).

Short wavelength AF (SW-AF, excitation 488 nm, emission > 500 nm) gives valuable information to monitor lipofuscin in the RPE, it may be used as a diagnostic and monitoring tool by measuring the amount of lipofuscin in the RPE cells in both clinical practice and experimental studies (Schmitz-Valckenberg et al., 2008, Taubitz et al., 2019). Another ocular lipofuscin analysis method is high-performance liquid chromatography (HPLC) quantitation, including collecting granules from homogenized RPE tissue, extracting, and measuring (Sparrow et al., 2013).

1.3.3 Melanolipofuscin

The formation and aggregation of melanolipofuscin (MLF) granules also indicate the decrease in lipofuscin degradation ability. MLF is a complex granule that combines the features of melanosome and lipofuscin granules (Figure.1). In the RPE of aged human eyes, Stargardt patients, and Stargardt mice,

melanolipofuscin is prominent (Taubitz et al., 2018, Fang et al., 2020, Taubitz et al., 2019); it may play a role in the genesis of AMD (Warburton et al., 2007). According to Feeney-Burns, MLF accumulation more accurately represents the start of AMD than lipofuscin (Feeney-Burns et al., 1984).

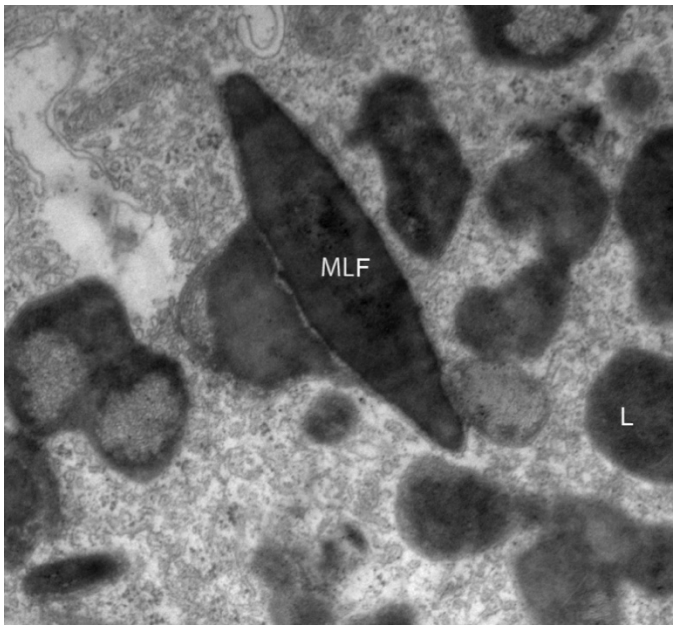

Figure 1. Melanolipofuscin Structure under EM.

Melanolippofuscin overserved in 2-year-old pigmented *Abca4*$^{-/-}$ mouse. MLF, Melanolipofuscin; L, Lipofuscin.

The underlying mechanism of MLF formation is yet not clarified. Warburton et al (Warburton et al., 2007) suggested that MLF, unlike Lipofuscin, lacks photoreceptor-specific proteins, implying that MLF does not arise from phagocytosis of photoreceptor outer segments as Lipofuscin does, or from the fusion of melanosomes with lipofuscin. The presence of RPE and melanosome-specific proteins, on the other hand, indicates that MLF is accumulated as a result of autophagocytosis by the melanosome (Warburton et al., 2007). Schraermeyer et al (Schraermeyer et al., 1999) suggested that melanosomes are involved in lysosome-like degradation of photoreceptor outer segments; by the injection of gold-labeled rod outer segments into the retina, the gold particles were detected later in the space between the limiting membrane and melanin granule matrix. The hypothesis is that the undegradable substances related to photoreceptor disc membranes may be transferred from RPE

phagosomes to melanosomes and stay there after other disc membrane-derived components have been digested (Schraermeyer et al., 1999).

1.4 Current Treatment for lipofuscin-related diseases

So far, there is no approved therapy for Stargardt disease or dry AMD. Efforts are made for searching potential therapeutic strategies for both disorders, stem cell replacement, compound administration, and gene therapy are a few examples.

1.4.1 Pharmacological therapy

Multiple pharmacological clinical trials have been studied in humans or are presently being tested in humans regarding Stargardt disease or dry AMD, 16 trials were summarized in table 1 (nine of them were from Cremers et al's review) (Cremers et al., 2020). Trials that were suspended, terminated, or withdrawn were not taken into consideration. Because the buildup of lipofuscin is the principal problem in this disease, many therapies are aimed at lowering the synthesis, build-up, and removal of lipofuscin in the retina. Remofuscin was reported to be capable of removing lipofuscin from monkey RPE after oral administration (Julien and Schraermeyer, 2012). Remofuscin could reverse lipofuscin formation in aged primary human RPE cells and showed non-cytotoxicity in elderly Stargardt disease mice RPE cells in vitro, according to the same research group (Fang et al., 2022). In the mouse model of advanced Stargardt disease, removing lipofuscin following a single intravitreal injection of Remofuscin even leads to rescue from retinal degeneration and an improvement in retinal functioning (Fang et al., 2022). The phase II clinical trial is now underway to determine the safety and efficacy of oral Remofuscin (EudraCT 2018-001496-20) (Fang et al., 2022).

Medication ALK-001, a deuterated form of vitamin A, is currently being tested in a phase II clinical trial (ClinicalTrials.gov NCT02402660) (Cremers et al., 2020, Sears et al., 2017). Charbel Issa et al demonstrated that vitamin A's propensity to dimerize is responsible for the bulk of lipofuscin accumulation, by substituting vitamin A with C20-D3-retinyl acetate (ALK-001), vitamin A dimerization and subsequent lipofuscinogenesis is slowed down (Charbel Issa et al., 2015). Retinol-binding protein 4 is a serum protein that transports Vitamin A, the

inhibition of retinol-binding protein 4 is thought to be a relatively safe strategy to reduce vitamin A delivery to the retina (MATA et al., 2013, Kim and Priefer, 2021). Tinlarebant and STG-001 (Stargazer) are two retinol-binding protein 4 antagonists that are currently being studied in clinical trials (ClinicalTrials.gov NCT05266014, NCT05244304, NCT04489511).

The RPE-specific 65 kDa retinoid isomerase (RPE65) is the rate-limiting enzyme in the visual cycle, converting all-trans-retinyl esters to 11-cis-retinol, the discovery of RPE65's molecular structure enabled the development of particular inhibitors-emixustat (ACU-4429) that slows the visual cycle and therefore the synthesis of all-trans-retinal (Sears et al., 2017, KUBOTA et al., 2014). The clinical trial conducted by Kubota et al confirmed emixustat's biological activity in Stargardt by demonstrating demonstrated dose-dependent reduction of rod b-wave amplitude recovery postphotobleaching (ClinicalTrials.gov NCT03033108) (Kubota et al., 2022).

Another potential drug is Zimura, which targets on complement system by inhibiting complement factor C5. The results of a pivotal phase 2/3 clinical trial revealed that the intravitreal injection of Zimura reduced geographic atrophy development significantly in AMD eyes (ClinicalTrials.gov NCT02686658) (Jaffe et al., 2021). Another trial is being carried out to assess the safety and efficacy of Zimura in Stargardt disease (ClinicalTrials.gov NCT03364153).

Three months of omega-3 fatty acid supplementation lowers A2E levels, lipofuscin granules, and C3 levels in the *Abca4*$^{-/-}$ Stargardt disease animal model, according to Prokopiou et al (Prokopiou et al., 2018). However, no improvement of docosahexaenoic acid (DHA) supplementation on macular function was found in an clinical trial with 11 Stargardt patients (ClinicalTrials.gov NCT00060749) (MacDonald and Sieving, 2018).

Saffron, a potential antioxidant, did not appear to provide any substantial improvement in visual function in the short term as reported by Piccardi et al (ClinicalTrials.gov NCT01278277) (Piccardi et al., 2019). The prospective therapeutic efficacy of 4-methylpyrazole was called into question because it did not have an effect on dark adaptation (Jurgensmeier et al., 2007). Additionally, metformin, a medicine for diabetes is also being investigated in a clinical trial for

ABCA4 retinopathy (ClinicalTrials.gov NCT04545736). In trials for AMD, fenretinide failed to slow the course of geographic atrophy or enhance vision (Hussain et al., 2018).

Table 1. Registered clinical trials of Compound administration for ABCA4-associated retinopathy.

Adapted from (Cremers et al., 2020) (9 trials were listed by Cremers et al).

ClinicalTrials.gov Identifier	Intervention	Phase	Recruitment Status
NCT00429936	Fenretinide	Phase 2	Completed
NCT04545736	Metformin	Phase 1/2	Recruiting
NCT05266014	Tinlarebant	Phase 1/2	Active, not recruiting
NCT05244304	Tinlarebant	Phase 3	Recruiting
NCT04489511	STG-001 (Stargazer)	Phase 2	Completed
NCT00346853	4-Methylpyrazole (alcohol dehydrogenase inhibitor)	Phase 1	Completed
NCT04239625	ALK-001 (chemically modified vitamin A)	Phase 2	Enrolling by invitation
NCT02402660	ALK-001 (chemically modified vitamin A)	Phase 2	Recruiting
NCT00060749	DHA (omega-3 fatty acid)	Phase 1	Completed
NCT03033108	Emixustat (inhibitor of *RPE65*)	Phase 2	Completed
NCT03772665	Emixustat (inhibitor of RPE65)	Phase 3	Active, not recruiting
NCT03297515	Madeos (omega-3 fatty acid)	Not available	Completed
NCT01278277	Saffron (neuroprotectant)	Phase 1/2	Unknown
2018-001496-20	Soraprazan (Remofuscin)	Phase 2	Active
NCT03364153	Zimura (inhibitor of complement factor C5)	Phase 2	Recruiting

NCT02686658	Zimura (inhibitor of complement factor C5)	Phase 2/3	Completed

1.4.2 Stem cell replacement therapy

Stem cell replacement therapies are also been investigated as a treatment option for restoring impaired RPE function caused by lipofuscin accumulation. Stem cells originating vary from bone marrow-derived cells to human embryonic stem cells (hESCs) have been studied or are undergoing clinical trials (Cremers et al., 2020). Although some studies were reported to be effective, giving RPE cells (or cells destined to become RPE) will most likely have little long-term benefit because ABCA4 is mainly expressed in photoreceptors (Cremers et al., 2020).

1.4.3 Gene therapy

Since ABCA4 gene mutations have been linked to autosomal recessive Stargardt disease, gene therapies were used. Adeno-associated virus(AAV) vectors have been widely used in the delivery of therapeutic transgenes. However, although the attempt to package a large AAV transgene containing the entire ABCA4 (human ABCA4 cDNA is around 7 kb) coding region yielded promising results, it is difficult to create homogeneous AAV preparations containing designated transgenes consistently (Piotter et al., 2021, Auricchio et al., 2015). Lentiviral vectors are another possibility due to their 8 kb packaging capacity, which allows them to carry even the longest coding sequences (Semple-Rowland and Berry, 2014). A Phase 1/2 clinical trial of lentivirus vector-based gene therapy was done to deliver the ABCA4 gene via subretinal injection of the lentivirus vector (ClinicalTrials.gov NCT01367444). This trial was terminated based on the Sponsor's decision. No results from this trial were revealed. Due to the limitation of viral vectors outlined, nanoparticles provide an alternate carrier for bigger transgenes. According to Sun et al, subretinal gene therapy with ECO/pRHO–ABCA4 and ECO/pRHO–ABCA4–SV40 nanoparticles reduced A2E accumulation in *Abca4*$^{-/-}$ mice (Sun et al., 2021). Anti-sense oligonucleotides, small single-stranded fragments of artificial nucleotides which operate as RNA modulators, are also an option for gene therapy towards ABCA4 variants (Piotter et al., 2021, Albert et al., 2018).

1.5 Lipofuscin can be degraded by radicals generators

Ueda et al reported that bisretinoids photodegradation occurred in the eye, by using HPLC analysis of the mouse eyes after being exposed to different light conditions, they revealed a link between light and lower levels of the bisretinoids (Ueda et al., 2016). Lipofuscin is a photoinducible generator of superoxide anion, singlet oxygen, and hydrogen peroxide (Yamamoto et al., 2011, Ueda et al., 2016, Sparrow and Boulton, 2005). Those reactive forms of oxygen then will quench and photo oxidize bisretinoids (Wu et al., 2010). Fang et al showed that the mechanism causing lipofuscin degradation in Remofuscin treatment may involve reactive oxygen species generated by Remofuscin (Fang et al., 2022). Riboflavin , a superoxide generator, removed lipofuscin from the RPE of *Abca4*$^{-/-}$ mice (Schraermeyer U, 2019). Horseradish peroxidase has also been shown to cleave the RPE bisretinoid A2E (Wu et al., 2011). All these findings could point to a direct superoxide radical (O2•-) route for lipofuscin degradation. Phagosomes provide one of the most critical roles of the RPE, which is to ingest and digest shed photoreceptor membranes already containing bisretinoids (Feeney-Burns and Eldred, 1983). During disc outer segments phagocytosis, a variety of radicals including superoxide, hydroxyl radicals, and hydrogen peroxide (H_2O_2) are formed (Miceli et al., 1994). Because radicals are able to degrade bisretinoids (Wu et al., 2011, Kim et al., 2008), part of bisretinoids clearance may occur during phagocytosis.

Premi et al reported that superoxide and nitric oxide (NO•), when combined to create peroxynitrite (ONOO-), react with melanin to excite melanin electrons to a high energy state that is capable of chemical reactions (Premi et al., 2015). The laboratory production of bisretinoids needs two such high-energy stages, sigmatropic processes (Parish et al., 1998); This could be reversed by excited states created by melanin chemical reactions driven by superoxide and nitric oxide radicals.

1.6 Aim of the study

To test whether RPE melanin is required for a photoreceptor disc turnover mechanism and whether reagents that generate radicals enhance this pathway, unique thin lamellar membranes (TLMs) that resemble photoreceptors disc

remnants are investigated and effects of radicals generators are compared between pigmented and albino *Abca4*$^{-/-}$ mice.

2. Materials and Method

2.1 Reagents

Three different radical generators were used in this study. 3-morpholinosydnonimine(SIN-1), which spontaneously generate nitric oxide (NO•) and superoxide anion (Hogg et al., 1992), was obtained from Focus Biomolecules (Plymouth Meeting, PA USA). SIN-1 decomposes in the aqueous solution, releasing superoxide anion and NO•, which quickly combine to create peroxynitrite (ONOO-) (An et al., 2015). It's possible that SIN-1 also generates extremely reactive free radicals including nitrogen dioxide and carbonate radicals (Ho et al., 2012). Isosorbide dinitrate (ISDN), a medication for heart attack for more than 30 years as a nitric oxide donor (Schaumann, 1989, Blair, 2021), was ordered from Merus Labs Luxco II S.A R.L. (Grand Duchy Of Luxembourg). Horseradish peroxidase was purchased from Sigma-Aldrich (Darmstadt, Deutschland).

2.2 Mice

All experiments concerning animals were approved by the local animal welfare organization (Einrichtung für Tierschutz, Tierärztlichen Dienst und Labortierkunde der Eberhard Karls Universität Tübingen, Tuebingen, Germany) and local authorities (Regierungspräsidium Tübingen, Tuebingen, Germany) (authorization number: AK1/16). Pigmented *Abca4*$^{-/-}$ mice (129S4/SvJae-Abca4tm1Ght) were purchased from Charles River (Sulzfeld, Germany). Albino *Abca4*$^{-/-}$ mice (BALB/c-Abca4tm1Ght) were graciously given by R. Radu (University of California, Los Angeles, CA). All strains were bred in-house under a 12h lights (about 50 lx in cages)/12h dark cycle with ad libitum food and water (Lyu et al., 2022).

2.3 Generation of Ad-Tyr

The human tyrosinase cDNA is introduced into the adenoviral vector Ad-Tyr. It was generated using the published protocol (Julien et al., 2007).

2.4 Subretinal injection of Ad-Tyr

To test the melanin hypothesis, albino *Abca4*$^{-/-}$ mice, 3-4 months old, were used

for introducing melanogenesis. Isoflurane (Isoflurane CP®, CP-Pharma, Germany) inhalation (3.5% isoflurane and 25% oxygen) was used to anesthetize the mice. Pupils then were dilated using tropicamide (Pharmacy of the University of Tuebingen, Germany). To avoid corneal dryness, Methocel 2% (OmniVision, Puchheim, Germany) was applied. A surgical microscope was used to direct the injections. The injection eye (right) was positioned facing the light and the microscope. 1.5µL adenoviral vector Ad-Tyr (10^8 iu/ µl) per eye was used for injection. The position of the eyeball was modified by gently pushing on the conjunctiva with tweezers. Ad-Tyr was injected into the subretinal space of each mouse's right eye using a 10 µL NanoFil syringe with a 34-gauge needle (World Precision Instruments). The injection was carried out by introducing the syringe tip into the eyes tangentially via the sclera into the subretinal region without injuring the lens or retina (Figure.2). Left eyes stayed untreated. Additionally, the left eye of a few mice was injected with 1.5µl sterile phosphate buffered saline (PBS, Gibco®, Darmstadt, Germany) for comparison. After the operation, antibiotic ointment (GentamicinPOS®, Ursapharm, Saarbruecken, Germany) was used as a routine. Then the fundus in vivo of the mice was checked by customized ophthalmoscopy regularly. Until the funds showed brown-darkish spots, which was after 2 weeks, the fundus autofluorescence images were obtained by confocal scanning laser ophthalmoscopy (cSLO; Spectralis HRA+OCT, Heidelberg Engineering, Heidelberg, Germany). After that, the mice were sacrificed, eyes were enucleated. The timeline of Ad-Tyr injection was demonstrated in Figure.3.

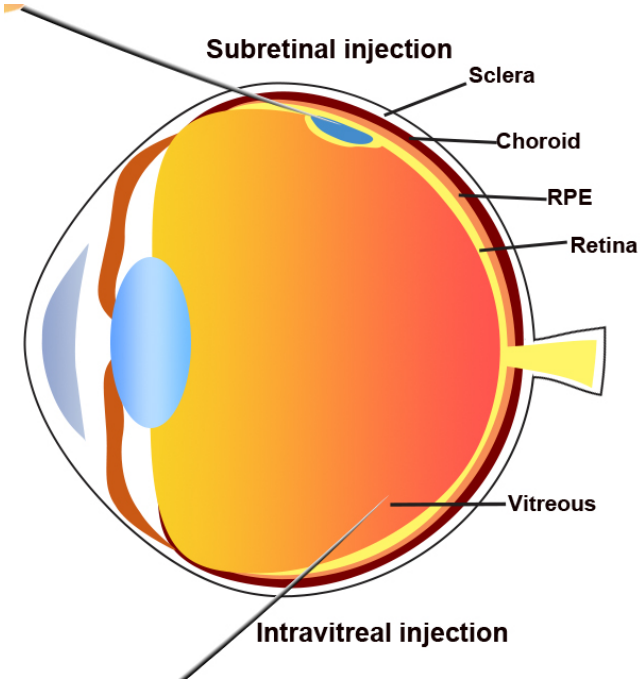

Figure 2. illustration of injection methods.

Subretinal injection, the syringe tip was inserted into the eyes tangentially via the sclera into the subretinal region; Intravitreal injection, the tip of the syringe was inserted into the eyes via the sclera into the vitreous.

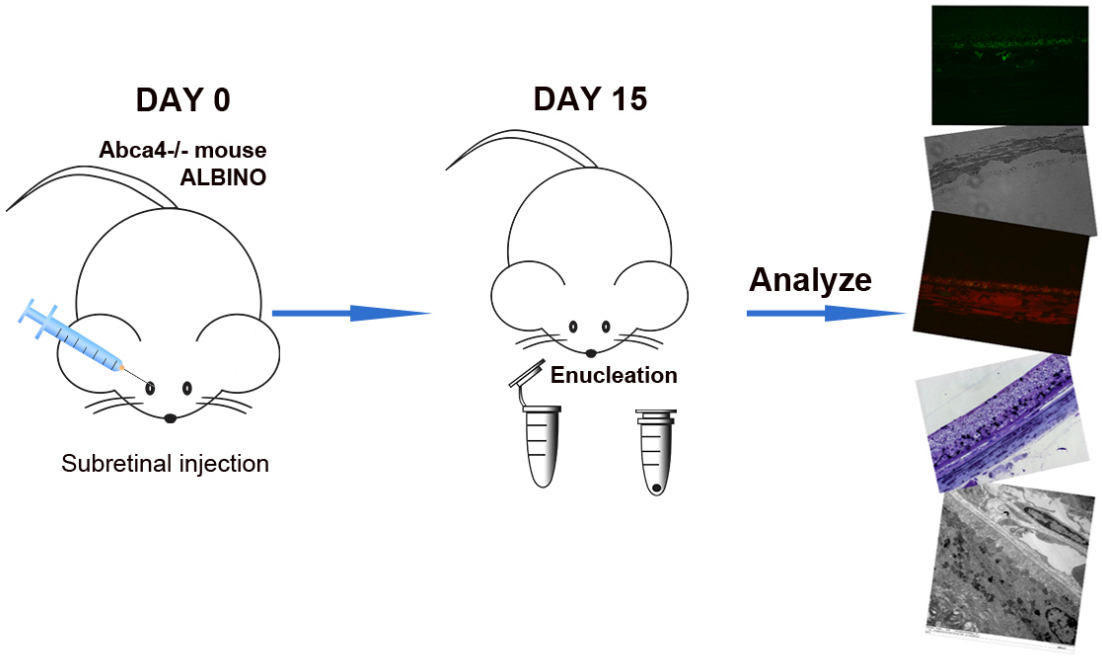

Figure 3. Experimental timeline.

The right eye of the animal was subretinal injected with 1.5μl Ad-Tyr. Two weeks later, the mice were investigated by cSLO to acquire fundus autofluorescence images on

both eyes. After cSLO, the mice were sacrificed, and the eyes were enucleated for histological analysis.

2.5 Intravitreal injection of radical generators

Pigmented *Abca4*$^{-/-}$ mice and albino *Abca4*$^{-/-}$ mice were used in this experiment. For SIN-1 injection, 2-year-old pigmented *Abca4*$^{-/-}$ mice were used. However, because of time limitations, 6 months old albino *Abca4*$^{-/-}$ mice were used instead. For horseradish peroxidase and ISDN treatments, 7 months old pigmented and albino *Abca4*$^{-/-}$ mice were used. SIN-1 was dissolved in sterile PBS to 65µg/µL. Horseradish peroxidase and ISDN were dissolved in PBS to the concentration of 70µg/µL and 40µg/µL respectively. Preoperative preparations were conducted as stated in **2.4**. A 10 µL NanoFil syringe with a 34-gauge needle (World Precision Instruments) was used for intravitreal injection procedure. The tip of the syringe was inserted into the eyes via the sclera into the vitreous without injuring the lens or retina (demonstrated in Figure.2). The right eyes of the first group of the animals were injected with 2µL prepared SIN-1 (pigmented and albino *Abca4*$^{-/-}$ mice). The right eyes of the second group of animals were treated with prepared horseradish peroxidase (pigmented and albino *Abca4*$^{-/-}$ mice). The right eyes of the third group of animals were treated with ISDN (pigmented *Abca4*$^{-/-}$ mice). All left eyes remained untreated. The injected eyes were treated with antibiotic ointment after. 2 days after the mice were sacrificed and eyes were enucleated. The timeline is shown in Figure.4.

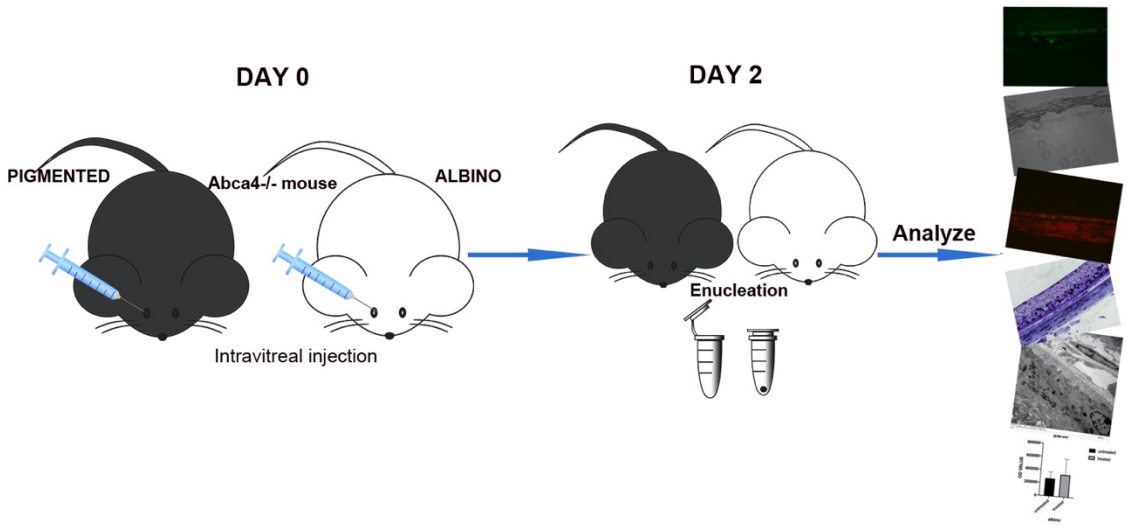

Figure 4: Experimental timeline.

Intravitreal injection of radical generator in the right eye of both pigmented and albino *Abca4*$^{-/-}$ mice, the eyes were enucleated for histological analysis after 2 days.

2.6 Fundus autofluorescence image acquisition

Fundus AF images were acquired using confocal scanning laser ophthalmoscopy before Ad-Tyr treated mice were sacrificed according to the procedure described previously (Fang et al., 2020). The device was installed with a 78-DPT non-contact slit lamp lens (Volk Optical, Inc., Mentor, OH 44060, USA). A custom-manufactured contact lens (100 DPT) was positioned on the cornea of the mouse. Briefly, intraperitoneal narcosis (0.05 mg/kg of fentanyl, 5 mg/kg of midazolam, and 0.5 mg/kg of medetomidine) was used to anesthetize the mice. The animal was then placed on the adjustable three-dimensional operating platform. Methocel and the contact lens were administered to the eye after the pupils had been fully dilated. The near-infrared reflectance (NIR-R) mode was first used to orient the camera and locate the areas of interest. Short-wavelength autofluorescence (SW-AF) (excitation 488 nm) images and near-infrared autofluorescence(NIR-AF) (excitation 788 nm) were recorded at the same time.

2.7 Sample preparation for light, fluorescence, and electron microscopy

Isoflurane inhalation and cervical dislocation were performed to sacrifice the animals. The eyeballs were immediately enucleated, then fixed in 5% glutaraldehyde (AppliChem, Darmstadt, Germany) at 4°C overnight. After removing cornea and lens, the eyecups were cut in half vertically through the optic disc. The eyecups were embedded in Epon using standard procedures (Taubitz et al., 2018). For electron microscopy and light microscopy, the half eyecups with optic nerve were postfixed with 1% Osmium tetraoxide solution (OsO4) (Carl Roth, Karlsruhe, Germany) in 0.1 M cacodylate buffer (pH 7.4) and then stained with saturated uranyl acetate (UAC) (Electron Microscopy Science, Hatfield, USA). For the preparation of fluorescence microscopy with the other halves without optic nerve, post-fixation and heavy metals staining were skipped. Dimethylarisinic acid sodium salt and Ethanol (absolute for analysis EMSURE®) were purchased from Merck (Darmstadt, Germany). Propylenoxid was from Serva (Heidelberg, Germany). The detailed Epon

embedding procedures of fluorescence microscopy and electron microscopy are shown in Table.2 and Table.3 respectively. Glycid ether 100 (53.6%), 2-Dodecenylsuccinic acid anhydride (6.7%), Methylnacid anhydride (38.28 %), and 2,4,6-Tris (dimethyl aminomethyl) phenol (1.5%) were used to make Epon. They were purchased from Serva (Heidelberg, Germany).

Table 2. Fluorescence microscopy embedding procedures.

Procedure	**Reagent**	**time**
Fixation	5% glutaraldehyde in 0.1M cacodylate buffer (Dimethylarisinic acid sodium salt in distilled water) (PH 7.4)	Overnight at 4℃
Washing	0.1M cacodylate buffer *3 times	10 min each
Dehydration	Ethanol 30-50-70%-70%-80%-95%	15 min each
	Absolute ethanol for analysis*2 times	20 min each
Intermedium	Propylenoxid*2 times	20 min each
Resin	Propylenoxid : Epon=1:1	2 h
	Epon	2 h
	Epon	1 h
Polymerization	60℃	48 h

Table 3. Electron microscopy embedding procedures.

Procedure	**Reagent**	**time**
Fixation	5% glutaraldehyde in 0.1M cacodylate buffer (PH 7.4)	Overnight at 4℃
Washing	0.1M cacodylate buffer *3 times	10 min each
Postfixation	1% OsO4	2 h
Washing	0.1M cacodylate buffer *3 times	10 min each
Dehydration	Ethanol 30-50-70%	15 min each
Block staining	Saturated UAC in 70% ethanol	Overnight at 4℃
Dehydration	Ethanol 70%-80%-95%	15 min each
	Absolute ethanol for analysis*2	20 min each

	times	
Intermedium	Propylenoxid*2 times	20 min each
Resin	Propylenoxid : Epon=1:1	2 h
	Epon	2 h
	Epon	1 h
Polymerization	60℃	48 h

The sections were made using Reichert-Jung Ultracut E ultramicrotome (Leica Biosystems, Nussloch, Germany). The choice of the diamond knife depends on the section thickness. Prior to use, the glass slides were coated with 0.01% Poly-L-lysine solution (Sigma-Aldrich, Schnelldorf, Germany). For light microscopy, 500nm semi-thin sections were prepared and stained with toluidine blue. Epon was used as a mounting medium, the slides were put in a 60℃ oven overnight. For electron microscopy, 70nm ultra-thin sections were prepared on formvar-coated grids, and then poststained with lead citrate. Briefly, the post-stain procedure includes putting the grid on a droplet of lead citrate for one minute under the condition that the section side faces the droplet. For fluorescence analysis, 500nm semi-thin sections were prepared and Dako fluorescent mounting media (Dako Omnis, Denmark) was used as a coverslip. Semi-thin sections were first stained with toluidine blue and investigated by light microscopy (Zeiss Axioplan2 imaging, Zeiss, Jena, Germany).

2.8 Electron microscopy investigation

The samples were investigated thoroughly for changes in RPE and choroid by a Zeiss transmission electron microscope (EM) (Zeiss, EM 902, Jena, Germany). To improve the image quality given in the results, brightness and contrast were post-processed.

2.9 Quantification of the area in vacuole-like structures occupied by thin lamellar membranes

Fourteen vacuole-like structures (described by Taubitz et al.) (Taubitz et al., 2018) of 7-month-old albino *Abca4*$^{-/-}$ mice in total were analyzed by Fiji software. Areas of thin lamellar membranes and flocculate residues in the vacuole were determined using the default threshold and normalized to the areas of the vacuole. The result is shown in a pie chart. The thickness of thin lamellar

membranes was measured in electron micrographs at 140000-fold magnification.

2.10 Quantification of the area in the RPE occupied by vacuoles

The total areas of vacuole-like structures were measured and normalized to the length of RPE in 7-month-old pigmented and albino *Abca4*$^{-/-}$ mice. The measurements were conducted with imageSP Software (Minsk, Belarus).

2.11 Quantification of the area in RPE cytoplasm occupied by lipofuscin melanin, and melanolipofuscin

The measurements were performed using Fiji software. Electron microscopy was used to capture images of ultrathin sections through the optic nerve head in order to quantify lipofuscin. Ten electron microscopy images of the RPE with a magnification of 7000 were obtained per eye, beginning at the optic nerve head. Lipofuscins were observed in *Abca4*$^{-/-}$ animals as varied-shaped granules with lower electron density (grey) but darker than the cytoplasm. Melanin granules were distinguished from lipofuscin by their uniform high electron density (black) and spindle, or spherical shapes. Melanolipofuscin is a combination of both.

Among SIN-1 treated pigmented and albino *Abca4*$^{-/-}$ mice, the regions of lipofuscin were quantified in 5 eyes per group. The measurement of the lipofuscin area including the lipofuscin part in the melanolipofuscin granules. The same manner of measurement was performed for melanin quantification. Additionally, I quantified the area of the entire melanolipofuscin granule separately. When I measured the cytoplasm regions, nuclei, microvilli, and basal labyrinth were not included.

2.12 Fluorescence microscopy investigation

Semi-thin samples were investigated by Zeiss Axioplan 2 microscope (Zeiss, Jena, Germany). A custom manufactured lipofuscin filter set (excitation 370/36 nm, emission 575/15) was used for SW-AF, and a commercial Cy7 filter set (excitation 708/75 nm, emission 809/81 nm) was used for NIR-AF, as described previously (Taubitz et al., 2019). Acquisition duration, as well as microscopy and software settings, were kept consistent for any set of samples for the comparison of fluorescence intensity. For the figures given in the results, brightness and contrast were post-processed by IrfanView software for a better

image quality. Image J software was used to merge images.

2.13 Semi-quantitative analysis of fluorescence intensities in the RPE

Whole sections were recorded by fluorescence microscopy for analysis. The measurements were conducted with Fiji software according to published method with modifications (Taubitz et al., 2019). For SW-AF intensity measurements, fluorescence areas were determined by the default threshold, and the integrated optical density (IOD) was measured. To account for the varying lengths of RPE in each image, the IOD was standardized to the length of RPE (pixel) in the corresponding pictures. For NIR-AF intensity measurement, the default threshold was used to determine the areas of interest in the RPE of NIR fluorescence and bright-field (BF) images, area and IOD were measured. The integrated optical density was then normalized to the area of the RPE pigment threshold in corresponding BF images because of varying amounts of pigment granules in the RPE.

2.14 Correlative fluorescence and electron microscopy

This procedure was conducted as described by Taubitz et al with modifications (Taubitz et al., 2019). 300nm thick ultra-thin sections were used to reach the requirements of both fluorescence and electron microscopy. This thickness enables enhanced detection of fluorescence granules compared to standard 70nm ultra-thin sections which are routinely used for electron microscopy, while still thin enough for electron microscopic examination (500nm semi-thin sections are too thick for the electron beam to penetrate). Non-osmicated sections were prepared on formvar-coated mesh grids. Grids were put on glass slides within a water drop, covered by the coverslip, then investigated with BF mode to locate the pigmented area under fluorescence microscopy. Then the areas of interest were investigated under NIR mode. Acquisition times were more prolonged than usual. After investigation, grids needed to be carefully removed from the coverslips with forceps to not destroy the sections. Since sections are fragile and already stressed by being coverslipped, post-staining is likely to cause complete section damage. Therefore, post-staining with lead citrate was operated carefully, then grids were air-dried and investigated by electron microscopy the next day. The lack of heavy-metal staining leads to low contrast,

but melanosomes are still identifiable. This procedure enables the investigation of NIR-AF signals of the pigmented granules. However, due to the section thickness, the NIR-AF signals were not strong enough, and the brightness and contrast of the figure shown in the results were post-processed.

2.15 Statistical analysis

Prism 8 software (GraphPad Software, Inc., La Jolla, CA) and Excel (Microsoft, Inc., Redmond, WA) were used for statistical analyses. To determine whether to use parametric or non-parametric test, all data sets were checked for normal distribution. The student t-test was used for normally distributed data and Mann–Whitney U test was used for non-normally distributed data. A two-tailed test was used in all statistical analyses. The null hypothesis stated that the two groups did not differ statistically, with $p<0.05$ considered statistically significant. The results were presented as Box plot.

3. Results

3.1 Thin lamellar membranes (TLMs) detected in melanolipofuscin granules in the RPE of pigmented *Abca4*$^{-/-}$ mice

Figure.5 and results related to Figure.5 were published on the preprint server bioRxiv (Lyu et al., 2022). The pigmented *Abca4*$^{-/-}$ mice were investigated by high magnification electron microscopy (50000-140000x). Most of the lipofuscin granules fused with melanosomes and formed melanolipofuscin that contains both properties as shown in Figure.5A. Thin membranes with 3-4 nm thickness (black arrowhead) were visible in the lipofuscin part of MLF granules in the form of multiple lamellae (Figure.5A). These TLMs were detected in melanolipofuscin granules in RPE cells regularly, they were also found in endothelial cells of the choriocapillaris (Fig.5B, C). In 140000x magnification, thin membranes surround the residual body within the endothelial cell (arrowheads) (Figure.5C). Besides, TLMs were also found in Bruch's membrane (Figure.6).

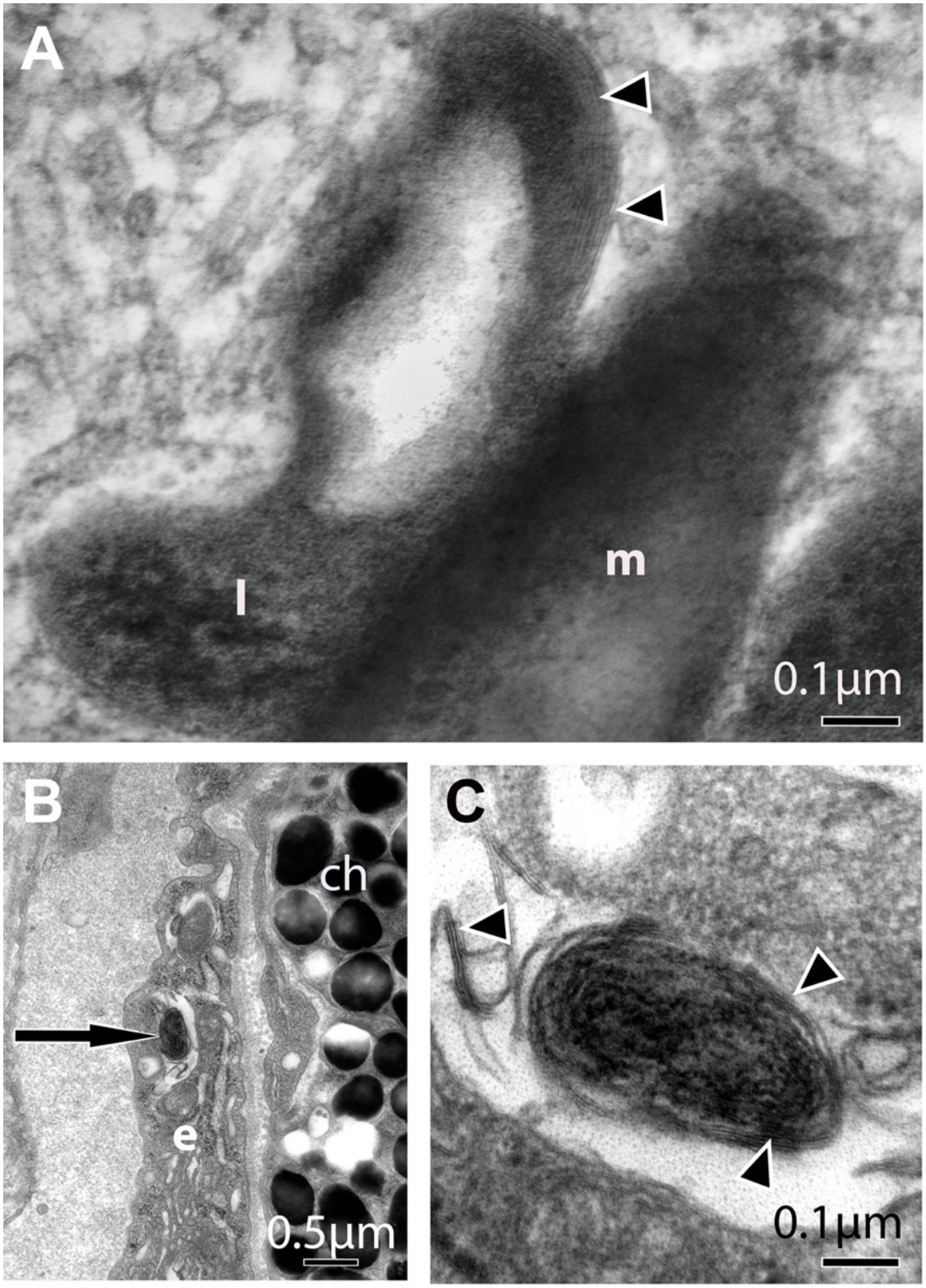

Figure 5. TLMs were detected in melanolipofuscin in pigmented *Abca4*$^{-/-}$ mice by electron microscopy.

(A) MLF granule can be seen in the RPE cytoplasm from a pigmented *Abca4*$^{-/-}$ mouse (50000x). The granule consists of melanin (m) with attached lipofuscin (l) that is less electron-dense than melanin. Thin membranes in the form of lamellae (arrowheads) are visible in the upper region of the lipofuscin portion. (B) TLMs are present in endothelial cells of the choriocapillaris (black arrow). (C) B in 140000x magnification, thin membranes surround the residual body within the endothelial cell (arrowheads). TLMs, thin lamellar membranes; m, melanin; l, lipofuscin; ch, choroidal melanocytes; (Lyu et al., 2022).

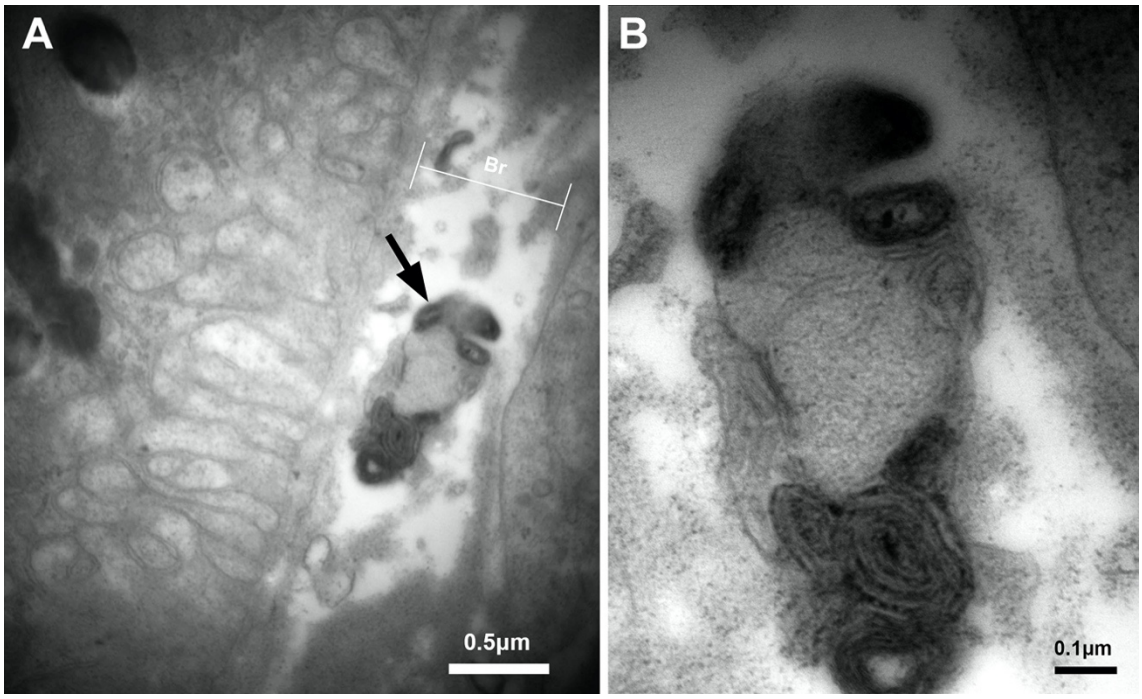

Figure 6. TLMs were detected in Bruch's membrane in pigmented *Abca4*$^{-/-}$ mice by electron microscopy.

(A) Thin lamellar membranes (TLMs) were also detected in the Bruch's membrane by electron microscopy (black arrow). (B) A in 85000x magnification, the fine lamellar structure can be seen. Br, Bruch's membrane; TLMs, thin lamellar membranes.

3.2 TLMs may originate from photoreceptor disc membranes

Figure.7 and results related to it were published on the preprint server bioRxiv (Lyu et al., 2022). TLMs were also identified free in the cytoplasm of RPE (Figure.7A) (black arrowhead). The fine lamellar membranes were detected again in the non-melanin part of melanolipofuscin (Figure.7A) (white arrowhead). The transformation in the MLF from the lipofuscin portion to the more electron-

dense melanin portion is interwoven (Figure.7A). Residual material is associated with the MLF granules and is surrounded by TLMs (Figure.7A) (black arrow). It is unclear whether it is incorporated into or released from the MLF granule, but the latter is more likely given the presence of such structures in the endothelium and circulation. The original photoreceptor disc membranes have fused inside phagosomes (Figure.7B) (white arrowhead), and they seem to be thinner and condensed under higher magnification (Figure.7C). This structure is similar to the TLMs found in the cytoplasm of RPE (Figure.7A) and endothelial cells (Figure.5B). For comparison, the relative sizes of the membranes of the original photoreceptor disc membranes and condensed TLMs from an albino *Abca4*$^{-/-}$ animal RPE vacuole are shown in Figure.7D under the same magnification.

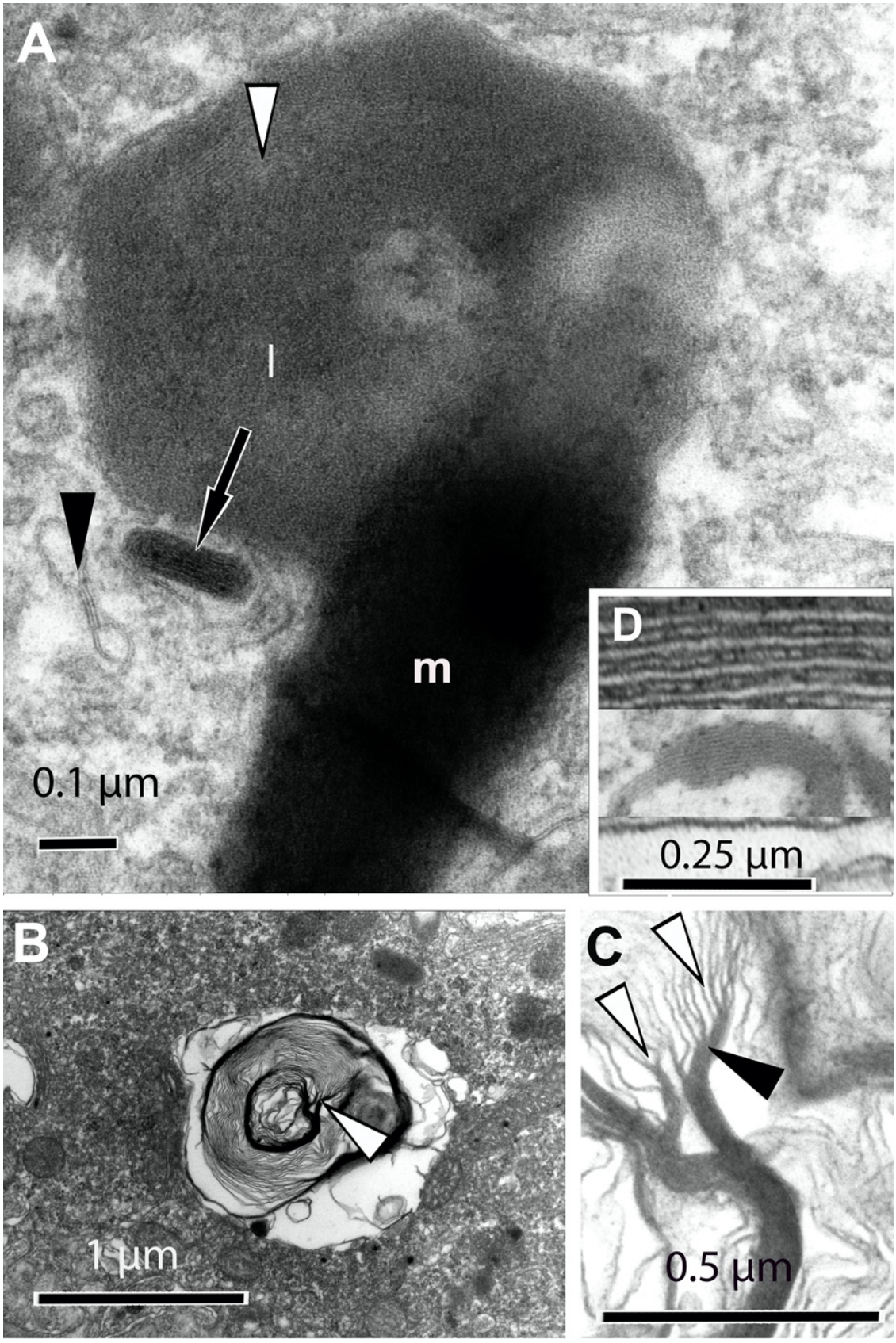

Figure 7. TLMs may originate from photoreceptor disc membranes.

(A) MLF granule in the RPE of pigmented *Abca4*$^{-/-}$ mouse under electron microscopy (50000x). The granule consists of melanin (m) with attached lipofuscin-like (l) material which is less electron-dense than the melanin. Although the lipofuscin content appears to be more homogenous, TLMs are still visible (white arrowhead). The transformation in the MLF from lipofuscin to the more electron-dense melanin is interwoven. TLMs were also detected free in the cytoplasm of RPE (black arrowhead). Residual material that shares the same features with the residual body in the endothelium (Figure.5B) can be seen associated with the MLF granules and is surrounded by TLMs (black arrow). (B) Phagosome with electron-dense membranes in the RPE of an albino *Abca4*$^{-/-}$ mouse (arrowhead). (C) Higher magnification of B marked with a white arrowhead. The original photoreceptor disk membranes (white arrowhead) are fused together (black arrowhead), and their structures are similar to the TLMs shown in Figure.5 and Figure.7A morphologically. (D) The relative sizes of the membranes of the original photoreceptor disc and condensed TLMs from an albino *Abca4*$^{-/-}$ animal are presented under the same magnification (50000x). TLMs, thin lamellar membranes; m, melanin; l, lipofuscin; (Lyu et al., 2022).

3.3 TLMs primarily accumulate in the vacuoles in the RPE of albino *Abca4*$^{-/-}$ mice

Figure.9, Figure.10B, and results related were published on the preprint server bioRxiv (Lyu et al., 2022). Under light microscopy, vacuole-like structures are regularly seen in the RPE of albino *Abca4*$^{-/-}$ mice (Figure.8). When investigated under electron microscopy, they are full of various heterogeneous materials including TLMs that are either electron-dense or opaque and flocculate residues (Figure.9A, B). These vacuole-like structures contain limiting membranes that are frequently partial or lacking, separating them from the cytoplasm (Figure.9B). 60% of the vacuole-like structures are occupied by the TLMs and flocculate residues (Figure.10A). Albinos have significantly more vacuole-like structures in the RPE than pigmented *Abca4*$^{-/-}$ mice (Figure.10B) (n=5 eyes/group, **$p<0.01$, unpaired t-test).

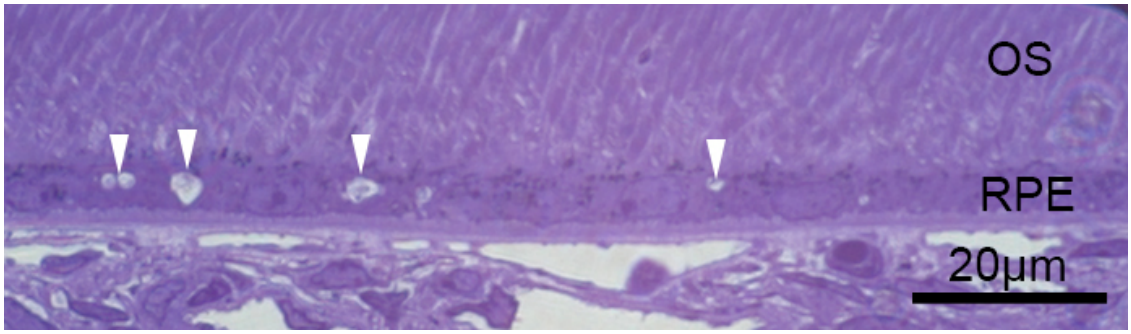

Figure 8. Vacuole-like structures in albino *Abca4*$^{-/-}$ mice under light microscopy. Under light microscopy, vacuole-like structures (white arrowheads) can be seen often in the RPE of albino *Abca4*$^{-/-}$ mice (6 months). OS, outer segments; RPE, retinal pigment epithelium.

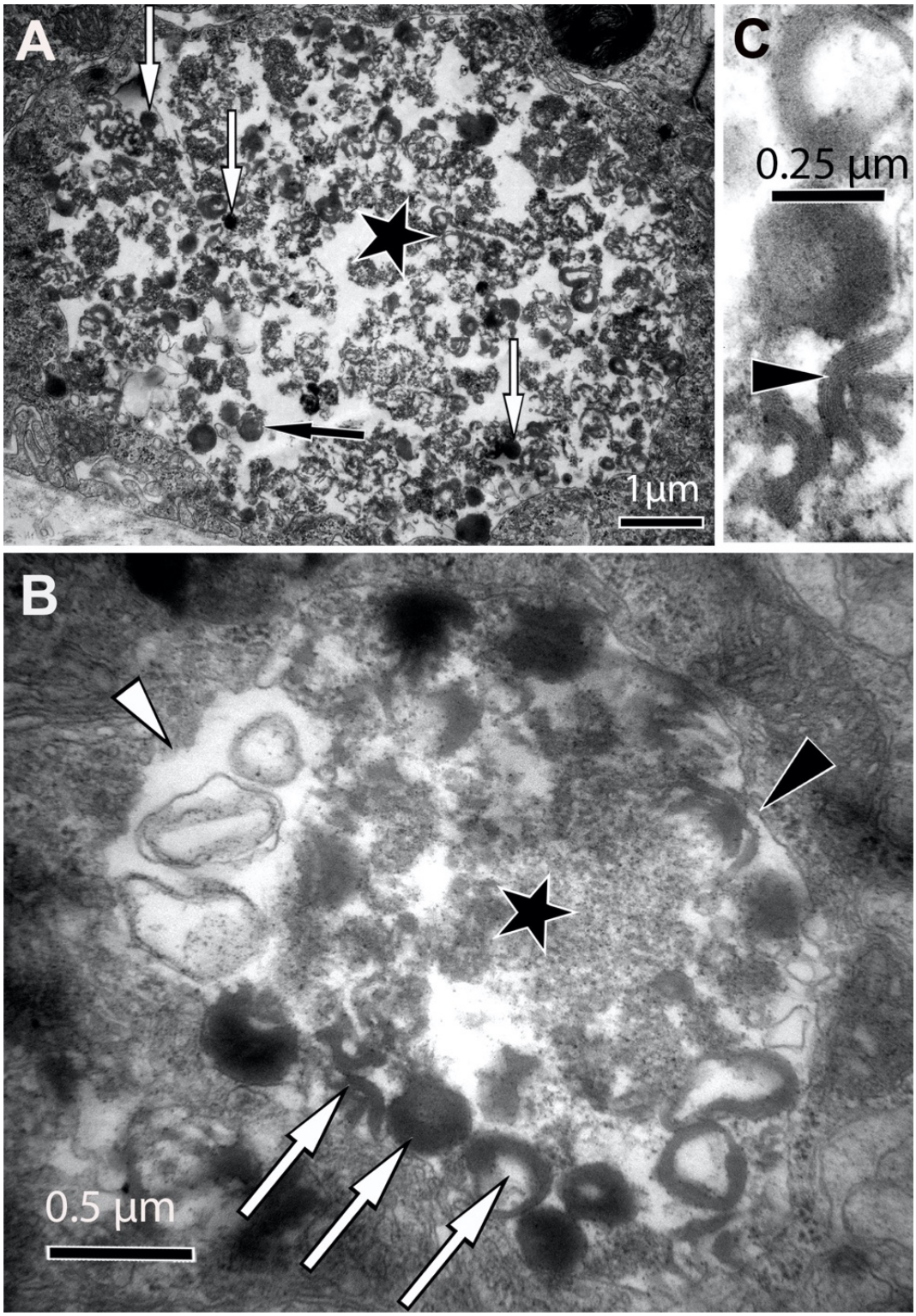

Figure 9. TLMs were detected in vacuoles in the RPE of albino *Abca4*$^{-/-}$ mice by electron microscopy.

(A) Under electron microscopy, vacuole-like structure (star) in albino *Abca4*$^{-/-}$ mice are full of various heterogeneous materials including TLMs that are either electron-dense (black arrow) or opaque (white arrows). (B) Fine lamellar membranes are detected

inside the vacuole (white arrows; magnified in C). Flocculate residues are also present in the vacuole (beside star). The vacuole-like structure contains limiting membranes that are frequently partial (black arrowhead) or lacking (white arrowhead), separating them from the cytoplasm. (C) The lamellar character of these residual bodies (arrowhead) is visible under higher magnification. TLMs, thin lamellar membranes; (Lyu et al., 2022).

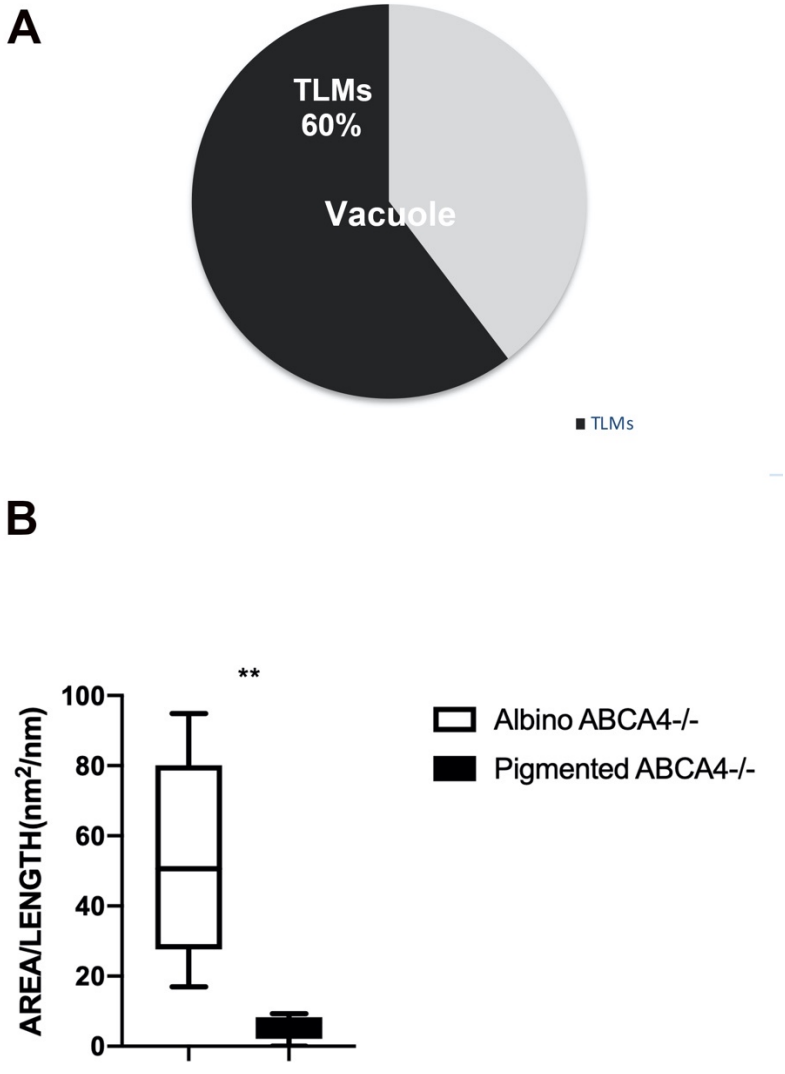

Figure 10. Quantification of vacuole occupied by TLMs and RPE occupied by vacuole-like materials.

(A) About 60% of the vacuole is occupied by the TLMs and flocculate residues (means, standard deviation: 0.603±0.089). 14 vacuoles in total were used for quantification. (B) Quantification by electron microscopy revealed that these vacuole-like structures are more frequently observed in albino *Abca4*$^{-/-}$ mice than in pigmented *Abca4*$^{-/-}$ mice (7-

month-old, n = 5 eyes/group, unpaired t-test, $^{**}p < 0.01$, Tukey boxplots), Figure.10B is adapted from (Lyu et al., 2022).

3.4 Tyrosinase-induced melanogenesis in the albino *Abca4*$^{-/-}$ mice

To prove the melanin hypothesis, the re-establish of melanin in the retina of albino *Abca4*$^{-/-}$ mice was done by the transfection of tyrosinase cDNA. Tyrosinase is the rate-limiting enzyme in melanin synthesis. Two weeks after subretinal injection of Ad-Tyr, brown-darkish spots were observed on the retinal in vivo by fundoscopy. After enucleation, brown-darkish areas surrounding the optic nerve head can be seen directly (Figure.11A). Under light microscopy, the pigmented granules which are normally invisible in the albino mouse were detected in the RPE (black arrowhead) and choroid (white arrowhead) (Figure.11B). Under electron microscopy, classical melanin containing pre-melanosomes were formed in choroidal melanocytes of albino *Abca4*$^{-/-}$ mice (Figure.12A). Melanofilaments that have a striated periodicity can be seen under higher magnification (Figure.12B).

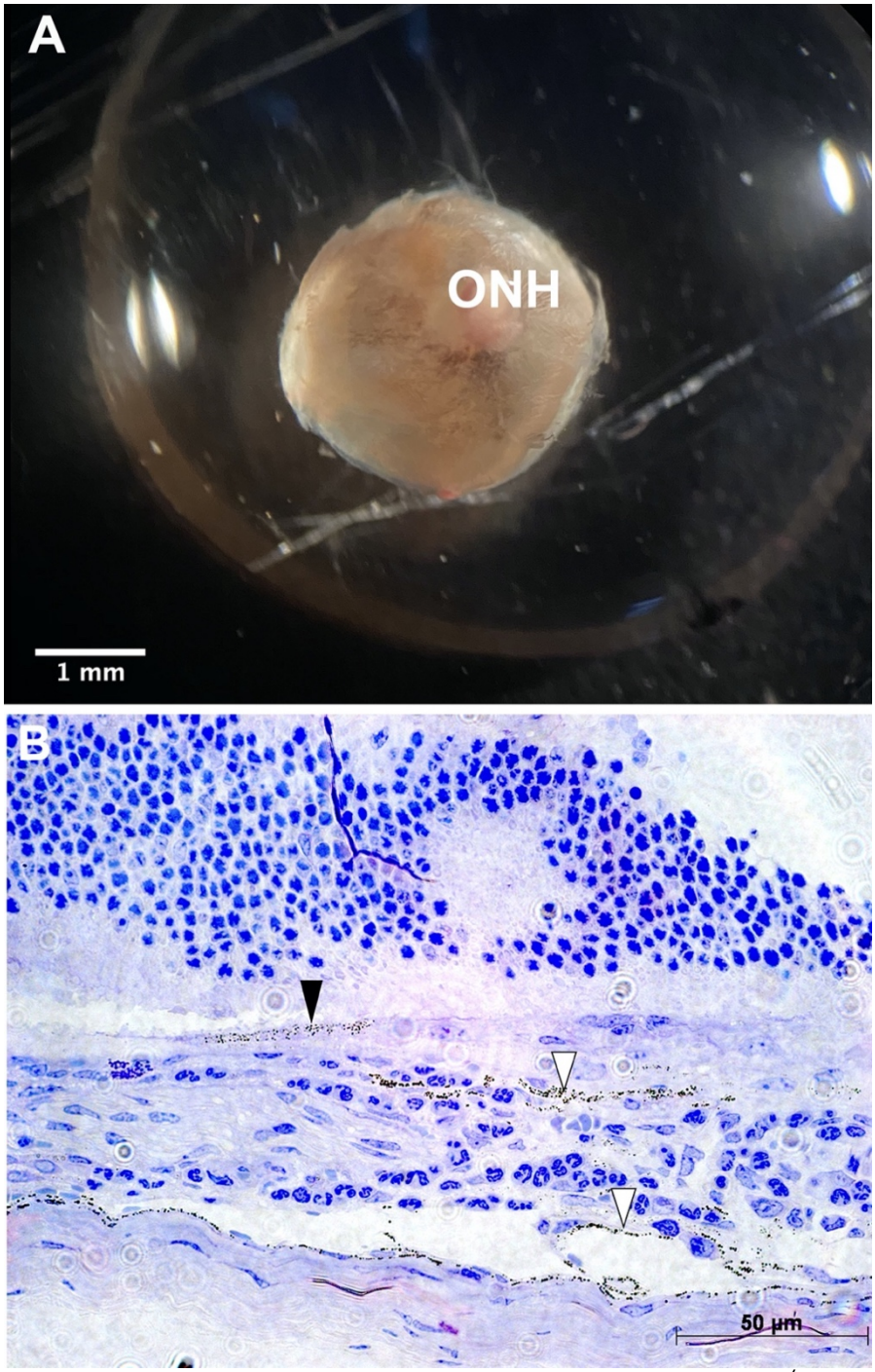

Figure 11. Tyrosinase-induced melanogenesis in the albino *Abca4*$^{-/-}$ mice.

(A) Brown-darkish spots surrounding the optic nerve were observed 2 weeks after tyrosinase cDNA transfection. ONH, optic nerve head. (B) Under light microscopy, pigmented granules can be seen in RPE (black arrowhead) and choroid (white arrowhead) 2 weeks after tyrosinase cDNA transfection.

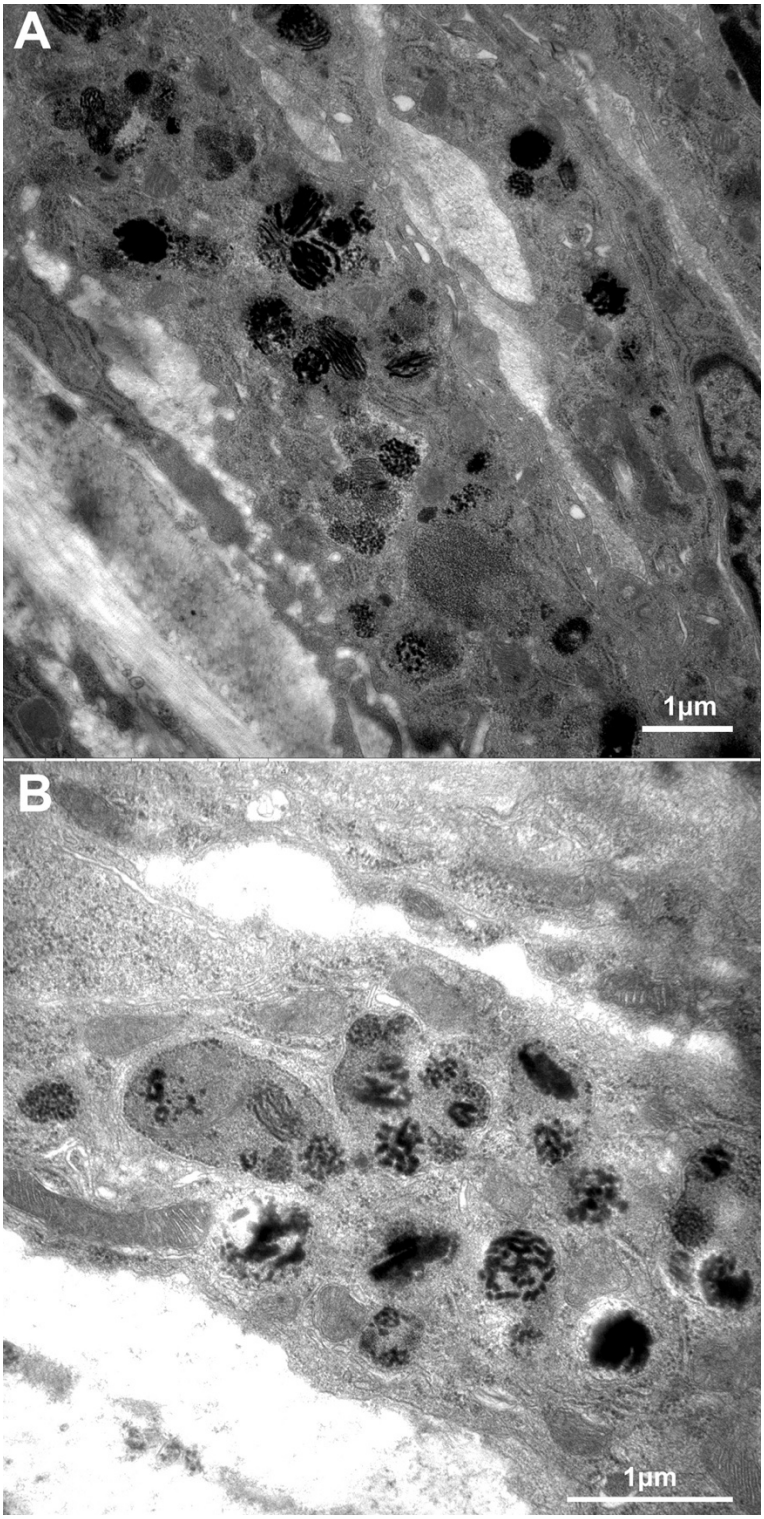

Figure 12. Tyrosinase-induced melanogenesis in choroidal melanocytes of albino *Abca4*$^{-/-}$ mice under electron microscopy.

(A) Different stages of pre-melanosomes were formed after transfection with the tyrosinase cDNA. (B) Melanofilaments that have a striated periodicity can be seen under higher magnification.

3.5 Tyrosinase-induced newly formed melanosomes show NIR-AF signals

Figure.14 and results related were published on the preprint server bioRxiv (Lyu et al., 2022). Round, electron-opaque granules were detected in the RPE of the albino *Abca4*$^{-/-}$ mice by electron microscopy (Figure.13), they were identified to be melanosomes. To confirm this, correlative fluorescence and electron microscopy on the same sections were performed. 300 nm thick sections were first investigated under fluorescence microscopy, then the same sections were investigated under electron microscopy. Figure.13 shows that melanosomes (black arrow) detected by electron microscopy showed NIR-AF signals (white arrow). Due to technical difficulties, the NIR-AF signal intensity is low, and the signals on the right upper side of the NIR-AF image were caused by the water used for covering the section (white arrowhead). In vivo fundus, NIR-AF is absent in the untreated eye of albino *Abca4*$^{-/-}$ mice (Figure.14A), while NIR-AF signals were detected 2 weeks after Ad-Tyr injection (Figure.14C). Injection could induce SW-AF signals because of tissue damage (Figure.14D, F), but the injection does not induce NIR-AF signals as shown in the PBS injected eye (Figure.14E).

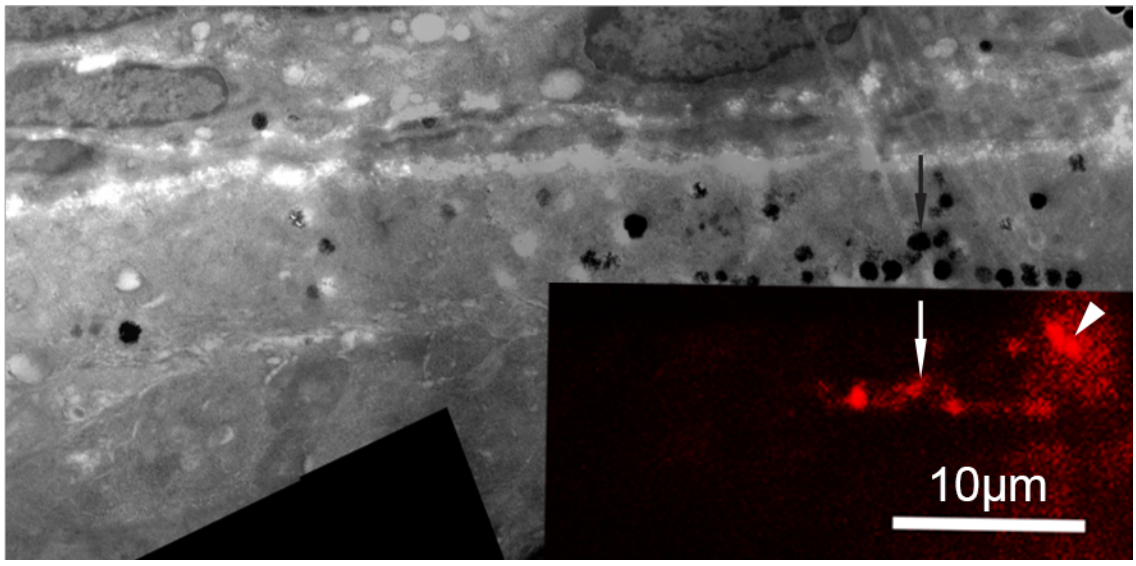

Figure 13. Correlative fluorescence and electron microscopy of the RPE of albino *Abca4*$^{-/-}$ mice after tyrosinase transfection.

300 nm section was investigated first by fluorescence microscopy and followed by electron microscopy investigation. Melanosomes (black arrow) shown in the electron

microscopy showed NIR-AF signals (white arrow). The white arrowhead shows the signal caused by water on the section.

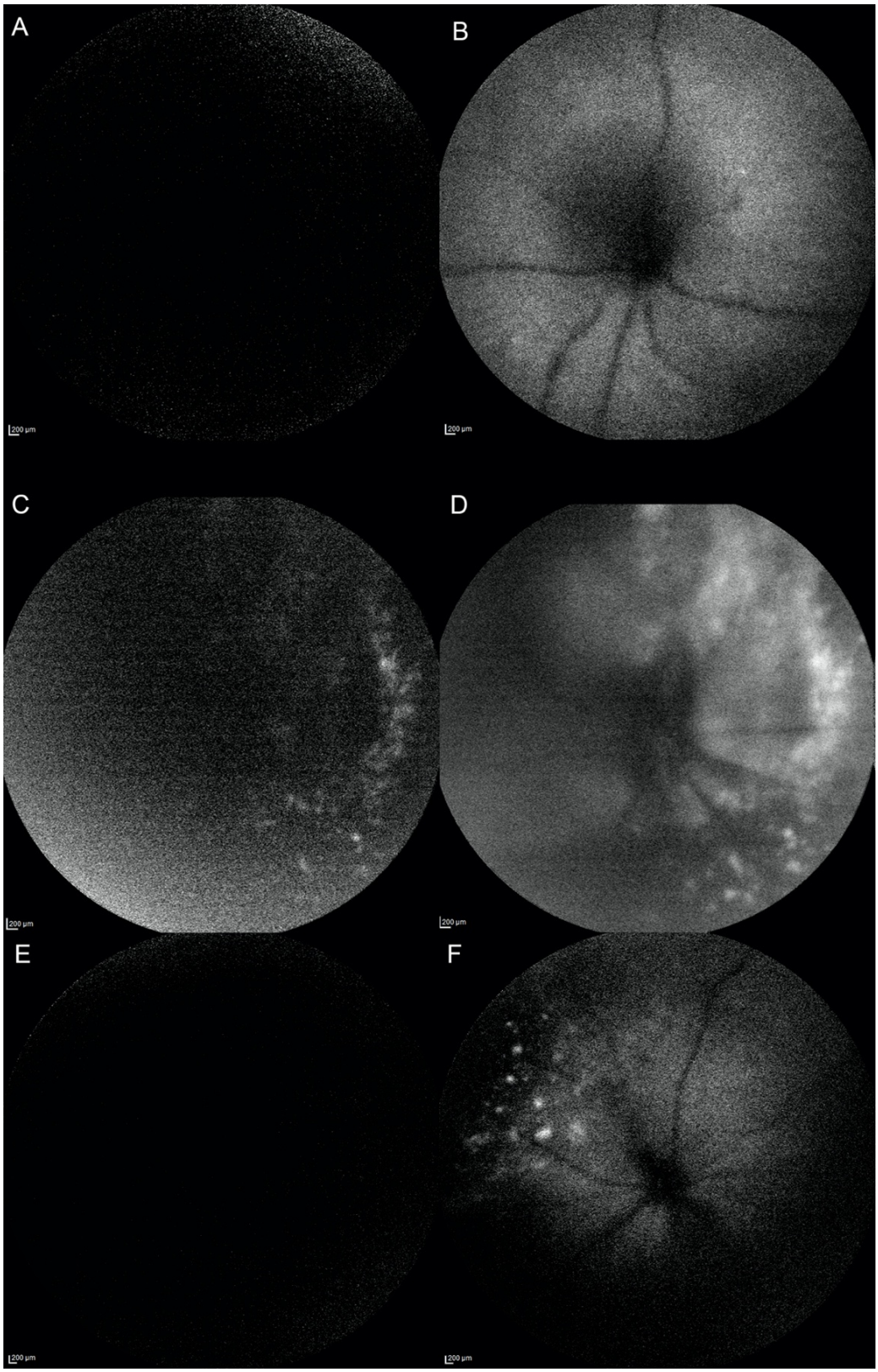

Figure 14. Fundus autofluorescence in vivo of albino *Abca4*$^{-/-}$ mice 2 weeks after tyrosinase transfection.

(A) Without Ad-Tyr injection, NIR-AF cannot be detected in the albino *Abca4*$^{-/-}$ mice. (B) SW-AF image of the untreated eye. (C) NIR-AF signals were detected 2 weeks after Ad-Tyr injection (treated eye from the same mouse). (D) Injection tissue damage resulted in strong SW-AF signals. (E) Eye injected with PBS, NIR-AF is absent. Injection does not cause NIR-AF signals. (F) The injection caused SW-AF signals. Ad-Tyr, adenovirus tyrosinase vector; adapted from (Lyu et al., 2022).

3.6 Transfecting albino *Abca4*$^{-/-}$ mice with tyrosinase cDNA induces RPE melanosome formation and reduces lipofuscin

Injection of Ad-Tyr also leads to melanosome (black arrow) formation in the RPE of albino *Abca4*$^{-/-}$ mice (Figure.15A). No classical pre-melanosome was detected in the RPE, indicating the melanogenesis might be different in the RPE from choroidal melanocytes. In the area where melanosomes were newly formed, the lipofuscin almost disappeared (Figure.15A). Without transfection, the RPE was filled with lipofuscin (Figure.15B).

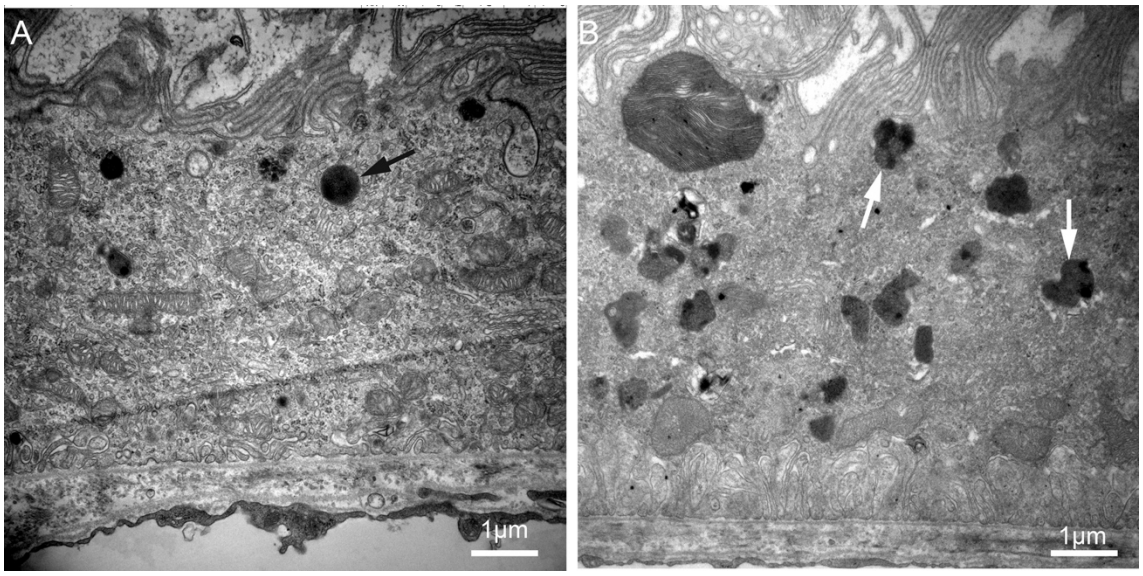

Figure 15. Melanosomes were formed in the RPE after tyrosinase transfection.

(A) Melanosomes were formed after Ad-Tyr subretinal injection. The lipofuscin can barely be seen. (B) Without transfection, the cytoplasm of RPE was full of lipofuscin.

3.7 SW-AF intensity is reduced in albino *Abca4*$^{-/-}$ mice after tyrosinase transfection

Figure.16 and results related were published on the preprint server bioRxiv (Lyu et al., 2022). Similar results were observed by fluorescence microscopy. After transfection of tyrosinase by subretinal administration of Ad-Tyr vector, newly formed melanosomes were detected in the RPE and choroid of the albino *Abca4*$^{-/-}$ mice as shown on the right side of the bright-field image (Figure.16A). As expected, these granules showed NIR-AF signals (Figure.16A) (white arrow). The left side shows the area without newly formed melanosomes in the same eye, there were no bright-field or NIR-AF signals (Figure.16A). A large amount of lipofuscin on the left side was shown by the widespread SW-AF signals (Figure.16A) (black arrowhead). Lipofuscin, detected as the SW-AF signal, almost disappeared in the region of newly produced melanosomes when compared to the left side (area without newly formed melanosomes) (Figure.16A). Figure.16B shows the magnified image of the overlay of the NIR-AF and SW-AF images, it's clear that the amount of lipofuscin decreased in the melanosomes newly formed area (Figure.16B).

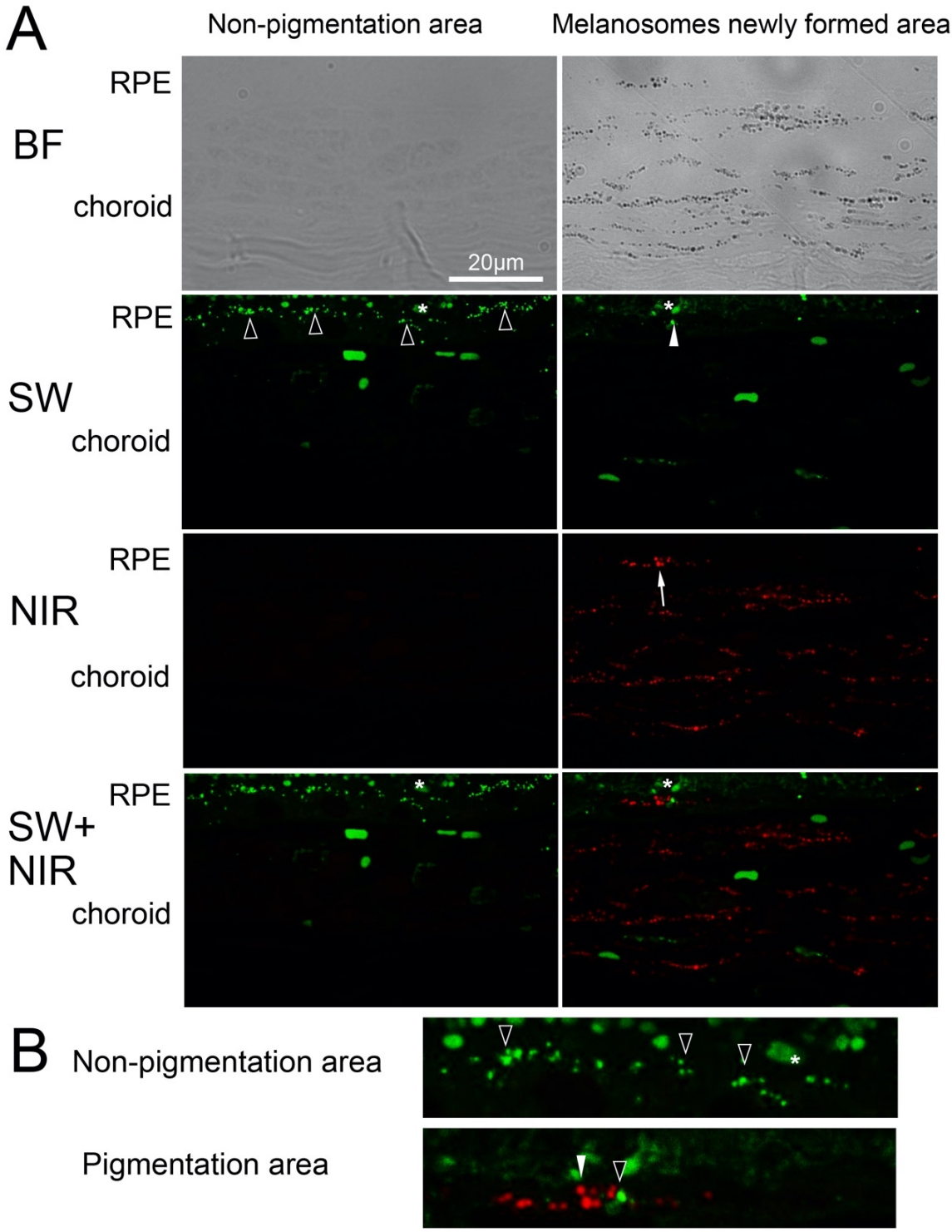

Figure 16. Representative fluorescence microscopy images after tyrosinase transfection in albino *Abca4*$^{-/-}$ mice.

(A) Left: No pigmented granules were observed in the bright-field (BF) image. Likewise, no NIR-AF (near-infrared autofluorescence) was detected. SW-AF (short-wavelength autofluorescence) reveals widespread signals, indicating the accumulation of lipofuscin

(black arrowhead). Right: Bright-field shows pigmented granules in both RPE and choroid. These granules were NIR-AF signal positive (white arrow). Around the melanosomes formed area (white arrowhead), SW-AF signals were significantly reduced than in the non-pigmentation area on the left side (black arrowhead). (B**)** Magnified overlay images of (A). The lipofuscin granules (black arrowhead) detected by SW-AF are nearly absent in the RPE where melanin were formed. The autofluorescent photoreceptor outer segments are marked by asterisks. BF, bright-field; SW-AF, short-wavelength autofluorescence; NIR-AF, near-infrared autofluorescence; (Lyu et al., 2022).

3.8 Light microscopy findings in pigmented and albino *Abca4*$^{-/-}$ mice after SIN-1 treatment

After SIN-1 injection, the mice were sacrificed after 48 hours. The eyes were fixed and then prepared for light microscopy, fluorescence microscopy, and electron microscopy. The toluidine blue stained sections were investigated first under light microscopy. All the images shown were taken from the area close to optic nerve. Figure.17A and B show the retina structure with and without SIN-1 treatment in the pigmented *Abca4*$^{-/-}$ mice. As shown, no significant changes in retina thickness and structure were observed after treatment. Similarly, there were no notable changes in retina thickness and structure following SIN-1 treatment in the albino *Abca4*$^{-/-}$ mice (Figure.17C, D). No evidence of toxicity was shown after SIN-1 treatment in either strain. Also, toxicity is out of the focus of this study.

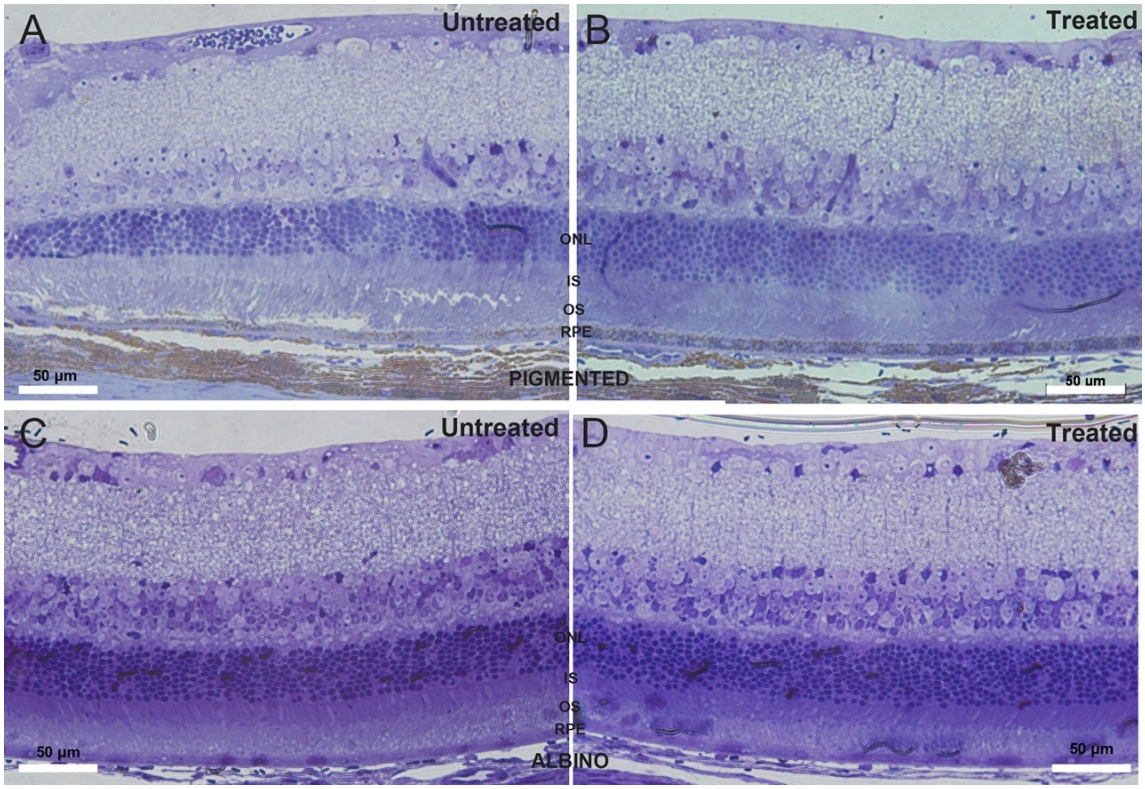

Figure 17. Retina structure overview after SIN-1 treatment in pigmented and albino *Abca4*$^{-/-}$ mice.

(A) The untreated eye of SIN-1 treated pigmented *Abca4*$^{-/-}$ mouse. (B) The treated eye of the same mouse. (C) The untreated eye of SIN-1 treated albino *Abca4*$^{-/-}$ mouse. (D) The treated eye of the same mouse.

3.9 Electron microscopy findings in pigmented and albino *Abca4*$^{-/-}$ mice after SIN-1 treatment

Results related to Figure.19 were published on the preprint server bioRxiv (Lyu et al., 2022). SIN-1 (3-morpholinosydnonimine) could decompose to superoxide (O2•-) and nitric oxide (NO•) spontaneously. Under electron microscopy, compared to the untreated eye (Figure.18A), the amount of lipofuscin in the RPE of pigmented *Abca4*$^{-/-}$ mice is reduced after intravitreal injection of SIN-1 (Figure.18B). And the amount of melanolipofuscin also decreased after treatment in the RPE of pigmented *Abca4*$^{-/-}$ mice (Figure.18A, B). The quantification confirmed these findings, that the amount of lipofuscin and melanolipofuscin significantly decreased after SIN-1 treatment (2-year-old pigmented *Abca4*$^{-/-}$ mice, n=5 eyes/group, ****p<0.0001, A, unpaired t-test, B , Mann–Whitney U test) (Figure.19A, B). The amount of melanin also decreased

after SIN-1 treatment (2-year-old pigmented *Abca4*$^{-/-}$ mice, n=5 eyes/group, *p<0.05, unpaired t-test) (Figure.19C). In albino *Abca4*$^{-/-}$ mice, the decrease of lipofuscin was not observed (Figure.18C, D). This was also confirmed by the quantification (6-month-old albino *Abca4*$^{-/-}$ mice, n=5 eyes/group, ns, p>0.05, Mann–Whitney U test) (Figure.19D). As mentioned in the method, the pigmented *Abca4*$^{-/-}$ mice used in this study were 2 years old while due to the time limitation the albino *Abca4*$^{-/-}$ mice were 6 months old. This explains why the amount of lipofuscin is generally higher in the pigmented *Abca4*$^{-/-}$ mice compared to albino *Abca4*$^{-/-}$ mice. No evidence of drug toxicity was shown by electron microscopy.

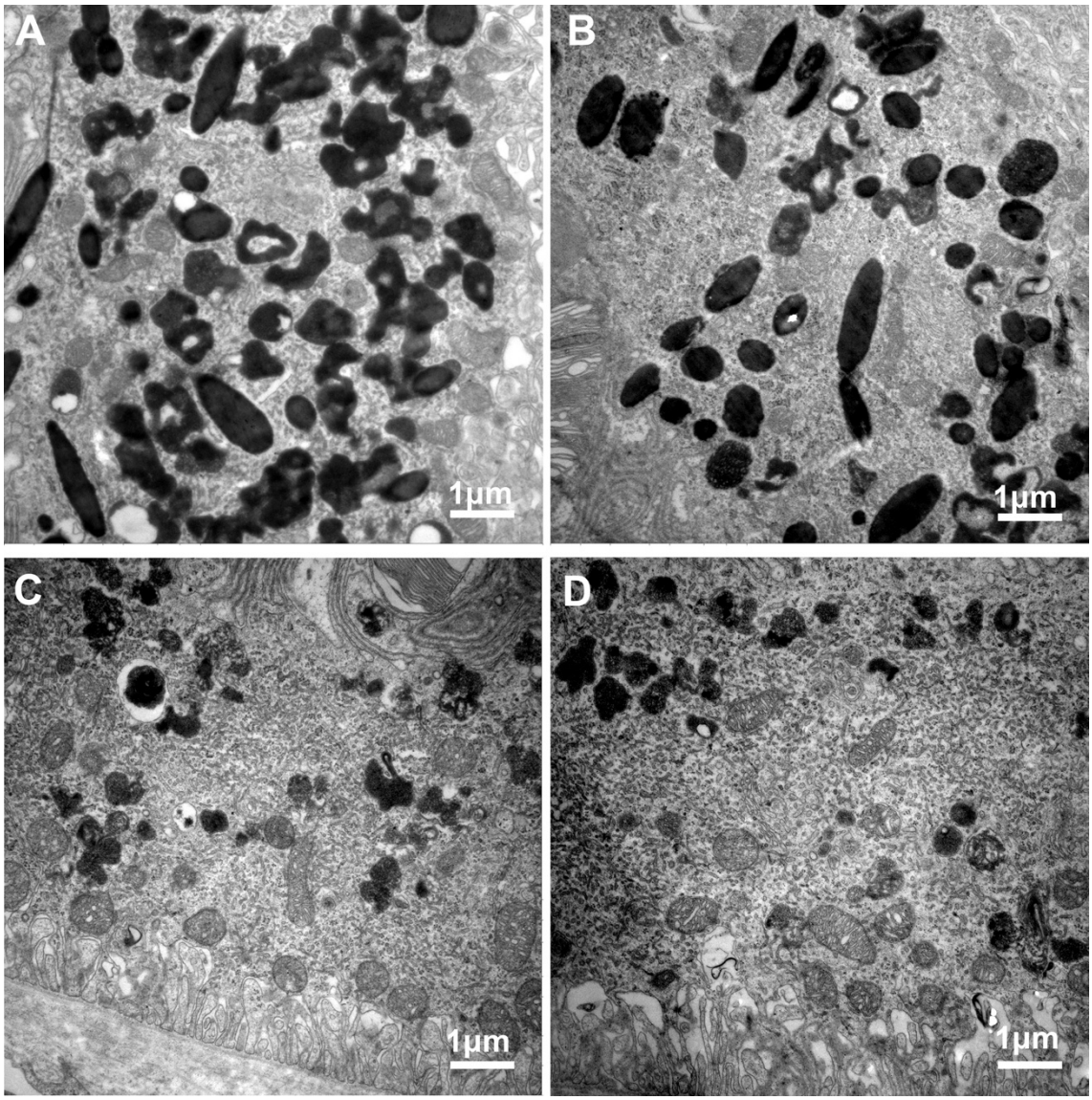

Figure 18. Representative electron microscopy images of RPE of pigmented and albino *Abca4*$^{-/-}$ mice treated with SIN-1.

(A) Pigmented *Abca4*$^{-/-}$ mouse, untreated left eye. The cytoplasm of the RPE is filled with lipofuscin and melanolipofuscin granules. (B) Pigmented *Abca4*$^{-/-}$ mouse, SIN-1 treated right eye from the same animal. The amount of lipofuscin and melanolipofuscin granules is reduced. (C) Albino *Abca4*$^{-/-}$ mouse, untreated left eye. The lipofuscin can be seen in the cytoplasm. (D) Albino *Abca4*$^{-/-}$ mouse, SIN-1 treated right eye from the same animal. The amount of lipofuscin is not reduced compared to C.

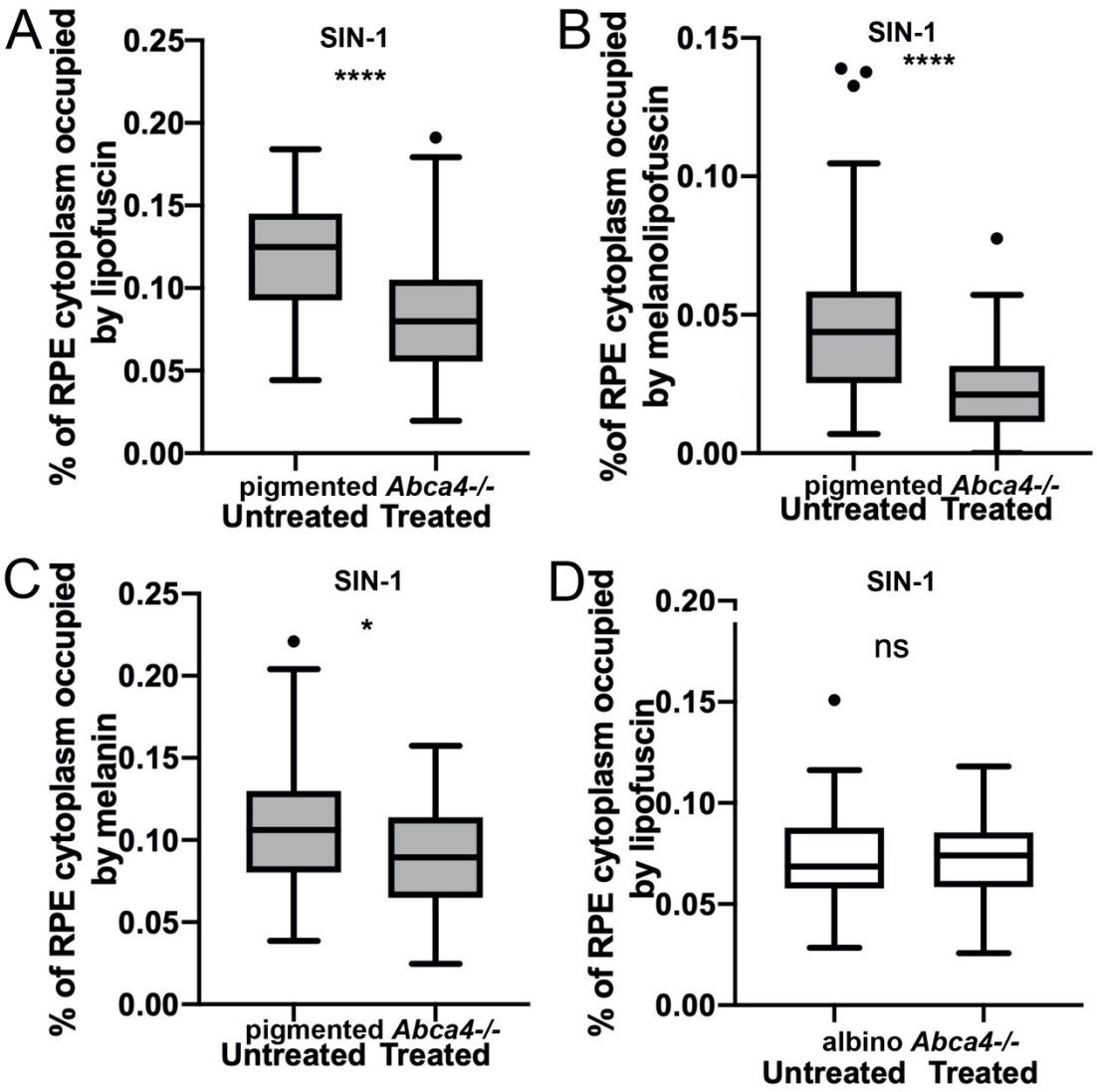

Figure 19. Quantification of electron microscopy images.

(A) Quantification of RPE cytoplasm occupied by lipofuscin in untreated and SIN-1 treated pigmented *Abca4*$^{-/-}$ mice, the amount of lipofuscin is reduced after treatment (2-

year-old pigmented *Abca4*$^{-/-}$ mice, n=5 eyes/group, ****p< 0.0001, unpaired t-test). (B) Quantification of the RPE cytoplasm occupied by melanolipofuscin in untreated and SIN-1 treated pigmented *Abca4*$^{-/-}$ mice, the amount of melanolipofuscin is reduced (2-year-old pigmented *Abca4*$^{-/-}$ mice, n=5 eyes/group, ****p<0.0001, Mann–Whitney U test). (C) Quantification of RPE cytoplasm occupied by melanin in untreated and SIN-1 treated pigmented *Abca4*$^{-/-}$ mice, the amount of melanin is reduced (2-year-old pigmented *Abca4*$^{-/-}$ mice, n=5 eyes/group, *$p<0.05$, unpaired t-test). (D) Quantification of RPE cytoplasm occupied by lipofuscin in untreated and SIN-1 treated albino *Abca4*$^{-/-}$ mice (6-month-old albino *Abca4*$^{-/-}$ mice, n=5 eyes/group, ns, not significant, $p>0.05$, Mann–Whitney U test). Data are presented by Tukey boxplots. Adapted from (Lyu et al., 2022).

3.10 Pre-melanosomes were detected in the RPE cells of pigmented *Abca4*$^{-/-}$ mice after SIN-1 treatment

Figure.20 and results related to Figure.20 were published on the preprint server bioRxiv (Lyu et al., 2022). After SIN-1 treatment, many pre-melanosomes (black arrow) and mature melanosomes (white arrow) were detected. The black arrowhead shows the MLF.

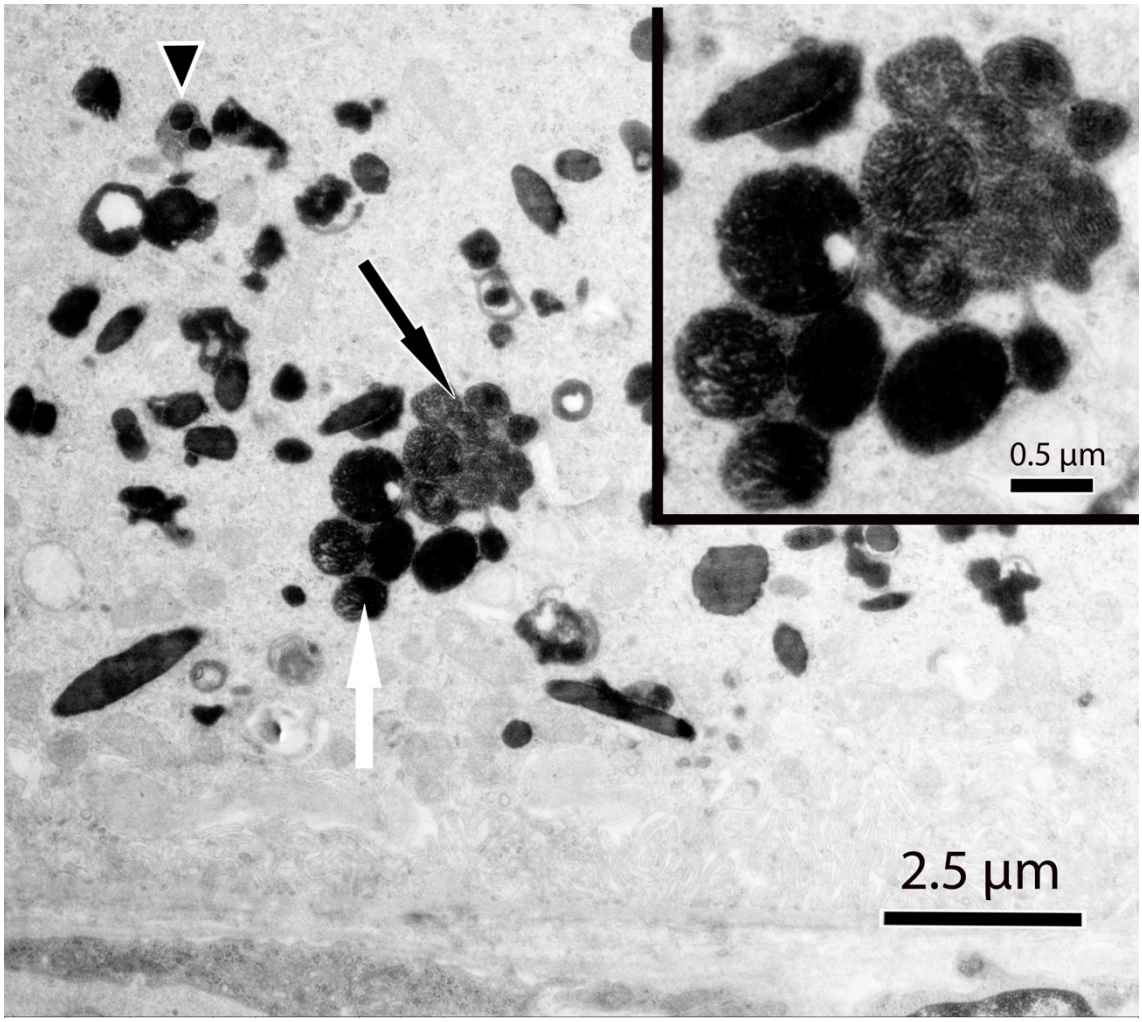

Figure 20. Pre-melanosomes were detected in the RPE of pigmented *Abca4*$^{-/-}$ mice after SIN-1 treatment.

Many early-stage (black arrow) and mature melanosomes (white arrow) were detected in the RPE after SIN-1 treatment. The inset shows the different stages of melanogenesis under higher magnification (Lyu et al., 2022).

3.11 Fluorescence microscopy findings in pigmented *Abca4*$^{-/-}$ mice after SIN-1 treatment

Figure.21 and results related to Figure. 21, Figure.22 were published on the preprint server bioRxiv (Lyu et al., 2022). Under the fluorescent microscopy (Figure.21), the NIR-AF signals located in both RPE and choroid correspond to the pigmented areas shown in the bright-field image were detected (Figure.21). After SIN-1 treatment, the SW-AF intensity decreased in pigmented *Abca4*$^{-/-}$ mice as compared to the untreated eye of the same mouse (Figure.21). The amount of melanin is also reduced as shown in bright-field. The MLF is shown

as yellow (overlapped red (melanin) and green (lipofuscin)), the amount of MLF decreased after SIN-1 injection as shown in the overlay of SW-AF and NIR-AF. The reduction of lipofuscin after treatment in pigmented *Abca4*$^{-/-}$ mice was confirmed by the semi-quantification of SW-AF intensity (2-year-old pigmented mice, n=6 eyes/group, *p<0.05, Mann–Whitney U test) (Figure.22A). No significant change in the NIR-AF intensity (averaged to each melanosome) in the RPE of pigmented *Abca4*$^{-/-}$ mice after SIN-1 treatment was observed (2-year-old pigmented mice, n=6 eyes/group, ns, p>0.05, Mann–Whitney U test) (Figure.22B).

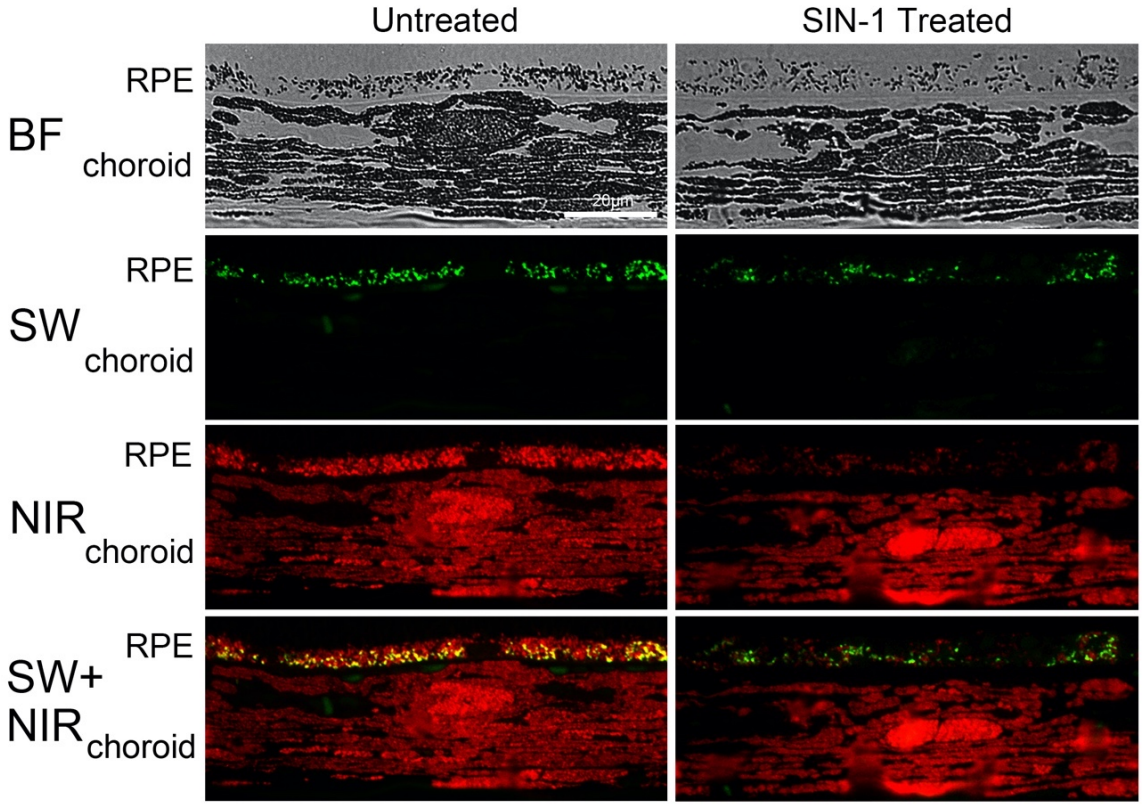

Figure 21. Representative AF images of pigmented *Abca4*$^{-/-}$ mice treated with SIN-1.

The SW-AF intensity is reduced after SIN-1 treatment in the pigmented *Abca4*$^{-/-}$ mice (second row). The yellow color (overlapped NIR-AF melanin signal (red) and SW-AF lipofuscin signal (green) shows areas that represent Melanolipofuscin (fourth row). The MLF amount is also reduced as compared to the untreated eye from the same animal. BF, bright-field; SW-AF, short-wavelength autofluorescence; NIR-AF, near-infrared autofluorescence; (Lyu et al., 2022).

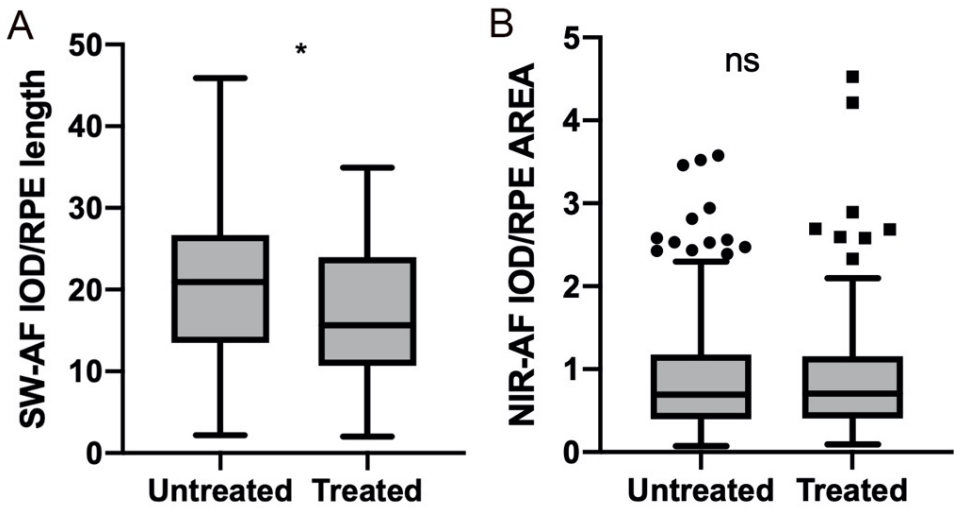

Figure 22. Semi-quantification of SW-AF intensity and NIR-AF intensity in pigmented *Abca4*$^{-/-}$ mice treated with SIN-1.

(A) Semi-quantification of SW-AF intensity in pigmented *Abca4*$^{-/-}$ mice treated with SIN-1 (2-year-old pigmented *Abca4*$^{-/-}$ mice, n=6 eyes/group, *$p<0.05$, Mann–Whitney U test), adapted from (Lyu et al., 2022). (B) Semi-quantification of NIR-AF intensity of the RPE of pigmented *Abca4*$^{-/-}$ mice treated with SIN-1 (2-year-old pigmented *Abca4*$^{-/-}$ mice, n=6 eyes/group, ns, not significant, $p>0.05$, Mann–Whitney U test). Data are presented by Tukey boxplots.

3.12 Fluorescence microscopy findings in albino *Abca4*$^{-/-}$ mice after SIN-1 treatment

Figure.23 and results related to Figure.23, Figure.24 were published on the preprint server bioRxiv (Lyu et al., 2022). In comparison to pigmented *Abca4*$^{-/-}$ mice, the reduction of lipofuscin after SIN-1 treatment was not observed in albino *Abca4*$^{-/-}$ mice (Figure.23). The albino mice do not show signals under NIR excitation. Semi-quantification of SW-AF intensity shows the same result that SIN-1 treatment did not effectively reduce the amount of lipofuscin in albino *Abca4*$^{-/-}$ mice (6-month-old albino mice, n=5 eyes/group, ns, $p>0.05$, Mann–Whitney U test) (Figure.24).

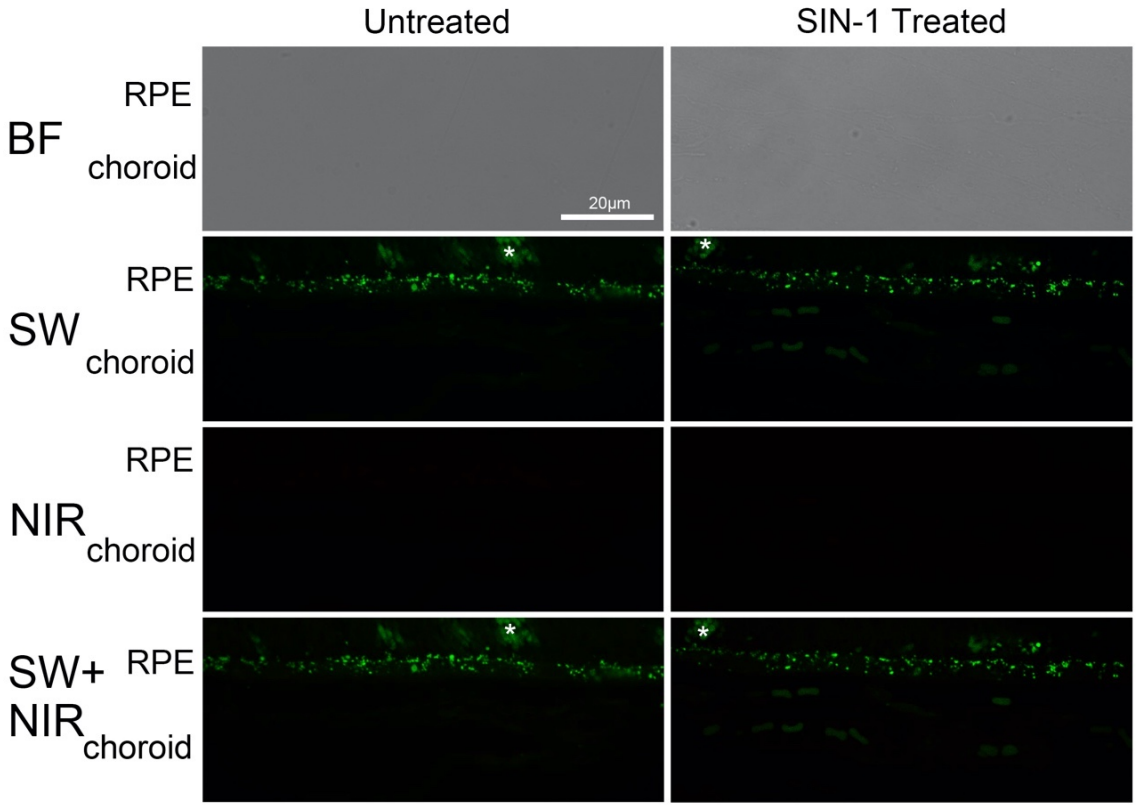

Figure 23. Representative AF images of albino *Abca4*$^{-/-}$ mice treated with SIN-1.

The reduction of SW-AF intensity was not observed in albino *Abca4*$^{-/-}$ mice after SIN-1 treatment. The albino mice do not show signals under NIR excitation because of the lack of melanin. BF, bright-field; SW-AF, short-wavelength autofluorescence; NIR-AF, near-infrared autofluorescence; (Lyu et al., 2022).

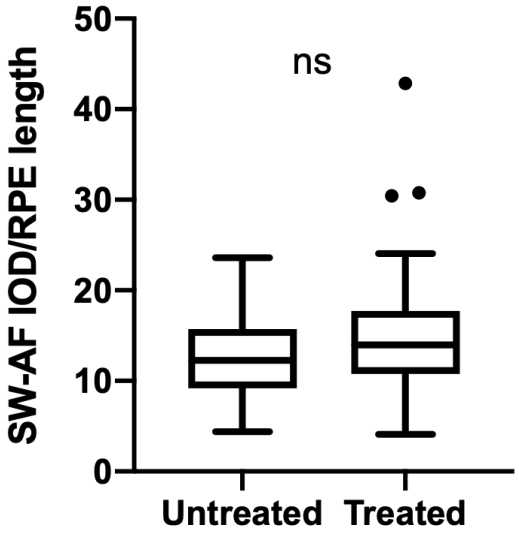

Figure 24. Semi-quantification of SW-AF intensity in albino *Abca4*$^{-/-}$ mice treated with SIN-1.

Semi-quantification of SW-AF intensity in albino *Abca4*$^{-/-}$ mice treated with SIN-1 (6-month-old albino *Abca4*$^{-/-}$ mice, n=5 eyes/group, ns, not significant, *p>0.05,* Mann–Whitney U test). Data are presented by Tukey boxplots, adapted from (Lyu et al., 2022).

3.13 Semi-quantification of SW-AF in pigmented and albino *Abca4*$^{-/-}$ mice after horseradish peroxidase treatment

The semi-quantification results shown in Figure.25 were published on the preprint server bioRxiv (Lyu et al., 2022). After treated with horseradish peroxidase, the reduction of SW-AF intensity was observed in the pigmented *Abca4*$^{-/-}$ mice (7-month-old pigmented *Abca4*$^{-/-}$ mice, n=3 eyes/group, ****p<0.0001, Mann–Whitney U test) (Figure.25A). In contrast, the horseradish peroxidase did not affect the SW-AF intensity in the albino Abca4$^{-/-}$ mice (7-month-old albino Abca4$^{-/-}$ mice, n=3 eyes/group, ns, p>0.05, Mann–Whitney U test) (Figure.25B).

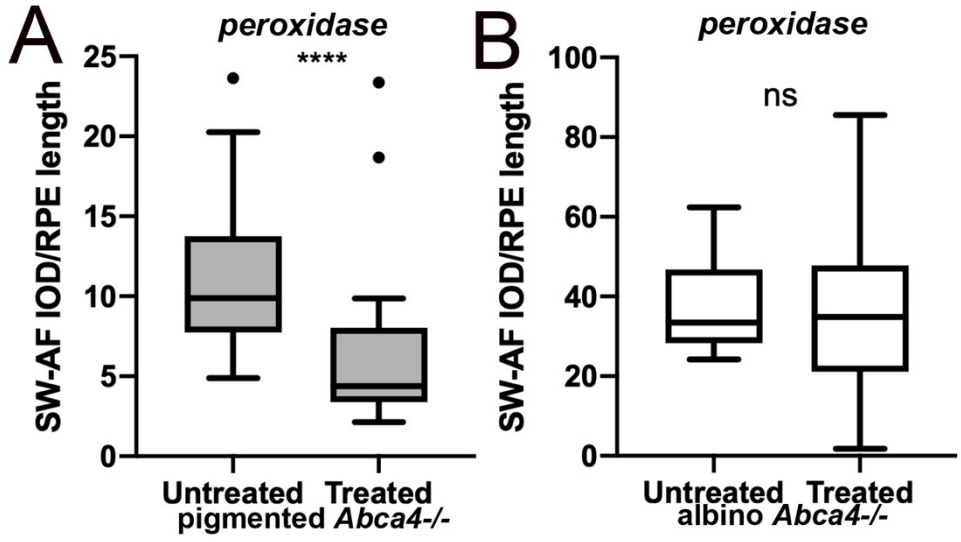

Figure 25. Semi-quantification of SW-AF intensity in pigmented and albino *Abca4*$^{-/-}$ mice treated with horseradish peroxidase.

(A) Semi-quantification of SW-AF intensity in pigmented *Abca4*$^{-/-}$ mice treated with horseradish peroxidase (7-month-old pigmented *Abca4*$^{-/-}$ mice, n=3 eyes/group, ****p<0.0001, Mann–Whitney U test). (B) Semi-quantification of SW-AF intensity in albino *Abca4*$^{-/-}$ mice treated with horseradish peroxidase (7-month-old albino *Abca4*$^{-/-}$ mice, n=3 eyes/group, ns, p>0.05, Mann–Whitney U test). Data are presented by Tukey boxplots, adapted from (Lyu et al., 2022).

3.14 Fluorescence microscopy findings in pigmented *Abca4*$^{-/-}$ mice after

ISDN treatment

The semi-quantification results shown in Figure.27 were published on the preprint server bioRxiv (Lyu et al., 2022). ISDN is a medicine used clinically for heart disease; it is a nitric oxide donor. As shown in Figure.26, the amount of lipofuscin is reduced after ISDN treatment. The semi-quantification showed that the lipofuscin decreased significantly after ISDN treatment (7-month-old pigmented *Abca4*$^{-/-}$ mice, n=3 eyes/group, ****p<0.0001, Mann–Whitney U test) (Figure.27). For reasons of missing the permission for animal experiments, ISDN treatment was not performed in albino *Abca4*$^{-/-}$ mice.

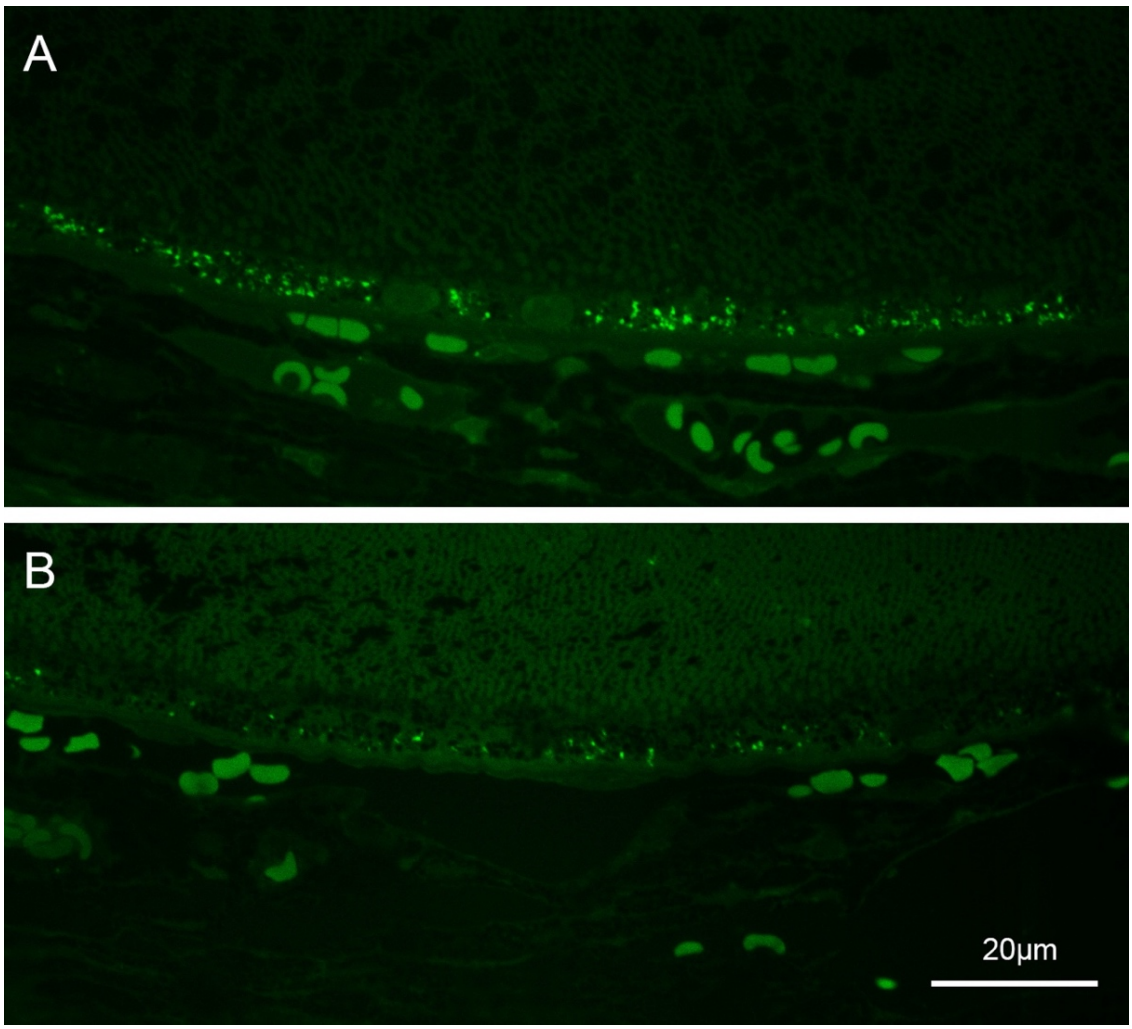

Figure 26. Representative AF images of pigmented *Abca4*$^{-/-}$ mice treated with ISDN.

(A)The untreated left eye. (B) The ISDN treated eye from the same mouse. The SW-AF signal intensity is reduced, representing the reduction of lipofuscin.

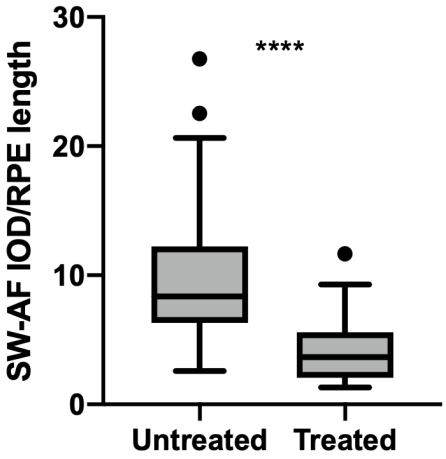

Figure 27. Semi-quantification of SW-AF intensity in pigmented *Abca4*$^{-/-}$ mice treated with ISDN.

Semi-quantification of SW-AF intensity in pigmented *Abca4*$^{-/-}$ mice treated with ISDN (7-month-old pigmented *Abca4*$^{-/-}$ mice, n=3 eyes/group, ****$P<0.0001$, Mann–Whitney U test). Data are presented by Tukey boxplots, adapted from (Lyu et al., 2022).

4. Discussion

4.1 Fate of photoreceptor discs

The amount of light-induced toxic materials inside photoreceptors rises daily (Sheline et al., 2010). The appropriate function and structure of the retina are required for light transduction by photoreceptors(Strauss, 2005). To preserve photoreceptor excitability, the photoreceptor outer segments are shed every day as a continuous renewal process. One whole photoreceptor outer segment has a 10-day turnover rate (Young and Bok, 1969, Strauss, 2005). The shed photoreceptor outer segments are then phagocytosed by RPE cells. In 70 years of human life, each cell digests billions of photoreceptor discs (Wavre-Shapton et al., 2014). The incomplete degradation of phagosomes eventually leads to lipofuscin deposit accumulation.

As observed in other species and in this study (Schraermeyer and Heimann, 1999, Schraermeyer and Stieve, 1994, Wavre-Shapton et al., 2014), photoreceptor discs of pigmented *Abca4*$^{-/-}$ mice are phagocytized by the RPE, partially degraded in lysosomes, and their products fused with RPE melanosomes, juxtaposing membranous material derived from photoreceptor discs. I found that most of the phagosomal membranes, including intra-phagosomal membranes derived from discs, are transformed into thin multi-

lamellar membranes (TLMs)–a structureless material with varied electron density (Figure.5, 7) that accumulate within MLF.

Schraermeyer first reported the fusion of phagosome and melanin in the RPE of the mature golden hamster (Schraermeyer, 1993). He suggested that melanin granules were involved in the pathway of the RPE handling non-degradable material. This was proved by subretinal injection of the gold-labeled outer segments to the rat eye (Schraermeyer et al., 1999), five days after outer segment residues and gold particles were found in the enlarged space between the melanin matrix and the limiting membrane in the RPE. After 12 days, only some gold particles can be found within melanosomes. He interpreted this as an indication that the phagosomal residues continue to be degraded in melanosomes whereas the indigestible gold particles remained longer within melanosomes. The fusion of phagosomes and melanosomes was also reported by Wavre-Shapton et al using cryo-immuno-electron microscopy (Wavre-Shapton et al., 2014). However, the residual phagosome content can't be fully digested, resulting in the formation of thin lamellar membranes (TLMs), which are likely being transported away together with other remaining materials through the choroidal vessels. Figure.7D demonstrated that the relative shape and structure of the TLMs are similar to the photoreceptor disc membranes but much thinner indicating that some material, probably protein, has been digested but other residues were not. Besides, the electron-dense structures were detected in the photoreceptor disc segments by tetramethylbenzidine reaction and intensive light exposure (Kayatz et al., 1999), and their structure is identical to the TLMs in the RPE. Through their experiments, it was also demonstrated that TLMs are able to induce chemical reactions. Originally Kayatz et al suggested that lipid peroxides are involved because TLMs appeared after the reaction with tetramethylbenzidine (Kayatz et al., 1999), therefore it is also possible that they are the result of a chemical reaction. It's likely that the bisretinoids are still associated with the original disc membrane, which also implies that the TLMs originate from the photoreceptor disc membranes.

4.2 RPE melanosomes are involved in the degradation of bisretinoids

Melanin is essential for the eye. Albinism patients suffer from foveal hypoplasia, and fundus hypopigmentation because of the defect in melanin biosynthesis(Liu et al., 2021). Aging is also accompanied by melanin declination in the RPE cells (Schmidt and Peisch, 1986). The amount of TLMs and lipofuscin are significantly higher in albino *Abca4*$^{-/-}$ mice than in pigmented ones (Figure.10) (Taubitz et al., 2018). Lipofuscin granules almost disappeared after the formation of melanosomes in the RPE of albino *Abca4*$^{-/-}$ mice (Figure.15, 16) while those newly formed granules were already oxidized and NIR fluorescent after a short time (Figure.13, 14). What role does melanin play in this process? RPE melanosomes are organelles that are related to lysosomes (Diment et al., 1995, Raposo and Marks, 2002) and contain lysosomal enzymes (Azarian et al., 2006), suggesting that melanosomes are likely to contribute to phagosome content degradation (Wavre-Shapton et al., 2014).

My data in this study also revealed the continuous degradation of photoreceptor disc membranes within the melanosomes (Figure.5A, 7A). The interaction between melanin and lipofuscin has also been reported by other researchers. Energy-dispersive X-ray microanalysis of human RPE pigment granules showed that the phosphorus level of the melanin component of melanolipofuscin is higher than individual melanosomes (Biesemeier et al., 2011). One of the components of lipofuscin is lipid (Terman and Brunk, 2004), the precursor of A2E also contains phosphorus (Jang et al., 2005), thus phosphorus can be considered a maker of lipofuscin. This finding indicates the molecular exchange between the lipofuscin and melanin components within melanolipofuscin. The complexes of DOPA-melanin with A2E were reported to even enhance the antioxidant property of DOPA-melanin compared with DOPA-melanin alone, suggesting the excess A2E in RPE cells loses its toxicity by bounding with the melanin in melanosome (Dontsov et al., 2013). Melanin has stable free radicals and can participate in redox reactions (Godechal and Gallez, 2011, Mostert et al., 2018). Melanin could not only absorb radicals (Ostrovsky et al., 1987) but also generate them (Sever et al., 1962), and is a superoxide(O_2-) donator (Lapina et al., 1984). Nitric oxide is also formed when melanin is

irradiated (Yacout et al., 2019). These properties have led to the suggestion that the redox properties of melanin lead to lipofuscin formation or degradation.

With regard to lipofuscin degradation, RPE melanin comprises redox-active metal ions including Fe, Cu, and Zn which are all engaged in the redox reaction (Biesemeier et al., 2011, Kim and Lee, 2021). Intracellular Fe promotes oxidative/degradation of the bisretinoid A2E in the presence of light (Zhao et al., 2021, Ueda et al., 2018). Even young rats that normally lack lipofuscin and MLF have formed these two types of granules in the RPE when given a zinc-deficient diet (Biesemeier et al., 2012, Julien et al., 2011). Furthermore, low zinc diet only causes low zinc in melanosomes of the RPE but not in choroidal melanocytes (Biesemeier et al., 2012). Studies have shown that lipofuscin can be degraded by radicals. For example, Fenton chemistry reactants could degrade A2E independently from light and produce dicarbonyls methylglyoxal and glyoxal in ARPE-19 cells otherwise inhibited by Fe chelator deferiprone (Ueda et al., 2018). Light-exposed melanin can itself generate superoxide which is able to degrade A2E-bisretinoid (Ueda et al., 2016). Recently Fang et al reported that Remofuscin could reverse the accumulation of lipofuscin in aged primary human RPE, they demonstrated the involvement of reactive oxygen species generated by Remofuscin in the lipofuscin degradation (Fang et al., 2022). It is reported that RPE pigments including melanin, lipofuscin and melanolipofuscin bind to Remofuscin (Julien-Schraermeyer et al., 2020). The treatment with Remofuscin was able to remove the lipofuscin from the monkey RPE as well (Julien and Schraermeyer, 2012). It is not clear why peroxidase can degrade A2E from RPE cells *in vitro* (Wu et al., 2011) since it consumes hydrogen peroxide rather than generating it, although horseradish peroxidase generates peroxyl and hydroperoxyl radicals (Berglund et al., 2002). Peroxidative activity was detected in the melanosomes of RPE in cattle (Schraermeyer and Stieve, 1994) and horseradish peroxidase removed lipofuscin from the RPE of pigmented *Abca4*$^{-/-}$ mice efficiently in the present study.

If the role of melanin is to generate radicals that degrade bisretinoids or lipofuscin directly, then an experimental prediction will be that peroxidase and drugs generating superoxide or other radicals will circumvent the melanin step

and even be effective in the albino *Abca4*$^{-/-}$ mice. They were not. The results of this study showed that SIN-1 (generator of $O_2^{\bullet-}$ and $NO^{\bullet}$), ISDN ($NO^{\bullet}$ generator), and horseradish peroxidase removed lipofuscin only in the pigmented *Abca4*$^{-/-}$ mice. Sundelin et al showed that melanin could inhibit lipofuscin formation in photoreceptor outer segments fed RPE cells when exposed to oxidative stress. The lipofuscin amounts were significantly higher in pigment-poor bovine cells and albino rabbit cells than in pigment-rich bovine RPE cells and pigmented rabbit cells after photoreceptor outer segments exposure (Sundelin et al., 2001). The highly pigmented human fetal RPE was also reported to be resistant to lipofuscin material whereas the amelanotic ARPE19 cells were not. The authors observed a mixture of undigestible autofluorescent material and melanin after being fed with oxidized outer segments which mimic melanolipofuscin in aged human RPE. They concluded that healthy pigmented RPE could sufficiently tolerate lipofuscin accumulation (Zhang et al., 2019). Those results, together with data of my study, indicate that melanin is directly involved in the degradation or detoxification of bisretinoids.

The chemiexcitation that creates chemical reaction products containing excited electrons is crucial in biology (White et al., 1974, Premi et al., 2015). Premi et al have shown the chemiexcitation pathway of melanin. The UV radiation to cells will cause the generation of nitric oxide (NO•) and superoxide (O2•–), these two radicals together form the strong oxidant peroxynitrite (ONOO–), and the formed peroxynitrite subsequently reacts with melanin then produce a dioxetane. The unstable dioxetane goes through spontaneous thermolysis, and the energy is transferred to excite the melanin fragment to the triplet state (Premi et al., 2015). SIN-1 is a reactive oxygen and nitrogen species generator, it decomposes in aqueous solution, releasing O2•– and NO• (Feelisch et al., 1989), which rapidly combine to create ONOO– for which it is also used as a peroxynitrite generator (Ho et al., 2012, Huie and Padmaja, 1993, Cuddy et al., 2012). A likely explanation for the lipofuscin and melanin reduction in the pigmented mice after SIN-1 treatment is that melanin chemiexcitation is engaged. Nitric oxide is naturally produced in the human RPE according to an investigation of the nitric oxide synthase expression in the retina of aged

humans and AMD eyes (Bhutto et al., 2010). Nitric oxide is also important for maintaining intraocular pressure homeostasis (Reina-Torres et al., 2021). Murdaugh et al detected nitro-A2E within the Bruch's membrane of aged humans (Murdaugh et al., 2010), suggesting the reaction of nitric oxide and A2E. Horseradish peroxidase could also create dioxetanes enzymatically, including on melanin, and can do so using its oxidase cycle that does not require H_2O_2 as oxidant (Berglund et al., 2002, Premi et al., 2015, Bechara et al., 1979, Baader et al., 1985). Taken together, melanin-dependent mechanisms are able to degrade lipofuscin but its removal also results in melanin destruction.

4.3 Stress responses opposing melanosome decline with age and disease

During bisretinoid degradation, toxic byproducts and radicals are formed (Ueda et al., 2016), therefore it would be an advantage that this event takes place in melanosomes. The membrane could limit the diffusion into the cytoplasm and the presence of melanin could also absorb the toxic byproducts and radicals.

The melanin-involved lipofuscin degradation pathway leads to the consumption of melanin. Dontsov et al revealed fluorescent melanin degradation products after exposing a combination of melanosomes and lipofuscin to blue light (Dontsov et al., 2017). They used blue light to irradiate the mixture of granules with the ratio of 1:5 of melanosome and lipofuscin for 90 min, this led to the development of fluorescent products because of melanin destruction. These fluorescent products were not present after the blue light irradiation of only melanosomes (Dontsov et al., 2017). The same group also discovered that the paramagnetic centers' concentration of human RPE is lower in the MLF than in melanin, suggesting the melanin degradation going on in the melanolipofuscin (Dontsov et al., 2017). They indicated that the decrease of melanin in RPE during aging is caused by the degradation of melanin located in melanolipofuscin by superoxide radicals generated by lipofuscin under the light (Dontsov et al., 2017).

NIR-AF is not an intrinsic melanin characteristic, it rises with age and photic or oxidative stress (Taubitz et al., 2019). In my current study, the young melanin granules already exhibited NIR-AF after 2 weeks while most of the lipofuscin granules were eliminated (Figure.16). Also, the reduction of lipofuscin was

accompanied by the reduction of melanin after injection of the O2•- and NO• donor SIN-1 in pigmented *Abca4*$^{-/-}$mice (Figures.19). The change in average NIR-AF intensity is not detected after SIN-1 treatment (Figure.22B). The explanation could be that the oxidized melanosomes with increased NIR-AF intensity were already degraded. Charbel Issa et al reported that the increased MLF with aging in the pigmented *Abca4*$^{-/-}$ mice is accompanied by decreased melanosomes. The rise in melanolipofuscin granules paralleled the rise in melanin-related NIR-AF (Charbel Issa et al., 2013), suggesting that interactions with lipofuscin lead to oxidation of melanosomes. Taubitz et al also revealed the NIR fluorescence of the melanosomes in the pigmented *Abca4*$^{-/-}$ mice with high amounts of MLF. While the melanosomes of age-matched wild type mice do not show NIR signals (Taubitz et al., 2019), again indicating the oxidation of melanin through overwhelming reaction with lipofuscin. In the process of chemiexcitation, melanosomes are also degraded (Premi et al., 2015). Therefore, the RPE melanin formed during embryogenesis would eventually run out.

On the other hand, melanogenesis was reported by Poliakov et al in the ARPE-19 cells challenged with rod outer segments that were treated with a low level of A2E for weeks. ARPE-19 cells produce melanin in response to the excess A2E accumulation (Poliakov et al., 2014). In this study, early-stage melanosomes were also observed after SIN-1 treatment (Figure.20). The rate of melanogenesis can be enhanced 40-fold by radicals (Wood and Schallreuter, 1991). Nitric oxide was reported to stimulate melanogenesis by enhancing tyrosinase gene expression (Roméro-Graillet et al., 1997, Sasaki et al., 2000). Post-natal melanin induction (Schraermeyer, 1992, Poliakov et al., 2014) may therefore be a stress response to excess lipofuscin because tyrosinase expression was detected after feeding cattle and humans RPE cells with outer segments (Schraermeyer et al., 2006, Julien et al., 2007).

4.4 Melanogenesis induced by tyrosinase cDNA and intravitreal injection delivery system

The formation of melanosomes in mammalian RPE cells is generally thought to only occur during embryogenesis and maturing during the first two years after

birth (Schraermeyer and Heimann, 1999, Biesemeier et al., 2010). Only a few studies reported melanogenesis in the mature RPE cells (Dorey et al., 1990, Schraermeyer, 1992, Poliakov et al., 2014). I presented clear evidence that melanogenesis can occur in adult mammal RPE after birth, the artificial formation of melanin in both RPE and choroidal melanocytes was achieved by the transfection of tyrosinase cDNA. Pre-melanosomes, which are thought to be required for melanogenesis in both melanocytes and RPE cells (Lopes et al., 2007, Biesemeier et al., 2010) were formed in the choroidal melanocytes of albino *Abca4*$^{-/-}$ mice (Figure.12). However, pre-melanosomes were not detected in the RPE cells. It's possible that the melanin synthesis pathway is different in the choroid and RPE. Biesemeier et al also demonstrated the occurrence of melanogenesis without the typical pre-melanosomes formation in the human RPE cell (Biesemeier et al., 2010). This study suggests the possibility of the restoration of melanization in the adult RPE for the rescue of function. However, the injection of Ad-Tyr also altered the RPE structure due to the side effects of adenovirus. A better approach to melanogenesis in the RPE would be the use of new AAV vectors.

Intravitreal injection was used for the delivery of SIN-1, ISDN, and peroxidase. It is a highly effective way of drug delivery to the eye and is wildly used for drugs developed for retinal diseases (Martin, 2018). Although peroxynitrite is not stable, it's more likely that SIN-1 diffuses through the RPE. Large proteins like Avastin reaches the choroid within 1-day after intravitreal injection (Schraermeyer and Julien, 2013). The intravitreal injection was sufficient for drug delivery and action in this study.

In this study, I detected TLMs that originate from photoreceptor membranes. Only preliminary descriptions about TLM were made before (Schraermeyer et al., 1998), it is still mostly unknown. However, TLMs are very prominent in *Abca4*$^{-/-}$ mice, this underlines the importance of TLMs. These TLMs are often related to melanolipofuscin and are more common in albino *Abca4*$^{-/-}$ mice. I discovered a natural mechanism by which lipofuscin in the RPE could be degraded with the support of melanosomes. Additionally, lipofuscin degradation can be enhanced by drugs generating nitric oxide. The failure of this

mechanism may account for the decline in visual acuity of Stargardt patients and for the onset of AMD with age. This study indicates (Figure.28) that leftover incomplete phagosomal degradation could merge with melanosomes. Radicals or chemical reactions generated by melanosomes or during the phagocytosis process, lipofuscin is degraded. Some of the phagosomal membranes are transformed into a homogeneous substance with varying electron densities that reside in the melanolipofuscin granules, lipofuscin, or cytoplasm. In the meantime, melanosomes also provide a protective environment against the oxidative stress produced during the degradation procedure. When lipofuscin cannot be entirely degraded because the burden is too great, as in Stargardt disease, or during aging, melanolipofuscins are formed and accumulated. These findings suggest a potential treatment approach to lipofuscin-related diseases such as Stargardt disease and AMD in the future.

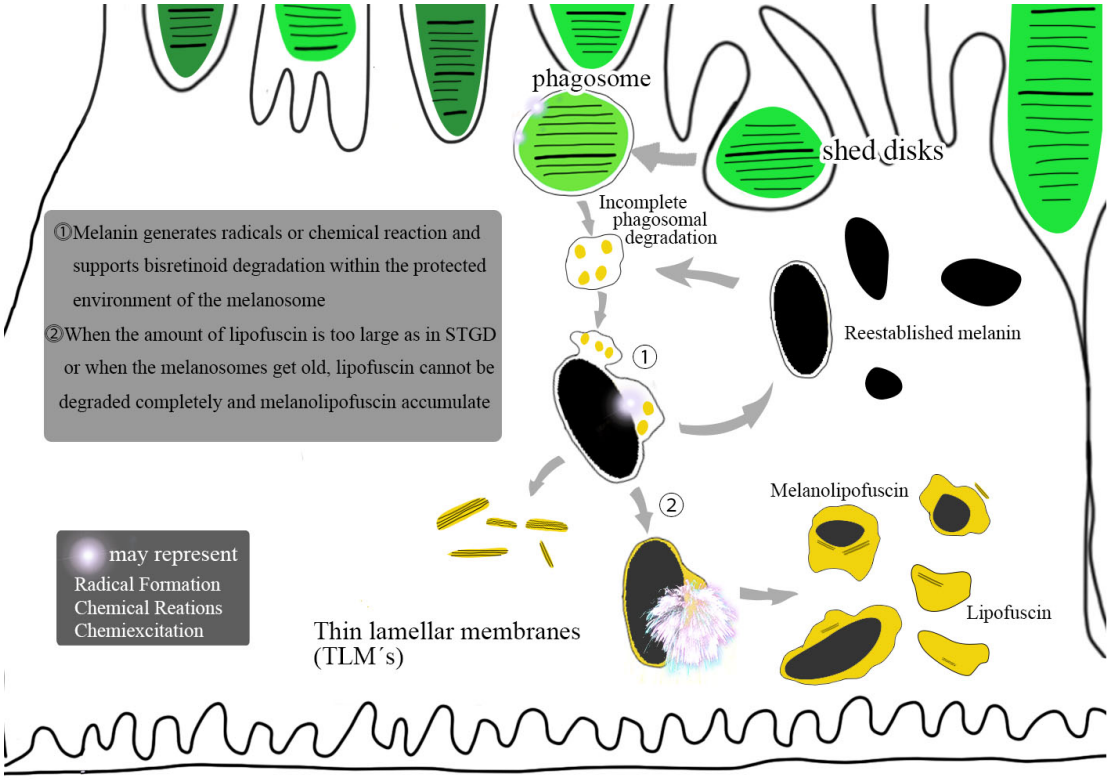

Figure 28. Bisretinoids degradation requires melanosomes and is enhanced by radicals.

Incomplete phagosomal degradation leftover fuse with melanosomes, with radicals created by melanin or during the phagocytosis process, lipofuscin could be degraded. Some phagosomal membranes are transformed into homogeneous substances with

variable electron densities that reside in melanolipofuscin granules, lipofuscin, or cytoplasm. In this scenario, melanosomes provide a protective environment against the oxidative damage caused during the degradation process. Lipofuscin cannot be entirely degraded when the burden is too great, as in Stargardt disease or aging, melanolipofuscins are formed.

5. Summary

Lipofuscin granules accumulate within the human RPE cell with age. The accumulation procedure is especially accelerated among Stargardt disease and age-related macular degeneration (AMD). Another pigment granule - melanolipofuscin (MLF) starts to accumulate throughout the pathogenic procedure and aging, indicating the reduction in the capacity to degrade lipofuscin. Studies have shown the major lipofuscin amount differs between pigmented and albino *Abca4*$^{-/-}$ mice as well as non-white people and white people. Lipofuscin accumulation is ameliorated by drugs that generate superoxide ($O_2^{\bullet-}$), and melanin together with superoxide and nitric oxide was discovered to be able to excite melanin electrons to a high-energy state for chemical reactions. Therefore, the present study was designed to test whether melanin is required for the photoreceptor disc clearance in the RPE and whether drugs generating $NO^{\bullet}$ enhance this process. The *Abca4*$^{-/-}$ mice - models for Stargardt disease and for lipofuscin-related diseases were used in this study. Subretinal injection of the adenovirus tyrosinase vector was performed to induce melanin formation in the albino *Abca4*$^{-/-}$ mouse. Additionally, intravitreous injections of reagents (3-morpholinosydnonimine (SIN-1) or isosorbide dinitrate (ISDN)) and horseradish peroxidase that generate radicals were performed in both pigmented and albino *Abca4*$^{-/-}$ mice. Fundoscopy was measured in vivo, and electron microscopy, fluorescence microscopy, and immunofluorescence stain were used in the method. This study demonstrated the unique thin lamellar membranes (TLM) that are more often found in the albinos *Abca4*$^{-/-}$ mice than in the pigmented mice, It also showed that these TLMs originate from incomplete digestion of photoreceptor disc membranes. The results also provided an explanation of the formation of MLF - it originates from the inability of melanin to continue to degrade bisretinoids because melanin is aged or the amount of bisretinoids is

overwhelmed as in Stargardt disease. Melanogenesis in adult mammal RPE after birth by adenoviral tyrosinase vector was presented. The newly formed melanin granules were near-infrared positive and oxidized within 2 weeks. And the reduction of lipofuscin was detected in the area where melanin was newly formed. The results showed a marked decrease in lipofuscin amount in the RPE cell of pigmented *Abca4*$^{-/-}$ mice after SIN-1, ISDN, or peroxidase treatments. By contrast, neither SIN-1 nor peroxidase was able to remove lipofuscin from albino *Abca4*$^{-/-}$ mice. Therefore, the current study showed a natural mechanism by which lipofuscin in RPE cells can be degraded with the support of melanosomes, and this pathway can be enhanced by drugs generating superoxide or nitric oxide.

6. Zusammenfassung

Lipofuszingranula sammeln sich mit zunehmendem Alter in der menschlichen RPE-Zelle an. Besonders beschleunigt wird der Akkumulationsvorgang bei Morbus Stargardt und altersbedingter Makuladegeneration (AMD). Ein weiteres Pigmentgranulat – Melanolipofuscin (MLF) – beginnt sich während des pathogenen Vorgangs und des Alterns anzusammeln, was auf die Verringerung der Fähigkeit zum Abbau von Lipofuscin hinweist. Studien haben gezeigt, dass sich die Hauptmenge an Lipofuszin zwischen pigmentierten und Albino-*Abca4*$^{-/-}$-Mäusen sowie zwischen nicht-weißen und weißen Menschen unterscheidet. Die Anreicherung von Lipofuszin wird durch Arzneimittel verbessert, die Superoxid (O2•-) erzeugen, und es wurde entdeckt, dass Melanin zusammen mit Superoxid und Stickoxid Melaninelektronen in einen hochenergetischen Zustand für chemische Reaktionen anregen kann. Daher wurde die vorliegende Studie entwickelt, um zu testen, ob Melanin für die Clearance der Photorezeptor Disk im RPE erforderlich ist und ob Medikamente, die NO• erzeugen, diesen Prozess verstärken. Die *Abca4*$^{-/-}$-Maus-Modelle für die Stargardt - Krankheit und für Lipofuszin-bedingte Krankheiten wurden in dieser Studie verwendet. Eine subretinale Injektion des Adenovirus-Tyrosinase-Vektors wurde durchgeführt, um die Melaninbildung in die Albino-*Abca4*$^{-/-}$-Mäuse einzuleiten. Zusätzlich wurden intravitrealen Injektionen von Reagenzien (3-Morpholinosydnonimin (SIN-1) oder Isosorbiddinitrat (ISDN)) und

Meerrettichperoxidase, die Radikale erzeugen, sowohl bei pigmentierten als auch bei Albino-*Abca4*$^{-/-}$-Mäusen durchgeführt. Die Fundoskopie wurde in vivo gemessen, und bei dem Verfahren wurden Elektronenmikroskopie, Fluoreszenzmikroskopie und Immunfluoreszenzfärbung verwendet. Diese Studie demonstrierte die einzigartigen dünnen lamellaren Membranen (TLM), die häufiger bei Albino- *Abca4*$^{-/-}$-Mäusen als bei pigmentierten Mäusen gefunden werden. Sie zeigte auch, dass diese TLMs aus einer unvollständigen Verdauung von Photorezeptorscheibenmembranen stammen. Die Ergebnisse lieferten auch eine Erklärung für die Bildung von MLF – es stammt aus der Unfähigkeit von Melanin, weiterhin Bisretinoide abzubauen, weil Melanin gealtert ist oder die Menge an Bisretinoiden wie bei der Stargardt-Krankheit zu groß ist. Es wurde die Melanogenese in erwachsenen Säuger-RPE nach der Geburt durch einen Adenovirus-Tyrosinase-Vektor vorgestellt. Die neu gebildeten Melaninkörnchen waren im nahen Infrarot positiv und oxidierten innerhalb von 2 Wochen. Und die Reduktion von Lipofuszin wurde in dem Bereich nachgewiesen, in dem Melanin neu gebildet wurde. Die Ergebnisse zeigten eine deutliche Abnahme der Lipofuszinmenge in den RPE-Zellen pigmentierter *Abca4*$^{-/-}$ Mäuse nach SIN-1-, ISDN-oder Peroxidase-Behandlungen. Im Gegensatz dazu war weder SIN-1 noch Peroxidase in der Lage, Lipofuszin aus Albino *Abca4*$^{-/-}$ Mäusen zu entfernen. Daher zeigte die aktuelle Studie einen natürlichen Mechanismus, durch den Lipofuszin in RPE-Zellen mit Unterstützung von Melanosomen abgebaut wird, und dieser Weg kann durch Medikamente verstärkt werden, die Superoxid oder Stickoxid erzeugen.

7. Bibliography

ABALEM, M. F., OMARI, A. A., SCHLEGEL, D., KHAN, N. W. & JAYASUNDERA, T. 2019. Macular hyperpigmentary changes in ABCA4-Stargardt disease. *Int J Retina Vitreous,* 5**,** 9.

ADHI, M., READ, S. P., FERRARA, D., WEBER, M., DUKER, J. S. & WAHEED, N. K. 2015. Morphology and Vascular Layers of the Choroid in Stargardt Disease Analyzed Using Spectral-Domain Optical Coherence Tomography. *Am J Ophthalmol,* 160**,** 1276-1284 e1.

ADLER, L. T., BOYER, N. P., CHEN, C., ABLONCZY, Z., CROUCH, R. K. & KOUTALOS, Y. 2015. The 11-cis Retinal Origins of Lipofuscin in the Retina. *Prog Mol Biol Transl Sci,* 134**,** e1-12.

ALBERT, S., GARANTO, A., SANGERMANO, R., KHAN, M., BAX, N. M., HOYNG, C. B., ZERNANT, J., LEE, W., ALLIKMETS, R., COLLIN, R. W. J. & CREMERS, F. P. M. 2018. Identification and Rescue of Splice Defects Caused by Two Neighboring Deep-Intronic ABCA4 Mutations Underlying Stargardt Disease. *Am J Hum Genet,* 102**,** 517-527.

ALLIKMETS, R., SINGH N FAU - SUN, H., SUN H FAU - SHROYER, N. F., SHROYER NF FAU - HUTCHINSON, A., HUTCHINSON A FAU - CHIDAMBARAM, A., CHIDAMBARAM A FAU - GERRARD, B., GERRARD B FAU - BAIRD, L., BAIRD L FAU - STAUFFER, D., STAUFFER D FAU - PEIFFER, A., PEIFFER A FAU - RATTNER, A., RATTNER A FAU - SMALLWOOD, P., SMALLWOOD P FAU - LI, Y., LI Y FAU - ANDERSON, K. L., ANDERSON KL FAU - LEWIS, R. A., LEWIS RA FAU - NATHANS, J., NATHANS J FAU - LEPPERT, M., LEPPERT M FAU - DEAN, M., DEAN M FAU - LUPSKI, J. R. & LUPSKI, J. R. 1997. A photoreceptor cell-specific ATP-binding transporter gene (ABCR) is mutated in recessive Stargardt macular dystrophy. *Nature genetics,* 15**,** 236-246.

AN, J. M., MOON, S. A., HONG, S. Y., KANG, J. W. & SEO, J. T. 2015. Neuroprotective effect of 3-morpholinosydnonimine against Zn^{2+}-induced PC12 cell death. *Eur J Pharmacol,* 748**,** 37-44.

ARRIGO, A., ROMANO, F., ARAGONA, E., DI NUNZIO, C., SPERTI, A., BANDELLO, F. & BATTAGLIA PARODI, M. 2019. OCTA-Based Identification of Different Vascular Patterns in Stargardt Disease. *Transl Vis Sci Technol,* 8**,** 26.

AURICCHIO, A., TRAPANI, I. & ALLIKMETS, R. 2015. Gene Therapy of ABCA4-Associated Diseases. *Cold Spring Harb Perspect Med,* 5**,** a017301.

AZARIAN, S. M., MCLEOD, I., LILLO, C., GIBBS, D., YATES, J. R. & WILLIAMS, D. S. 2006. Proteomic analysis of mature melanosomes from the retinal pigmented epithelium. *J Proteome Res,* 5**,** 521-9.

BAADER, W. J., BOHNE, C., CILENTO, G. & DUNFORD, H. B. 1985. Peroxidase-catalyzed formation of triplet acetone and chemiluminescence from isobutyraldehyde and molecular oxygen. *J Biol Chem,* 260**,** 10217-25.

BANDELLO, F., SACCONI, R., QUERQUES, L., CORBELLI, E., CICINELLI, M. V. & QUERQUES, G. 2017. Recent advances in the management of dry age-related macular degeneration: A review. *F1000Res,* 6**,** 245.

BATTAGLIA PARODI, M., IACONO, P., PAPAYANNIS, A., ALTO, G., BUZZOTTA, A., ARRIGO, A., CICINELLI, M. V. & BANDELLO, F. 2020. Near-infrared fundus autofluorescence in early age-related macular degeneration. *Eur J Ophthalmol,* 30**,** 1448-1453.

BAX, N. M., VALKENBURG, D., LAMBERTUS, S., KLEVERING, B. J., BOON, C. J. F., HOLZ, F. G., CREMERS, F. P. M., FLECKENSTEIN, M., HOYNG, C. B., LINDNER, M. & TEAM, F. T. F. S. A. S. 2019. Foveal Sparing in Central Retinal Dystrophies. *Invest Ophthalmol Vis Sci,* 60**,** 3456-3467.

BECHARA, E. J. H., OLIVEIRA, O. M. M. F., DURAN, N., BAPTISTA, R. C. D. & CILENTO, G. 1979. PEROXIDASE CATALYZED GENERATION OF TRIPLET ACETONE. 30**,** 101-110.

BERGLUND, G. I., CARLSSON, G. H., SMITH, A. T., SZÖKE, H., HENRIKSEN, A. & HAJDU, J. 2002. The catalytic pathway of horseradish peroxidase at high resolution. *Nature,* 417**,** 463-468.

BHUTTO, I. A., BABA, T., MERGES, C., MCLEOD, D. S. & LUTTY, G. A. 2010. Low nitric oxide synthases (NOSs) in eyes with age-related macular degeneration (AMD). *Exp Eye Res,* 90**,** 155-67.

BIESEMEIER, A., JULIEN, S., KOKKINOU, D., SCHRAERMEYER, U. & EIBL, O. 2012. A low zinc diet leads to loss of Zn in melanosomes of the RPE but not in melanosomes of the choroidal melanocytes. *Metallomics,* 4**,** 323-32.

BIESEMEIER, A., KREPPEL, F., KOCHANEK, S. & SCHRAERMEYER, U. 2010. The classical pathway of melanogenesis is not essential for melanin synthesis in the adult retinal pigment epithelium. *Cell Tissue Res,* 339**,** 551-60.

BIESEMEIER, A., SCHRAERMEYER, U. & EIBL, O. 2011. Chemical composition of melanosomes, lipofuscin and melanolipofuscin granules of human RPE tissues. *Exp Eye Res,* 93**,** 29-39.

BLAIR, H. A. 2021. Dapagliflozin: A Review in Symptomatic Heart Failure with Reduced Ejection Fraction. *Am J Cardiovasc Drugs*.

BOULTON, M. & DAYHAW-BARKER, P. 2001. The role of the retinal pigment epithelium: topographical variation and ageing changes. *Eye (Lond),* 15**,** 384-9.

BOULTON, M., RÓZANOWSKA, M., RÓZANOWSKI, B. & WESS, T. 2004. The photoreactivity of ocular lipofuscin. *Photochem Photobiol Sci.,* 3**,** 759.764.

BOYER, N. P., HIGBEE, D., CURRIN, M. B., BLAKELEY, L. R., CHEN, C., ABLONCZY, Z., CROUCH, R. K. & KOUTALOS, Y. 2012. Lipofuscin and N-retinylidene-N-retinylethanolamine (A2E) accumulate in retinal pigment epithelium in absence of light exposure: their origin is 11-cis-retinal. *J Biol Chem,* 287**,** 22276-86.

BRESSLER, S. B., MUÑOZ, B., SOLOMON, S. D., WEST, S. K. & TEAM, T. S. E. E. S. 2008. Racial Differences in the Prevalence of Age-Related Macular Degeneration: The Salisbury Eye Evaluation (SEE) Project. *Arch Ophthalmol* 126**,** 241-245.

CĂLIN, E. F., PATONI POPESCU, S. I., COMAN CERNAT, C. C., PATONI, C., POPESCU, M. N. & MUȘAT, O. 2021. Lipofuscin: a key compound in ophthalmic practice. *Rom J Ophthalmol,* 65**,** 109-113.

CASADEVALL, A., CORDERO, R. J. B., BRYAN, R., NOSANCHUK, J. & DADACHOVA, E. 2017. Melanin, Radiation, and Energy Transduction in Fungi. *Microbiol Spectr,* 5.

CHANG, M. A., BRESSLER, S. B., MUNOZ, B. & WEST, S. K. 2008. Racial differences and other risk factors for incidence and progression of age-related macular degeneration: Salisbury Eye Evaluation (SEE) Project. *Invest Ophthalmol Vis Sci,* 49**,** 2395-402.

CHARBEL ISSA, P., BARNARD, A. R., HERRMANN, P., WASHINGTON, I. & MACLAREN, R. E. 2015. Rescue of the Stargardt phenotype in Abca4

knockout mice through inhibition of vitamin A dimerization. *Proc Natl Acad Sci U S A,* 112**,** 8415-20.

CHARBEL ISSA, P., BARNARD, A. R., SINGH, M. S., CARTER, E., JIANG, Z., RADU, R. A., SCHRAERMEYER, U. & MACLAREN, R. E. 2013. Fundus autofluorescence in the Abca4(-/-) mouse model of Stargardt disease--correlation with accumulation of A2E, retinal function, and histology. *Invest Ophthalmol Vis Sci,* 54**,** 5602-12.

CREMERS, F. P., VAN DE POL, D. J., VAN DRIEL, M., DEN HOLLANDER, A. I., VAN HAREN, F. J., KNOERS, N. V., TIJMES, N., BERGEN, A. A., ROHRSCHNEIDER, K., BLANKENAGEL, A., PINCKERS, A. J., DEUTMAN, A. F. & HOYNG, C. B. 1998. Autosomal recessive retinitis pigmentosa and cone-rod dystrophy caused by splice site mutations in the Stargardt's disease gene ABCR. *Hum Mol Genet,* 7**,** 355-62.

CREMERS, F. P. M., LEE, W., COLLIN, R. W. J. & ALLIKMETS, R. 2020. Clinical spectrum, genetic complexity and therapeutic approaches for retinal disease caused by ABCA4 mutations. *Prog Retin Eye Res***,** 100861.

CUDDY, L. K., GORDON, A. C., BLACK, S. A., JAWORSKI, E., FERGUSON, S. S. & RYLETT, R. J. 2012. Peroxynitrite donor SIN-1 alters high-affinity choline transporter activity by modifying its intracellular trafficking. *J Neurosci,* 32**,** 5573-84.

DAYHAW-BARKER, P., DAVIES, S., SHAMSI, F., ROZANOWSKA, M. B., ROZANOWSKI, B. & BOULTON, M. 2001. The phototoxicity of aged RPE melanosomes. *Invest Ophthalmol Vis Sci,* 42**,** S755-S755.

DIMENT, S., EIDELMAN, M., RODRIGUEZ, G. M. & ORLOW, S. J. 1995. Lysosomal hydrolases are present in melanosomes and are elevated in melanizing cells. *J Biol Chem,* 270**,** 4213-5.

DONTSOV, A., YAKOVLEVA, M., TROFIMOVA, N., SAKINA, N., GULIN, A., AYBUSH, A., GOSTEV, F., VASIN, A., FELDMAN, T. & OSTROVSKY, M. 2022. Water-Soluble Products of Photooxidative Destruction of the Bisretinoid A2E Cause Proteins Modification in the Dark. *Int J Mol Sci,* 23.

DONTSOV, A. E., KOROMYSLOVA, A. D. & SAKINA, N. L. 2013. Lipofuscin component A2E does not reduce antioxidant activity of DOPA-melanin. *Bull Exp Biol Med,* 154**,** 624-7.

DONTSOV, A. E., SAKINA, N. L. & OSTROVSKY, M. A. 2017. Loss of Melanin by Eye Retinal Pigment Epithelium Cells Is Associated with Its Oxidative Destruction in Melanolipofuscin Granules. *Biochemistry (Mosc),* 82**,** 916-924.

DOREY, C. K., TORRES, X. & SWART, T. 1990. Evidence of melanogenesis in porcine retinal pigment epithelial cells in vitro. *Exp Eye Res,* 50**,** 1-10.

DUNCKER, T., MARSIGLIA, M., LEE, W., ZERNANT, J., TSANG, S. H., ALLIKMETS, R., GREENSTEIN, V. C. & SPARROW, J. R. 2014. Correlations Among Near-Infrared and Short-Wavelength Autofluorescence and Spectral-Domain Optical Coherence Tomography in Recessive Stargardt Disease. *Invest Ophthalmol Vis Sci.,* 55**,** 8134-8143.

ERGUN, E., HERMANN, B., WIRTITSCH, M., UNTERHUBER, A., KO, T. H., SATTMANN, H., SCHOLDA, C., FUJIMOTO, J. G., STUR, M. &

DREXLER, W. 2005. Assessment of central visual function in Stargardt's disease/fundus flavimaculatus with ultrahigh-resolution optical coherence tomography. *Invest Ophthalmol Vis Sci,* 46**,** 310-6.

FANG, Y., TAUBITZ, T., TSCHULAKOW, A. V., HEIDUSCHKA, P., SZEWCZYK, G., BURNET, M., PETERS, T., BIESEMEIER, A., SARNA, T., SCHRAERMEYER, U. & JULIEN-SCHRAERMEYER, S. 2022. Removal of RPE lipofuscin results in rescue from retinal degeneration in a mouse model of advanced Stargardt disease: Role of reactive oxygen species. *Free Radic Biol Med,* 182**,** 132-149.

FANG, Y., TSCHULAKOW, A., TAUBITZ, T., ILLING, B., BIESEMEIER, A., JULIEN-SCHRAERMEYER, S., RADU, R. A., JIANG, Z. & SCHRAERMEYER, U. 2020. Fundus autofluorescence, spectral-domain optical coherence tomography, and histology correlations in a Stargardt disease mouse model. *FASEB J,* 34**,** 3693-3714.

FEELISCH, M., OSTROWSKI, J. & NOACK, E. 1989. On the mechanism of NO release from sydnonimines. *J Cardiovasc Pharmacol,* 14**,** S13-S22.

FEENEY, L. 1978. Lipofuscin and melanin of human retinal pigment epithelium. Fluorescence, enzyme cytochemical, and ultrastructural studies. *IInvest Ophthalmol Vis Sci,* 17**,** 583-600.

FEENEY-BURNS, L. 1980. The pigments of the retinal pigment epithelium. *Curr Top Eye Res,* 2**,** 119-78.

FEENEY-BURNS, L. & ELDRED, G. E. 1983. The fate of the phagosome: conversion to 'age pigment' and impact in human retinal pigment epithelium. *Trans Ophthalmol Soc U K (1962),* 103 (Pt 4)**,** 416-21.

FEENEY-BURNS, L., HILDERBRAND, E. S. & ELDRIDGE, S. 1984. Aging human RPE: morphometric analysis of macular, equatorial, and peripheral cells. *Invest Ophthalmol Vis Sci,* 25**,** 195-200.

FRIEDMAN, D. S., KATZ, J., BRESSLER, N. M., RAHMANI, B. & TIELSCH, J. M. 1999. Racial differences in the prevalence of age-related macular degeneration: the Baltimore Eye Survey. *Ophthalmology,* 106**,** 1049-55.

FUJINAMI, K., LOIS, N., DAVIDSON, A. E., MACKAY, D. S., HOGG, C. R., STONE, E. M., TSUNODA, K., TSUBOTA, K., BUNCE, C., ROBSON, A. G., MOORE, A. T., WEBSTER, A. R., HOLDER, G. E. & MICHAELIDES, M. 2013a. A longitudinal study of stargardt disease: clinical and electrophysiologic assessment, progression, and genotype correlations. *Am J Ophthalmol,* 155**,** 1075-1088 e13.

FUJINAMI, K., LOIS, N., MUKHERJEE, R., MCBAIN, V. A., TSUNODA, K., TSUBOTA, K., STONE, E. M., FITZKE, F. W., BUNCE, C., MOORE, A. T., WEBSTER, A. R. & MICHAELIDES, M. 2013b. A longitudinal study of Stargardt disease: quantitative assessment of fundus autofluorescence, progression, and genotype correlations. *Invest Ophthalmol Vis Sci,* 54**,** 8181-90.

FUJINAMI, K., SERGOUNIOTIS, P. I., DAVIDSON, A. E., WRIGHT, G., CHANA, R. K., TSUNODA, K., TSUBOTA, K., EGAN, C. A., ROBSON, A. G., MOORE, A. T., HOLDER, G. E., MICHAELIDES, M. & WEBSTER, A. R. 2013c. Clinical and molecular analysis of Stargardt disease with preserved foveal structure and function. *Am J Ophthalmol,* 156**,** 487-501.e1.

GODECHAL, Q. & GALLEZ, B. 2011. The contribution of electron paramagnetic resonance to melanoma research. *J Skin Cancer,* 2011**,** 273280.
GREENBERG, J. P., DUNCKER, T., WOODS, R. L., SMITH, R. T., SPARROW, J. R. & DELORI, F. C. 2013. Quantitative fundus autofluorescence in healthy eyes. *Invest Ophthalmol Vis Sci,* 54**,** 5684-93.
GREENSTEIN, V. C., SCHUMAN, A. D., LEE, W., DUNCKER, T., ZERNANT, J., ALLIKMETS, R., HOOD, D. C. & SPARROW, J. R. 2015. Near-infrared autofluorescence: its relationship to short-wavelength autofluorescence and optical coherence tomography in recessive stargardt disease. *Invest Ophthalmol Vis Sci,* 56**,** 3226-34.
HAJI ABDOLLAHI, S. & HIROSE, T. 2013. Stargardt-Fundus flavimaculatus: recent advancements and treatment. *Semin Ophthalmol,* 28**,** 372-6.
HILL, H. Z. 1992. The function of melanin or six blind people examine an elephant. *Bioessays,* 14**,** 49-56.
HO, S. C., CHIU, S. J. & HU, T. M. 2012. Comparative kinetics of thiol oxidation in two distinct free-radical generating systems: SIN-1 versus AAPH. *Free Radic Res,* 46**,** 1190-200.
HOGG, N., DARLEY-USMAR, V. M., WILSON, M. T. & MONCADA, S. 1992. Production of hydroxyl radicals from the simultaneous generation of superoxide and nitric oxide. *Biochem J,* 281 (Pt 2)**,** 419-24.
HU, D. N., SIMON, J. D. & SARNA, T. 2008. Role of ocular melanin in ophthalmic physiology and pathology. *Photochem Photobiol,* 84**,** 639-44.
HUIE, R. E. & PADMAJA, S. 1993. The reaction of no with superoxide. *Free Radic Res Commun,* 18**,** 195-9.
HUSSAIN, R. M., CIULLA, T. A., BERROCAL, A. M., GREGORI, N. Z., FLYNN, H. W., JR. & LAM, B. L. 2018. Stargardt macular dystrophy and evolving therapies. *Expert Opin Biol Ther,* 18**,** 1049-1059.
JAFFE, G. J., WESTBY, K., CSAKY, K. G., MONÉS, J., PEARLMAN, J. A., PATEL, S. S., JOONDEPH, B. C., RANDOLPH, J., MASONSON, H. & REZAEI, K. A. 2021. C5 Inhibitor Avacincaptad Pegol for Geographic Atrophy Due to Age-Related Macular Degeneration: A Randomized Pivotal Phase 2/3 Trial. *Ophthalmology,* 128**,** 576-586.
JANG, Y. P., MATSUDA, H., ITAGAKI, Y., NAKANISHI, K. & SPARROW, J. R. 2005. Characterization of peroxy-A2E and furan-A2E photooxidation products and detection in human and mouse retinal pigment epithelial cell lipofuscin. *J Biol Chem,* 280**,** 39732-9.
JIN, G., ZOU, M., CHEN, A., ZHANG, Y., YOUNG, C. A., WANG, S. B. & ZHENG, D. 2019. Prevalence of age-related macular degeneration in Chinese populations worldwide: A systematic review and meta-analysis. *Clin Exp Ophthalmol,* 47**,** 1019-1027.
JULIEN, S., BIESEMEIER, A., KOKKINOU, D., EIBL, O. & SCHRAERMEYER, U. 2011. Zinc deficiency leads to lipofuscin accumulation in the retinal pigment epithelium of pigmented rats. *PLoS One,* 6**,** e29245.
JULIEN, S., KOCIOK, N., KREPPEL, F., KOPITZ, J., KOCHANEK, S., BIESEMEIER, A., BLITGEN-HEINECKE, P., HEIDUSCHKA, P. & SCHRAERMEYER, U. 2007. Tyrosinase biosynthesis and trafficking in adult human retinal pigment epithelial cells. *Graefes Arch Clin Exp Ophthalmol,* 245**,** 1495-505.

JULIEN, S. & SCHRAERMEYER, U. 2012. Lipofuscin can be eliminated from the retinal pigment epithelium of monkeys. *Neurobiol Aging,* 33**,** 2390–2397.

JULIEN-SCHRAERMEYER, S., ILLING, B., TSCHULAKOW, A., TAUBITZ, T., GUEZGUEZ, J., BURNET, M. & SCHRAERMEYER, U. 2020. Penetration, distribution, and elimination of remofuscin/soraprazan in Stargardt mouse eyes following a single intravitreal injection using pharmacokinetics and transmission electron microscopic autoradiography: Implication for the local treatment of Stargardt's disease and dry age-related macular degeneration. *Pharmacol Res Perspect,* 8**,** e00683.

JURGENSMEIER, C., BHOSALE, P. & BERNSTEIN, P. S. 2007. Evaluation of 4-methylpyrazole as a potential therapeutic dark adaptation inhibitor. *Curr Eye Res,* 32**,** 911-5.

KAYATZ, P., HEIMANN, K. & SCHRAERMEYER, U. 1999. Ultrastructural localization of light-induced lipid peroxides in the rat retina. *Invest Ophthalmol Vis Sci,* 40**,** 2314-21.

KEILHAUER, C. N. & DELORI, F. C. 2006. Near-infrared autofluorescence imaging of the fundus: visualization of ocular melanin. *Invest Ophthalmol Vis Sci,* 47**,** 3556-64.

KENNEDY, C. J., RAKOCZY, P. E. & CONSTABLE, I. J. 1995. Lipofuscin of the retinal pigment epithelium: A review. *Eye,* 9**,** 763-771.

KHAN, K. N., KASILIAN, M., MAHROO, O. A. R., TANNA, P., KALITZEOS, A., ROBSON, A. G., TSUNODA, K., IWATA, T., MOORE, A. T., FUJINAMI, K. & MICHAELIDES, M. 2018. Early Patterns of Macular Degeneration in ABCA4-Associated Retinopathy. *Ophthalmology,* 125**,** 735-746.

KIM, N. & LEE, H. J. 2021. Redox-Active Metal Ions and Amyloid-Degrading Enzymes in Alzheimer's Disease. *Int J Mol Sci,* 22.

KIM, N. & PRIEFER, R. 2021. Retinol binding protein 4 antagonists and protein synthesis inhibitors: Potential for therapeutic development. *Eur J Med Chem,* 226**,** 113856.

KIM, S. R., JOCKUSCH, S., ITAGAKI, Y., TURRO, N. J. & SPARROW, J. R. 2008. Mechanisms Involved in A2E Oxidation. *Exp Eye Res. ,* 86**,** 975–982.

KOTHAMASI, D., WANNIJN, J., VAN HEES, M., NAUTS, R., VAN GOMPEL, A., VANHOUDT, N. & VANDENHOVE, H. 2019. Exposure to ionizing radiation affects the growth of ectomycorrhizal fungi and induces increased melanin production and increased capacities of reactive oxygen species scavenging enzymes. *J Environ Radioact,* 197**,** 16-22.

KUBOTA, R., AL-FAYOUMI, S., MALLIKAARJUN, S., SHIVA PATIL, P., CLAES BAVIK, P. & CHANDLER, J. W. 2014. Phase 1, dose-ranging study of emixustat hydrochloride (ACU-4429), a novel visual cycle modulator, in healthy volunteers. *Retina,* 34**,** 603-609.

KUBOTA, R., BIRCH, D. G., GREGORY, J. K. & KOESTER, J. M. 2022. Randomised study evaluating the pharmacodynamics of emixustat hydrochloride in subjects with macular atrophy secondary to Stargardt disease. *Br J Ophthalmol,* 106**,** 403-408.

LAMBERTUS, S., LINDNER, M., BAX, N. M., MAUSCHITZ, M. M., NADAL, J., SCHMID, M., SCHMITZ-VALCKENBERG, S., DEN HOLLANDER, A. I., WEBER, B. H., HOLZ, F. G., VAN DER WILT, G. J., FLECKENSTEIN, M., HOYNG, C. B. & FOVEAL SPARING ATROPHY STUDY, T. 2016. Progression of Late-Onset Stargardt Disease. *Invest Ophthalmol Vis Sci,* 57**,** 5186-5191.

LAMBERTUS, S., VAN HUET, R. A., BAX, N. M., HOEFSLOOT, L. H., CREMERS, F. P., BOON, C. J., KLEVERING, B. J. & HOYNG, C. B. 2015. Early-onset stargardt disease: phenotypic and genotypic characteristics. *Ophthalmology,* 122**,** 335-44.

LAPINA, V. A., DONTSOV, A. E. & OSTROVSKIĬ, M. A. 1984. [Generation of superoxides during the interaction of melanins with oxygen]. *Biokhimiia,* 49**,** 1712-8.

LENIS, T. L., HU, J., NG, S. Y., JIANG, Z., SARFARE, S., LLOYD, M. B., ESPOSITO, N. J., SAMUEL, W., JAWORSKI, C., BOK, D., FINNEMANN, S. C., RADEKE, M. J., REDMOND, T. M., TRAVIS, G. H. & RADU, R. A. 2018. Expression of ABCA4 in the retinal pigment epithelium and its implications for Stargardt macular degeneration. *Proc Natl Acad Sci U S A*.

LIU, S., KUHT, H. J., MOON, E. H., MACONACHIE, G. D. E. & THOMAS, M. G. 2021. Current and emerging treatments for albinism. *Surv Ophthalmol,* 66**,** 362-377.

LOIS, N., HOLDER, G. E., BUNCE, C., FITZKE, F. W. & BIRD, A. C. 2001. Phenotypic Subtypes of Stargardt Macular Dystrophy–Fundus Flavimaculatus. *Arch Ophthalmol.,* 119**,** 359-369.

LOPES, V. S., WASMEIER, C., SEABRA, M. C. & FUTTER, C. E. 2007. Melanosome maturation defect in Rab38-deficient retinal pigment epithelium results in instability of immature melanosomes during transient melanogenesis. *Mol Biol Cell,* 18**,** 3914-27.

LYU, Y., TSCHULAKOW, A. V. & SCHRAERMEYER, U. 2022. Melanosomes degrade lipofuscin and precursors that are derived from photoreceptor membrane turnover in the retinal pigment epithelium—an explanation for the origin of the melanolipofuscin granule. *bioRxiv***,** 2022.02.16.480523.

MACDONALD, I. M. & SIEVING, P. A. 2018. Investigation of the effect of dietary docosahexaenoic acid (DHA) supplementation on macular function in subjects with autosomal recessive Stargardt macular dystrophy. *Ophthalmic Genet,* 39**,** 477-486.

MAEDA, A., MAEDA, T., GOLCZAK, M. & PALCZEWSKI, K. 2008. Retinopathy in mice induced by disrupted all-trans-retinal clearance. *J Biol Chem,* 283**,** 26684-93.

MARTIN, D. F. 2018. Evolution of Intravitreal Therapy for Retinal Diseases-From CMV to CNV: The LXXIV Edward Jackson Memorial Lecture. *Am J Ophthalmol,* 191**,** xli-lviii.

MATA, N. L., LICHTER, J. B., VOGEL, R., HAN, Y., BUI, T. V., SINGERMAN, L. J. & FACS, F. 2013. Investigation of oral fenretinide for treatment of geographic atrophy in age-related macular degeneration. *Retina,* 33**,** 498-507.

MICELI, M. V., LILES, M. R. & NEWSOME, D. A. 1994. Evaluation of oxidative processes in human pigment epithelial cells associated with retinal outer segment phagocytosis. *Exp Cell Res,* 214**,** 242-9.
MICHAELIDES, M., HUNT, D. M. & MOORE, A. T. 2003. The genetics of inherited macular dystrophies. *J Med Genet,* 40**,** 641-50.
MIHAI, D. M. & WASHINGTON, I. 2014. Vitamin A dimers trigger the protracted death of retinal pigment epithelium cells. *Cell Death Dis,* 5**,** e1348.
MOLDAY, R. S. 2007. ATP-binding cassette transporter ABCA4: molecular properties and role in vision and macular degeneration. *J Bioenerg Biomembr,* 39**,** 507-17.
MOSTERT, A. B., RIENECKER, S. B., NOBLE, C., HANSON, G. R. & MEREDITH, P. 2018. The photoreactive free radical in eumelanin. *Sci Adv,* 4**,** eaaq1293.
MURDAUGH, L. S., WANG, Z., DEL PRIORE, L. V., DILLON, J. & GAILLARD, E. R. 2010. Age-related accumulation of 3-nitrotyrosine and nitro-A2E in human Bruch's membrane. *Exp Eye Res,* 90**,** 564-71.
NG, K.-P., GUGIU, B., RENGANATHAN, K., DAVIES, M. W., GU, X., CRABB, J. S., KIM, S. R., RÓŻANOWSKA, M. B., BONILHA, V. L., RAYBORN, M. E., SALOMON, R. G., SPARROW, J. R., BOULTON, M. E., HOLLYFIELD, J. G. & CRABB, J. W. 2008. Retinal Pigment Epithelium Lipofuscin Proteomics. *Mol Cell Proteomics,* 7**,** 1397-1405.
NOWAK, J. Z. 2006. Age-related macular degeneration (AMD): pathogenesis and therapy. *Pharmacol Rep,* 58**,** 353-63.
ORLOW, S. J. 1995. Melanosomes are specialized members of the lysosomal lineage of organelles. *J Invest Dermatol,* 105**,** 3-7.
OSTROVSKY, M. A., SAKINA, N. L. & DONTSOV, A. E. 1987. An antioxidative role of ocular screening pigments. *Vision Res,* 27**,** 893-9.
PAN, C., BANERJEE, K., LEHMANN, G. L., ALMEIDA, D., HAJJAR, K. A., BENEDICTO, I., JIANG, Z., RADU, R. A., THOMPSON, D. H., RODRIGUEZ-BOULAN, E. & NOCIARI, M. M. 2021. Lipofuscin causes atypical necroptosis through lysosomal membrane permeabilization. *Proc Natl Acad Sci U S A,* 118.
PARISH, C. A., HASHIMOTO, M., NAKANISHI, K., DILLON, J. & SPARROW, J. 1998. Isolation and one-step preparation of A2E and iso-A2E, fluorophores from human retinal pigment epithelium. *Proc. Natl. Acad. Sci. USA,* 95**,** 14609–14613.
PICCARDI, M., FADDA, A., MARTELLI, F., MARANGONI, D., MAGLI, A., MINNELLA, A. M., BERTELLI, M., DI MARCO, S., BISTI, S. & FALSINI, B. 2019. Antioxidant Saffron and Central Retinal Function in ABCA4-Related Stargardt Macular Dystrophy. *Nutrients,* 11.
PIOTTER, E., MCCLEMENTS, M. E. & MACLAREN, R. E. 2021. Therapy Approaches for Stargardt Disease. *Biomolecules,* 11.
POLIAKOV, E., STRUNNIKOVA, N. V., JIANG, J.-K., MARTINEZ, B., PARIKH, T., LAKKARAJU, A., THOMAS, C., BROOKS, B. P. & REDMOND, T. M. 2014. Multiple A2E treatments lead to melanization of rod outer segment–challenged ARPE-19 cells. *Mol Vis***,** 285-300.
PREMI, S., WALLISCH, S., MANO, C. M., WEINER, A. B., BACCHIOCCHI, A., WAKAMATSU, K., BECHARA, E. J., HALABAN, R., DOUKI, T. &

BRASH, D. E. 2015. Photochemistry. Chemiexcitation of melanin derivatives induces DNA photoproducts long after UV exposure. *Science,* 347**,** 842-7.

PROKOPIOU, E., KOLOVOS, P., KALOGEROU, M., NEOKLEOUS, A., NICOLAOU, O., SOKRATOUS, K., KYRIACOU, K. & GEORGIOU, T. 2018. Omega-3 Fatty Acids Supplementation: Therapeutic Potential in a Mouse Model of Stargardt Disease. *Invest Ophthalmol Vis Sci,* 59**,** 2757-2767.

QUAZI, F. & MOLDAY, R. S. 2014. ATP-binding cassette transporter ABCA4 and chemical isomerization protect photoreceptor cells from the toxic accumulation of excess 11-cis-retinal. *Proc Natl Acad Sci U S A,* 111**,** 5024-9.

RADU, R. A., HU, J., YUAN, Q., WELCH, D. L., MAKSHANOFF, J., LLOYD, M., MCMULLEN, S., TRAVIS, G. H. & BOK, D. 2011. Complement system dysregulation and inflammation in the retinal pigment epithelium of a mouse model for Stargardt macular degeneration. *J Biol Chem,* 286**,** 18593-601.

RADU, R. A., MATA, N. L., BAGLA, A. & TRAVIS, G. H. 2004. Light exposure stimulates formation of A2E oxiranes in a mouse model of Stargardt's macular degeneration. *Proc Natl Acad Sci U S A,* 101**,** 5928-33.

RADU, R. A., YUAN, Q., HU, J., PENG, J. H., LLOYD, M., NUSINOWITZ, S., BOK, D. & TRAVIS, G. H. 2008. Accelerated accumulation of lipofuscin pigments in the RPE of a mouse model for ABCA4-mediated retinal dystrophies following Vitamin A supplementation. *Invest Ophthalmol Vis Sci,* 49**,** 3821-9.

RAMKUMAR, H. L., ZHANG, J. & CHAN, C. C. 2010. Retinal ultrastructure of murine models of dry age-related macular degeneration (AMD). *Prog Retin Eye Res,* 29**,** 169-90.

RAPOSO, G. & MARKS, M. S. 2002. The dark side of lysosome-related organelles: specialization of the endocytic pathway for melanosome biogenesis. *Traffic,* 3**,** 237-48.

REINA-TORRES, E., DE IESO, M. L., PASQUALE, L. R., MADEKUROZWA, M., VAN BATENBURG-SHERWOOD, J., OVERBY, D. R. & STAMER, W. D. 2021. The vital role for nitric oxide in intraocular pressure homeostasis. *Prog Retin Eye Res,* 83**,** 100922.

RITTER, M., ZOTTER, S., SCHMIDT, W. M., BITTNER, R. E., DEAK, G. G., PIRCHER, M., SACU, S., HITZENBERGER, C. K., SCHMIDT-ERFURTH, U. M. & MACULA STUDY GROUP, V. 2013. Characterization of stargardt disease using polarization-sensitive optical coherence tomography and fundus autofluorescence imaging. *Invest Ophthalmol Vis Sci,* 54**,** 6416-25.

ROMÉRO-GRAILLET, C., ABERDAM, E., CLÉMENT, M., ORTONNE, J.-P. & BALLOTTI, R. 1997. Nitric oxide produced by ultraviolet-irradiated keratinocytes stimulates melanogenesis. *J Clin Invest,* 99**,** 635-642.

ROTENSTREICH, Y., FISHMAN, G. A. & ANDERSON, R. J. 2003. Visual acuity loss and clinical observations in a large series of patients with stargardt disease. *Ophthalmology,* 110**,** 1151-1158.

RÓZANOWSKA, M., KORYTOWSKI, W., RÓZANOWSKI, B., SKUMATZ, C., BOULTON, M. E., BURKE, J. M. & SARNA, T. 2002. Photoreactivity of aged human RPE melanosomes: a comparison with lipofuscin. *Invest Ophthalmol Vis Sci,* 43**,** 2088-96.

RÓZANOWSKI, B., BURKE, J., SARNA, T. & RÓZANOWSKA, M. 2008a. The pro-oxidant effects of interactions of ascorbate with photoexcited melanin fade away with aging of the retina. *Photochem Photobiol,* 84**,** 658-70.

RÓZANOWSKI, B., CUENCO, J., DAVIES, S., SHAMSI, F. A., ZADŁO, A., DAYHAW-BARKER, P., RÓZANOWSKA, M., SARNA, T. & BOULTON, M. E. 2008b. The phototoxicity of aged human retinal melanosomes. *Photochem Photobiol,* 84**,** 650-7.

SARNA, T. 1992. Properties and function of the ocular melanin--a photobiophysical view. *J Photochem Photobiol B,* 12**,** 215-58.

SARNA, T., BURKE, J. M., KORYTOWSKI, W., ROZANOWSKA, M., SKUMATZ, C. M., ZAREBA, A. & ZAREBA, M. 2003. Loss of melanin from human RPE with aging: possible role of melanin photooxidation. *Exp Eye Res,* 76**,** 89-98.

SASAKI, M., HORIKOSHI, T., UCHIWA, H. & MIYACHI, Y. 2000. Up-regulation of tyrosinase gene by nitric oxide in human melanocytes. *Pigment Cell Res,* 13**,** 248-52.

SCHAUMANN, W. 1989. Pharmacokinetics of isosorbide dinitrate and isosorbide-5-mononitrate. *Int J Clin Pharmacol Ther Toxicol,* 27**,** 445-53.

SCHMIDT, S. Y. & PEISCH, R. D. 1986. Melanin concentration in normal human retinal pigment epithelium. Regional variation and age-related reduction. *Invest Ophthalmol Vis Sci,* 27**,** 1063-7.

SCHMITZ-VALCKENBERG, S., HOLZ, F. G., BIRD, A. C. & SPAIDE, R. F. 2008. Fundus autofluorescence imaging: review and perspectives. *Retina,* 28**,** 385-409.

SCHRAERMEYER, U. 1992. Evidence for melanogenesis in the retinal pigment epithelium of adult cattle and golden hamster. *Comp Biochem Physiol B,* 103**,** 435-42.

SCHRAERMEYER, U. 1993. Does melanin turnover occur in the eyes of adult vertebrates? *Pigment Cell Res,* 6**,** 193-204.

SCHRAERMEYER, U., ADDICKS, K., KOCIOK, N., ESSER, P. & HEIMANN, K. 1998. Capillaries are present in Bruch's membrane at the ora serrata in the human eye. *Invest Ophthalmol Vis Sci,* 39**,** 1076-84.

SCHRAERMEYER U, F. Y., TAUBITZ T, TSCHULAKOW A 2019. Degradation of lipofuscin in Stargardt mice can be enhanced by the superoxide generator riboflavin - a hypothesis for melanolipofuscin formation(abstract). *Invest Ophthalmol Vis Sci,* 60.

SCHRAERMEYER, U. & HEIMANN, K. 1999. Current understanding on the role of retinal pigment epithelium and its pigmentation. *Pigment Cell Res,* 12**,** 219-36.

SCHRAERMEYER, U. & JULIEN, S. 2013. Effects of bevacizumab in retina and choroid after intravitreal injection into monkey eyes. *Expert Opin Biol Ther,* 13**,** 157-67.

SCHRAERMEYER, U., KOPITZ, J., PETERS, S., HENKE-FAHLE, S., BLITGEN-HEINECKE, P., KOKKINOU, D., SCHWARZ, T. & BARTZ-

SCHMIDT, K. U. 2006. Tyrosinase biosynthesis in adult mammalian retinal pigment epithelial cells. *Exp Eye Res,* 83**,** 315-21.
SCHRAERMEYER, U., PETERS, S., THUMANN, G., KOCIOK, N. & HEIMANN, K. 1999. Melanin granules of retinal pigment epithelium are connected with the lysosomal degradation pathway. *Exp Eye Res,* 68**,** 237-45.
SCHRAERMEYER, U. & STIEVE, H. 1994. A newly discovered pathway of melanin formation in cultured retinal pigment epithelium of cattle. *Cell Tissue Res,* 276**,** 273-9.
SEAGLE, B. L., REZAI, K. A., KOBORI, Y., GASYNA, E. M., REZAEI, K. A. & NORRIS, J. R., JR. 2005. Melanin photoprotection in the human retinal pigment epithelium and its correlation with light-induced cell apoptosis. *Proc Natl Acad Sci U S A,* 102**,** 8978-83.
SEARS, A. E., BERNSTEIN, P. S., CIDECIYAN, A. V., HOYNG, C., CHARBEL ISSA, P., PALCZEWSKI, K., ROSENFELD, P. J., SADDA, S., SCHRAERMEYER, U., SPARROW, J. R., WASHINGTON, I. & SCHOLL, H. P. N. 2017. Towards Treatment of Stargardt Disease: Workshop Organized and Sponsored by the Foundation Fighting Blindness. *Transl Vis Sci Technol,* 6**,** 6.
SEMPLE-ROWLAND, S. L. & BERRY, J. 2014. Use of lentiviral vectors to deliver and express bicistronic transgenes in developing chicken embryos. *Methods,* 66**,** 466-73.
SEVER, R. J., COPE, F. W. & POLIS, B. D. 1962. Generation by visible light of labile free radicals in the melanin granules of the eye. *Science,* 137**,** 128-9.
SHELINE, C. T., ZHOU, Y. & BAI, S. 2010. Light-induced photoreceptor and RPE degeneration involve zinc toxicity and are attenuated by pyruvate, nicotinamide, or cyclic light. *Mol Vis,* 16**,** 2639-52.
SPARROW, J. R., BLONSKA, A., FLYNN, E., DUNCKER, T., GREENBERG, J. P., SECONDI, R., UEDA, K. & DELORI, F. C. 2013. Quantitative fundus autofluorescence in mice: correlation with HPLC quantitation of RPE lipofuscin and measurement of retina outer nuclear layer thickness. *Invest Ophthalmol Vis Sci,* 54**,** 2812-20.
SPARROW, J. R. & BOULTON, M. 2005. RPE lipofuscin and its role in retinal pathobiology. *Exp Eye Res,* 80**,** 595-606.
SPARROW, J. R., GREGORY-ROBERTS, E., YAMAMOTO, K., BLONSKA, A., GHOSH, S. K., UEDA, K. & ZHOU, J. 2012. The bisretinoids of retinal pigment epithelium. *Prog Retin Eye Res,* 31**,** 121-35.
SPARROW, J. R., NAKANISHI, K. & PARISH, C. A. 2000. The Lipofuscin Fluorophore A2E Mediates Blue Light– Induced Damage to Retinal Pigmented Epithelial Cells. *Invest Ophthalmol Vis Sci,* 41**,** 1981–1989.
STAHL, A. 2020. The Diagnosis and Treatment of Age-Related Macular Degeneration. *Dtsch Arztebl Int,* 117**,** 513-520.
STARGARDT, K. 1909. Ueber familiare progressive Degeneration in der Makulagegend des Augues. *Albrecht V Graefes Arch Opthamology,* 71**,** 534–550.
STRAUSS, O. 2005. The retinal pigment epithelium in visual function. *Physiol Rev,* 85**,** 845-81.

SUN, D., SUN, W., GAO, S. Q., WEI, C., NADERI, A., SCHILB, A. L., SCHEIDT, J., LEE, S., KERN, T. S., PALCZEWSKI, K. & LU, Z. R. 2021. Formulation and efficacy of ECO/pRHO-ABCA4-SV40 nanoparticles for nonviral gene therapy of Stargardt disease in a mouse model. *J Control Release,* 330**,** 329-340.

SUNDELIN, S. P., NILSSON, S. E. & BRUNK, U. T. 2001. Lipofuscin-formation in cultured retinal pigment epithelial cells is related to their melanin content. *Free Radic Biol Med,* 30**,** 74-81.

TANAKA, K., LEE, W., ZERNANT, J., SCHUERCH, K., CICCONE, L., TSANG, S. H., SPARROW, J. R. & ALLIKMETS, R. 2018. The Rapid-Onset Chorioretinopathy Phenotype of ABCA4 Disease. *Ophthalmology,* 125**,** 89-99.

TANNA, P., STRAUSS, R. W., FUJINAMI, K. & MICHAELIDES, M. 2017. Stargardt disease: clinical features, molecular genetics, animal models and therapeutic options. *Br J Ophthalmol,* 101**,** 25-30.

TAUBITZ, T., FANG, Y., BIESEMEIER, A., JULIEN-SCHRAERMEYER, S. & SCHRAERMEYER, U. 2019. Age, lipofuscin and melanin oxidation affect fundus near-infrared autofluorescence. *EBioMedicine,* 48**,** 592-604.

TAUBITZ, T., TSCHULAKOW, A. V., TIKHONOVICH, M., ILLING, B., FANG, Y., BIESEMEIER, A., JULIEN-SCHRAERMEYER, S. & SCHRAERMEYER, U. 2018. Ultrastructural alterations in the retinal pigment epithelium and photoreceptors of a Stargardt patient and three Stargardt mouse models: indication for the central role of RPE melanin in oxidative stress. *PeerJ,* 6**,** e5215.

TERMAN, A. & BRUNK, U. T. 2004. Lipofuscin. *Int J Biochem Cell Biol,* 36**,** 1400-4.

THOMAS, C. J., MIRZA, R. G. & GILL, M. K. 2021. Age-Related Macular Degeneration. *Med Clin North Am,* 105**,** 473-491.

TSANG, S. H. & SHARMA, T. 2018. Stargardt Disease. *Adv Exp Med Biol,* 1085**,** 139-151.

UEDA, K., KIM, H. J., ZHAO, J., SONG, Y., DUNAIEF, J. L. & SPARROW, J. R. 2018. Iron promotes oxidative cell death caused by bisretinoids of retina. *Proc Natl Acad Sci U S A,* 115**,** 4963-4968.

UEDA, K., ZHAO, J., KIM, H. J. & SPARROW, J. R. 2016. Photodegradation of retinal bisretinoids in mouse models and implications for macular degeneration. *Proc Natl Acad Sci U S A***,** 6904–6909.

VAN DRIEL, M. A., MAUGERI, A., KLEVERING, B. J., HOYNG, C. B. & CREMERS, F. P. 1998. ABCR unites what ophthalmologists divide(s). *Ophthalmic Genet,* 19**,** 117-22.

VAN HUET, R. A., BAX, N. M., WESTENENG-VAN HAAFTEN, S. C., MUHAMAD, M., ZONNEVELD-VRIELING, M. N., HOEFSLOOT, L. H., CREMERS, F. P., BOON, C. J., KLEVERING, B. J. & HOYNG, C. B. 2014. Foveal sparing in Stargardt disease. *Invest Ophthalmol Vis Sci,* 55**,** 7467-78.

WARBURTON, S., DAVIS, W. E., SOUTHWICK, K., XIN, H., WOOLLEY, A. T., BURTON, G. F. & THULIN, C. D. 2007. Proteomic and phototoxic characterization of melanolipofuscin: Correlation to disease and model for its origin. *Mol Vis,* 13**,** 318-29.

WASSELL, J., DAVIES S FAU - BARDSLEY, W., BARDSLEY W FAU - BOULTON, M. & BOULTON, M. 1999. The Photoreactivity of the Retinal Age Pigment Lipofuscin. *J Biol Chem,* 274**,** 23828–23832.

WAVRE-SHAPTON, S. T., MESCHEDE, I. P., SEABRA, M. C. & FUTTER, C. E. 2014. Phagosome maturation during endosome interaction revealed by partial rhodopsin processing in retinal pigment epithelium. *J Cell Sci,* 127**,** 3852-61.

WEITER, J. J., DELORI, F. C., WING, G. L. & FITCH, K. A. 1986. Retinal pigment epithelial lipofuscin and melanin and choroidal melanin in human eyes. *Invest Ophthalmol Vis Sci,* 27**,** 145-52.

WENG, J., MATA, N. L., AZARIAN, S. M., TZEKOV, R. T., BIRCH, D. G. & TRAVIS, G. H. 1999. Insights into the Function of Rim Protein in Photoreceptors and Etiology of Stargardt's Disease from the Phenotype in abcr Knockout Mice. *Cell,* 98**,** 13-23.

WESTERFELD, C. & MUKAI, S. 2008. Stargardt's disease and the ABCR gene. *Semin Ophthalmol,* 23**,** 59-65.

WHITE, E. H., MIANO, J. D., WATKINS, C. J. & BREAUX, E. J. 1974. Chemically produced excited states. *Angew Chem Int Ed Engl,* 13**,** 229-243.

WONG, W. L., SU, X., LI, X., CHEUNG, C. M., KLEIN, R., CHENG, C. Y. & WONG, T. Y. 2014. Global prevalence of age-related macular degeneration and disease burden projection for 2020 and 2040: a systematic review and meta-analysis. *Lancet Glob Health,* 2**,** e106-16.

WOOD, J. M. & SCHALLREUTER, K. U. 1991. Studies on the reactions between human tyrosinase, superoxide anion, hydrogen peroxide and thiols. *Biochim Biophys Acta,* 1074**,** 378-85.

WU, L., NAGASAKI, T. & SPARROW, J. R. 2010. Photoreceptor cell degeneration in Abcr (-/-) mice. *Adv Exp Med Biol,* 664**,** 533-9.

WU, Y., ZHOU, J., FISHKIN, N., RITTMANN, B. E. & SPARROW, J. R. 2011. Enzymatic degradation of A2E, a retinal pigment epithelial lipofuscin bisretinoid. *J Am Chem Soc,* 133**,** 849-57.

YACOUT, S. M., MCILWAIN, K. L., MIRZA, S. P. & GAILLARD, E. R. 2019. Characterization of Retinal Pigment Epithelial Melanin and Degraded Synthetic Melanin Using Mass Spectrometry and In Vitro Biochemical Diagnostics. *Photochem Photobiol,* 95**,** 183-191.

YAMAMOTO, K., YOON, K. D., UEDA, K., HASHIMOTO, M. & SPARROW, J. R. 2011. A novel bisretinoid of retina is an adduct on glycerophosphoethanolamine. *Invest Ophthalmol Vis Sci,* 52**,** 9084-90.

YAMAMOTO, K., ZHOU, J., HUNTER, J. J., WILLIAMS, D. R. & SPARROW, J. R. 2012. Toward an understanding of bisretinoid autofluorescence bleaching and recovery. *Invest Ophthalmol Vis Sci,* 53**,** 3536-44.

YOUNG, R. W. & BOK, D. 1969. Participation of the retinal pigment epithelium in the rod outer segment renewal process. *J Cell Biol,* 42**,** 392-403.

ZERNANT, J., XIE, Y. A., AYUSO, C., RIVEIRO-ALVAREZ, R., LOPEZ-MARTINEZ, M. A., SIMONELLI, F., TESTA, F., GORIN, M. B., STROM, S. P., BERTELSEN, M., ROSENBERG, T., BOONE, P. M., YUAN, B., AYYAGARI, R., NAGY, P. L., TSANG, S. H., GOURAS, P., COLLISON, F. T., LUPSKI, J. R., FISHMAN, G. A. & ALLIKMETS, R. 2014. Analysis

of the ABCA4 genomic locus in Stargardt disease. *Hum Mol Genet,* 23**,** 6797-806.

ZHANG, Q., PRESSWALLA, F., CALTON, M., CHARNIGA, C., STERN, J., TEMPLE, S., VOLLRATH, D., ZACKS, D. N., ALI, R. R., THOMPSON, D. A. & MILLER, J. M. L. 2019. Highly Differentiated Human Fetal RPE Cultures Are Resistant to the Accumulation and Toxicity of Lipofuscin-Like Material. *Invest Ophthalmol Vis Sci,* 60**,** 3468-3479.

ZHAO, J., KIM, H. J., UEDA, K., ZHANG, K., MONTENEGRO, D., DUNAIEF, J. L. & SPARROW, J. R. 2021. A vicious cycle of bisretinoid formation and oxidation relevant to recessive Stargardt disease. *J Biol Chem,* 296**,** 100259.

ZHOU, J., KIM, S. R., WESTLUND, B. S. & SPARROW, J. R. 2009. Complement activation by bisretinoid constituents of RPE lipofuscin. *Invest Ophthalmol Vis Sci,* 50**,** 1392-9.

8. Declaration of Contributions

The dissertation work was carried out at the division of experimental vitreoretinal surgery, center for ophthalmology, institute of ophthalmic research, University of Tuebingen under the supervision of Prof. Dr. rer. nat. Ulrich Schraermeyer.

The study was designed by Prof. Dr. rer. nat. Ulrich Schraermeyer.

After training by laboratory members Dr. Tatjana Taubitz and Dr. Alexander Tschulakow, I carried out cSLO with the assistance of Dr. Alexander Tschulakow. I prepared the ultrathin sections for electron microscopy with the assistance of Antonina Burda. I carried out the rest of the experiments independently.

Statistical analysis was carried out independently by myself.

I confirm that I wrote the thesis myself under the supervision of Prof. Ulrich Schraermeyer and that any additional sources of information have been duly cited.

Signed_____

on _____ in Tübingen

9. Publication

Parts of the dissertation presented here have already appeared in the following publications:

Yanan Lyu, Alexander V. Tschulakow, Ulrich Schraermeyer. Melanosomes degrade lipofuscin and precursors that are derived from photoreceptor membrane turnover in the retinal pigment epithelium—an explanation for the origin of the melanolipofuscin granule. bioRxiv 2022.02.16.480523; doi: https://doi.org/10.1101/2022.02.16.480523.

10. Acknowledgment

Words cannot express my gratitude to my supervisor Prof. Dr. Ulrich Schraermeyer, who has not only provided me the opportunity to work on the project but also given me so much help. I still remember the countless time that him seating in front of electron microscopy and discussed the results with me. I could not have achieved what I did without his support. I would also like to give my thanks to PD Dr. Sylvie Julien-Schraermeyer, who has given me much advice in both my professional and personal life. They both gave me invaluable patience and support.

My sincere thanks should also be given to Dr. Tatjana Taubitz, who helped me so much during my first year with professional training and tremendous support. Thanks should also go to Dr. Alexander Tschulakow for his assistance in my research work. Many thanks to Shan Liu and Yuan Fang for their help to teach me experimental skills and for useful advice.

My sincere appreciation also goes to Antonina Burda for the great technical assistance she gave. Thanks to Judith Birch for all the help with the paperwork. I am also grateful to Kun Wang for her company and support in the past three years.

Thanks to the financial support from the China Scholarship Council.

My special thanks also go to my family(my mom, my sister, and my aunts) for their support during the difficult covid time. I would also like to thank my friends Timo Frankenbach, Yingyue Tang, Valentina Romagnano for their emotional support and accompany for my difficult times.